Graphitic structures: from planar to spheres, toroids and helices

By M. Terrones[1], W. K. Hsu[1], J. P. Hare[1], H. W. Kroto[1], H. Terrones[2] and D. R. M. Walton[1]

[1]*School of Chemistry and Molecular Sciences, University of Sussex, Brighton BN1 9QJ, UK*

[2]*Instituto de Física, UNAM, Apartado Postal 20-364, 01000, México, D.F. México*

Following the discovery of C_{60} (Buckminsterfullerene), nanotubes and graphitic onions, new graphitic-type carbon structures, possessing great stability were predicted theoretically and identified experimentally. The chief characteristic associated with many of these new structures is the presence of pentagons and heptagons in the predominantly hexagonal network leading to positive and/or negative curvature. In this paper, we discuss a range of fullerene-related graphitic sheet structures (e.g. corkscrew-like nanotubes, toroids, round giant fullerenes, etc.) and show that molecular simulation studies based on such curved graphene surfaces are in good agreement with experimental high-resolution transmission electron microscopy (HRTEM) observations. New production methods and possible ways of evaluating nanoscale graphitic structures (surfaces) are discussed. The novel materials may have applications in nanoscale engineering.

1. Introduction

C_{60}, the first hollow structure made entirely of carbon, was first detected in 1985 (Kroto *et al.* 1985) and produced in bulk five years later using a DC arc discharge between graphite rods in an inert gas atmosphere (e.g. Ar, He) (Krätschmer *et al.* 1990). Subsequently, other new forms of carbon such as nanotubes (needle-like concentric structures) (Iijima 1991), graphitic onions (giant concentric fullerenes first observed by Iijima (1980), see also Ugarte (1992) and Harris *et al.* (1994)), helix-shaped nanotubes (Amelinckx *et al.* 1994) and bent nanotubes (Hsu & Terrones 1994) were identified. Other layered materials, such as MoS_2 (Margulis *et al.* 1993), WS_2 (Tenne *et al.* 1992), BC_2N (Weng-Sieh *et al.* 1995), BC_3 (Weng-Sieh *et al.* 1995) and BN (Chopra *et al.* 1995), have recently been shown to form analogous structures.

From a simple theoretical point of view, pure graphite (hexagons only) can be rolled into open-ended needle-like structures (nanotubes). The inclusion of pentagons at the tips results in positive curvature leading to closure (30° declination) (Iijima 1980, 1991). The additional incorporation of heptagons results in negative (30° inclination) curvature (Mackay & Terrones 1991; Iijima 1992*b*).

In this paper we discuss these new forms of carbon, based on the high-resolution transmission electron microscopy (HRTEM) observations and molecular simulations using geometrical considerations, in an endeavour to understand their possible growth mechanisms.

Phil. Trans. R. Soc. Lond. A (1996) **354**, 2025–2054
Printed in Great Britain

2. C_{60} and concentric giant fullerenes

In 1985, when the third allotrope of carbon (C_{60}-Buckminsterfullerene) was discovered serendipitiously during laser vaporization of graphite (Kroto *et al.* 1985), the possibility of having other hollow cage structures made of carbon became a reality. C_{60}, the archetypal cage molecule, consists of 12 pentagons and 20 hexagons distributed symmetrically in a truncated icosahedron. According to Euler's law, twelve pentagons is the minimum required to close the structure. The general form of this law can be written; $F-E+V=\chi$, where F, E and V are the number of faces, edges and vertices respectively, and χ is the Euler characteristic—a geometric invariant associated with structures of the same shape or topology. For all polyhedra, $\chi=2$. For example, in a cube $F=6$, $E=12$ and $V=8$. For C_{60}, $F=32$ (12 pentagons and 20 hexagons), $E=90$, $V=60$.

For a graphitic network in which each edge is shared by two polygonal faces and each vertex is shared by three polygons, if pentagons, hexagons and heptagons only are considered,

$$F=N_5+N_6+N_7,$$

and

$$2E=3V=5N_5+6N_6+7N_7.$$

Putting this restriction into Euler's expression yields

$$N_5=N_7+12$$

The discovery of graphitic onions, first by Iijima (1980) in amorphous carbon films prepared by vacuum deposition and subsequently by Ugarte (1992) using high electron irradiation, has widened our appreciation of the shapes and growth mechanisms associated with graphite. Different approaches have been adopted in order to explain the sphericity of onions (figure 1*b*, *c*). Initially, they were considered to be nested icosahedral fullerenes containing only pentagonal and hexagonal rings (figure 1*a*) (Kroto & McKay 1988). One reason for considering icosahedral structures is that the average separation between successive shells (e.g. $C_{60}@C_{240}@C_{540}@C_{960}@C_{1500}$, etc.) should be close to that between graphite layers (e.g. 3.35 Å). In these models, the onion-like structures appear spherical if oriented along the five-fold axis, but faceted with respect to other orientations; the bigger the onion, the more pronounced the effect (figure 1*a*). Refinements of this proposal suggest that rounded structures can be generated by removing the cusps (pentagons and neighbouring atoms) from icosahedral fullerenes (Sarkar *et al.* 1996). In these models, it is also possible to introduce heptagons and additional pentagons, thus creating quasi-spherical onions (figure 2). By using invariants under rotation in order to measure the symmetry of such quasi-spherical fullerenes it is found that some of these structures, although quite spherical, are not symmetrical (neither icosahedral nor cubic, etc.), though they consist of highly graphitized domains.

Stone–Wales-type transformations (Stone & Wales 1986), which convert four adjacent hexagons into two pentagons and two heptagons, can be applied throughout the icosahedral onion structure to smooth out the cusp regions producing, in some cases, quasi-spherical fullerenes. In order to assess the sphericity of our structures, the distance r_i between each atom and the centre of mass has been calculated. For a perfect spherical arrangement, r_i corresponds to the radius of a sphere. In the quasi-spherical structures studied, r_i fluctuates; however, all r_i lie within a small range,

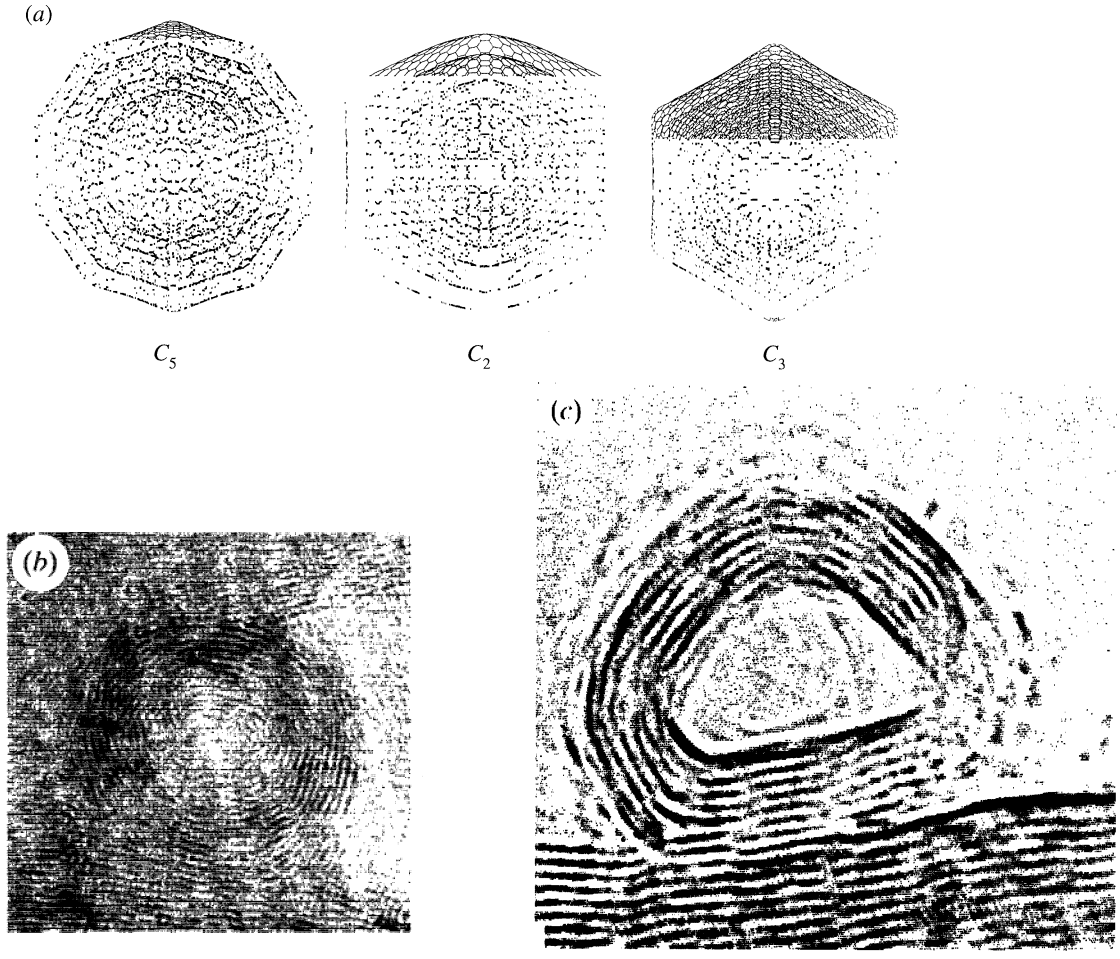

Figure 1. (*a*) Molecular modelling image of the structure $C_{960}@C_{1500}@C_{2160}@C_{2940}$ composed of four concentric perfect icosahedral giant fullerenes. The particle is viewed along three different symmetry axes (C5, C2 and C3, respectively) to show the way the shape varies with orientation to the observer. (*b*) Real round onion-like structure with *ca.* 15–20 layers. (*c*) Polyhedral (tetrahedron-like) structure possessing 8–10 layers. In (*b*) and (*c*) the interlayer spacing is close to that of graphite (e.g. 3.35 Å).

where Δr_i was estimated from the difference between the largest and the shortest r_i (see table 1). It is worth noting that as r_i increases—as the icosahedral fullerene grows—our structures show that Δr_i changes very little. Accordingly, C_{60} possesses a quasi-spherical icosahedral structure with $\Delta r_i = 6.4 \times 10^{-4}$ (almost spherical), and can therefore be used as the first shell in an onion structure.

It is also important to note that, in the quasi-spherical particles, we have found that the distance between layers, 3.35 Å, is close to the value observed in graphite and onions. For our initial analysis we have neglected van der Waals interactions.

Our quasi-spherical onions are not more stable than the symmetrically faceted giant fullerenes on which we based our calculations, this is because the number of pentagonal rings in the symmetric arrangements is just 12 and in the quasi-spherical fullerenes there are more than 12, together with heptagonal rings. However, under the conditions of formation (high electron irradiation), quasi-spherical structures

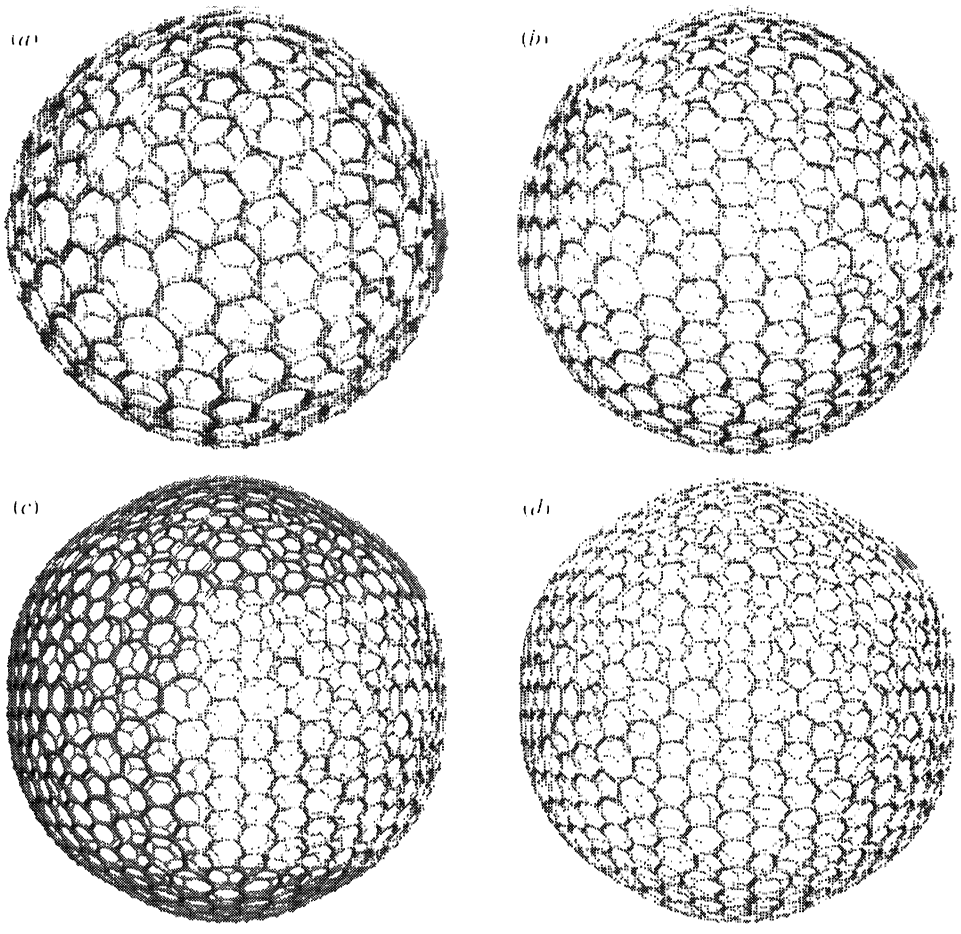

Figure 2. Quasi-spherical fullerenes with additional heptagonal and pentagonal rings: (*a*) D_{2h} C_{540} with 76 pentagons and 64 heptagons (non-cubic, non-icosahedral); (*b*) ico C_{888}-A with 60 heptagons and 72 pentagons (with traces of icosahedral symmetry); (*c*) ico C_{1500}-A with 132 pentagons and 120 heptagons (icosahedral I_h); (*d*) ico C_{1020}-B with 132 pentagons and 120 heptagons (icosahedral I_h symmetry).

appear to be preferred. A 'perfect' set of nested icosahedral cages would follow a predetermined sequence of sizes e.g. 60, 240, 540, 960, 1500, ..., etc. An interesting result from this analysis suggests that real quasi-spherical onions are not likely to be restricted in this way.

3. Nanotubes

In 1991, Iijima observed carbon nanotubes in the deposit formed on the cathode by the carbon arc discharge method used for bulk fullerene generation. Nanotubes consist of needle-like concentric structures. Two main growth mechanisms have been proposed for the formation of these nanotubes. The first (Iijima *et al.* 1992*a*, 1993) states that carbon atoms attach themselves to the edges of a growing carbon cylinder which closes when conditions are not suitable for growth. An alternative scheme (Endo & Kroto 1992) proposed that nanotubes are essentially elongated

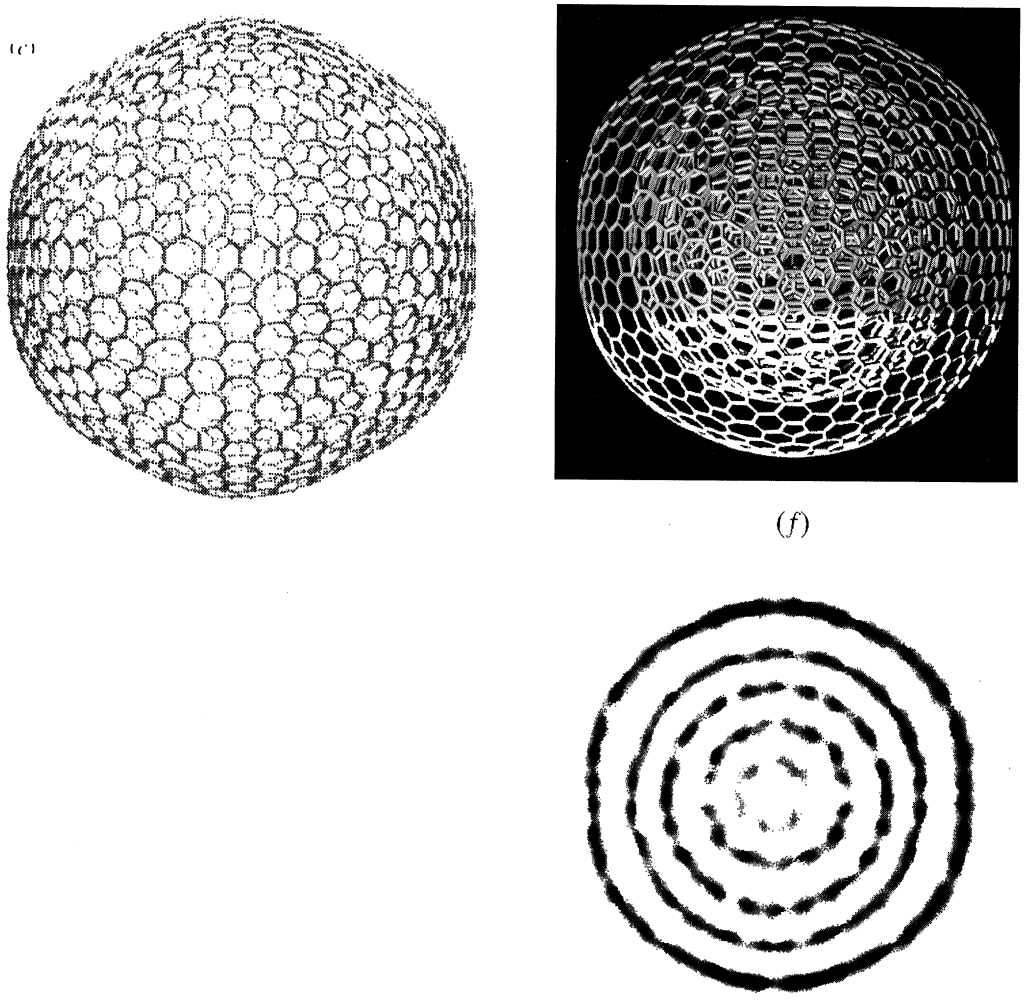

Figure 2. Quasi-spherical fullerenes with additional heptagonal and pentagonal rings: (*e*) ico C_{1620}-B (with traces of icosahedral symmetry) containing 192 pentagons and 180 heptagons; (*f*) nested quasi-spherical fullerenes made by introducing heptagonal and pentagonal carbon rings (along C_2 axes). The onion (top) and HRTEM simulation (bottom) are composed of C_{60}@C_{240}@D_{2h} C_{540}@C_{888}-A@C_{1500}-A.

giant fullerenes which grow by direct insertion of carbon species, accreted from the vapour phase, into the closed network.

It has recently been found that if hydrogen is used as a buffer gas in arc discharge experiments, the formation of C–H bonds at the point of tube growth inhibits the nanotube closure (Wang *et al.* 1995). This result supports the open-ended mechanism proposed by Iijima.

In addition to the arc discharge experiment or the Krätschmer–Huffman reactor, pyrolysis of hydrocarbons (e.g. benzene, acetylene, naphthalene, ethylene, etc.) in the presence of catalysts (e.g. Co, Ni and Fe) provides another route to fullerenes and carbon nanotubes. Before the discovery of fullerenes, pyrolytic nanofibres–nanotubes were actually observed by several authors (Endo *et al.* 1987; Dresselhaus *et al.* 1988).

Table 1. *Energy per atom relative to graphite, mean radius of the fullerene and the difference* Δr_i *of the largest and the shortest distance to the centre of mass of the fullerene*

structure	energy/atom (eV)	mean radius (Å)	Δr_i (Å)
C_{60} (I_h)	−0.6600	3.643	6.4×10^{-4}
C_{70} (D_{5h})	−0.6071	3.912	0.647
C_{240} (I_h)	−0.3136	7.253	0.198
C_{540} (I_h)	−0.1748	10.860	0.774
C_{960} (I_h)	−0.0987	14.440	1.570
C_{1500} (I_h)	−0.0631	18.014	2.415
D_{2h} C_{540}	−0.5591	10.962	0.492
ico C_{888}-A	−0.3648	14.008	0.699
ico C_{1020}-B	−0.5952	15.067	0.159
ico C_{1500}-A	−0.5539	18.201	0.591
ico C_{1620}-B	−0.5938	18.939	0.976

The growth mechanism was accounted for in terms of a metal (catalyst) particle, which was held to be responsible for the agglomeration of carbon and the subsequent axial growth of the fibre. The resulting tubules can be bent, curled or straight depending upon reaction conditions.

In the following sections we will discuss from the theoretical and experimental standpoint new types of graphitic structures formed by arc discharge and by pyrolysis. First, we consider the nature of nanotubes, and how the presence of odd-membered rings (pentagons and heptagons) may influence the electronic properties.

(*a*) *Straight nanotubes*

Carbon nanotubes consist of concentric hexagon-rich cylinders, made up of sp^2 hybridized carbon as in graphite, terminated by end-caps arising from the presence of pentagons. It is possible to construct a cylinder by rolling up a hexagonal graphene sheet in different ways, thereby creating tubes of various array geometries. Two of these are 'non-helical' because the graphite lattices at the top and the bottom of the tube are parallel. These arrangements are called 'armchair' and 'zig-zag'. In the armchair structure two C–C bonds of each hexagon are perpendicular to the tube axis, whereas in the zig-zag arrangement, two C–C bonds of each hexagon are parallel to the tubule axis (figure 3*a*, *b*). In all other conformations the C–C bonds in general lie at an angle to the tubule axis and a helical structure results (figure 3*c*, *d*).

Theoretical calculations indicate that the electronic properties for a single-walled nanotube will vary as a function of its diameter and helicity (Saito *et al.* 1992*a*, *b*; Hamada *et al.* 1992). The studies suggest that the behaviour ranges from semiconductor to metallic conductor, giving rise to the possibility of new interesting applications in solid-state chemistry and the development of nanoscale electronic devices.

(*b*) *Nanotube caps*

Two main factors distinguish carbon nanotubes from pyrolytic carbon fibres. First, the diameters and lengths of carbon fibres are one or two orders of magnitude greater than those of carbon nanotubules. Second, whereas nanotubes are invariably concen-

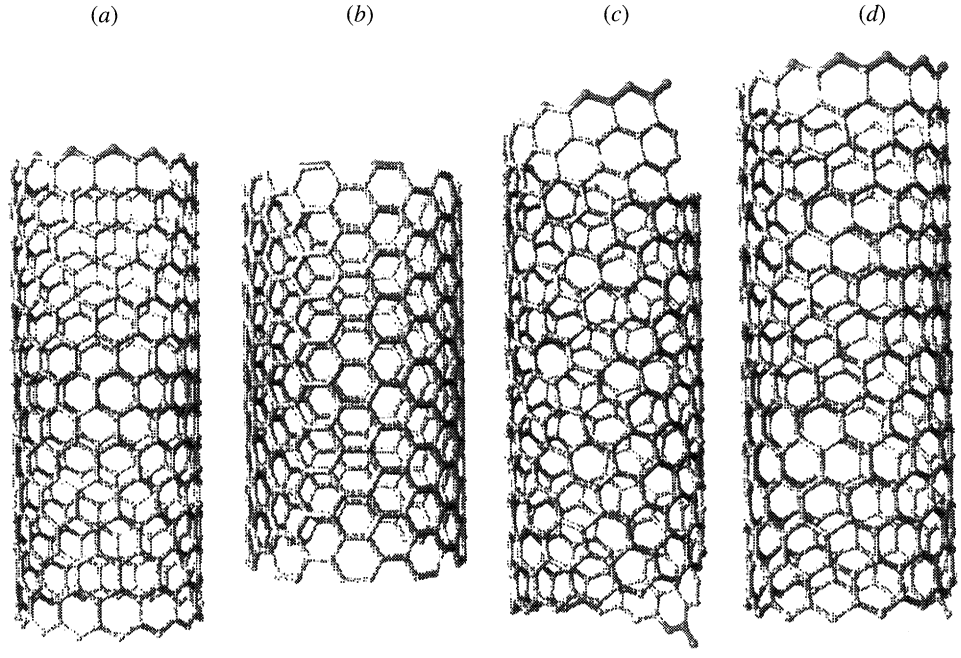

Figure 3. Simulated single-walled nanotubes with different helicities: (*a*) zig-zag arrangement; (*b*) armchair configuration; (*c*) and (*d*) two different helicities.

tric, pyrolytic carbon fibres (although sometimes concentric) often contain graphite-type layers distributed radially and oriented along the fibre axis. The nature of the pyrolytic fibre depends critically on the heat treatment and production technique (Dresselhaus *et al.* 1988, p. 16). It is noteworthy that the nanotube interlayer spacing is always *ca.* 3.4 Å, whereas pyrolytic carbon fibres exhibit a spacing in the 3.3–3.6 Å range (Dresselhaus *et al.* 1988, p. 52).

Nanotube end-caps can provide a rationale for the growth and helicity of the tube. C_{60} (Kroto *et al.* 1985), giant fullerenes (Kroto & McKay 1988) and nanotubes (Iijima *et al.* 1992*a*) require pentagons in order to achieve closure. Further to the comments in § 2, six pentagons (regularly or randomly distributed) are necessary and sufficient to bring about closure of one end of the nanotube. Energetically, these caps are expected to be reactive. Proof of this is provided by oxidation studies, which take place at *ca.* 750 °C in air or oxygen (Ebbesen *et al.* 1994), causing an axial oxidation starting from the tips. Figure 4 shows different types of nanotube caps and their associated morphology, depending upon the pentagonal arrangement within the cap.

(*c*) *Bent nanotubes*

Transmission electron microscope (TEM) images from the inner-core cathode deposit produced in the arc experiment under normal conditions (100 A, 20 V and 500 Torr He pressure) show the existence of 30°-bent nanotubes (figure 5). Theoretically, these bends are possible as a result of pentagon insertion (outer rim with positive curvature) coupled with inclusion of a heptagon (inner rim with negative curvature) on opposite sites of the tubule.

We believe that the appearance of these bent structures is due to changes during the experiment (e.g. current, He pressure, separation between graphite rods, etc.). In other words, when nanotube growth conditions are interrupted, growth may be

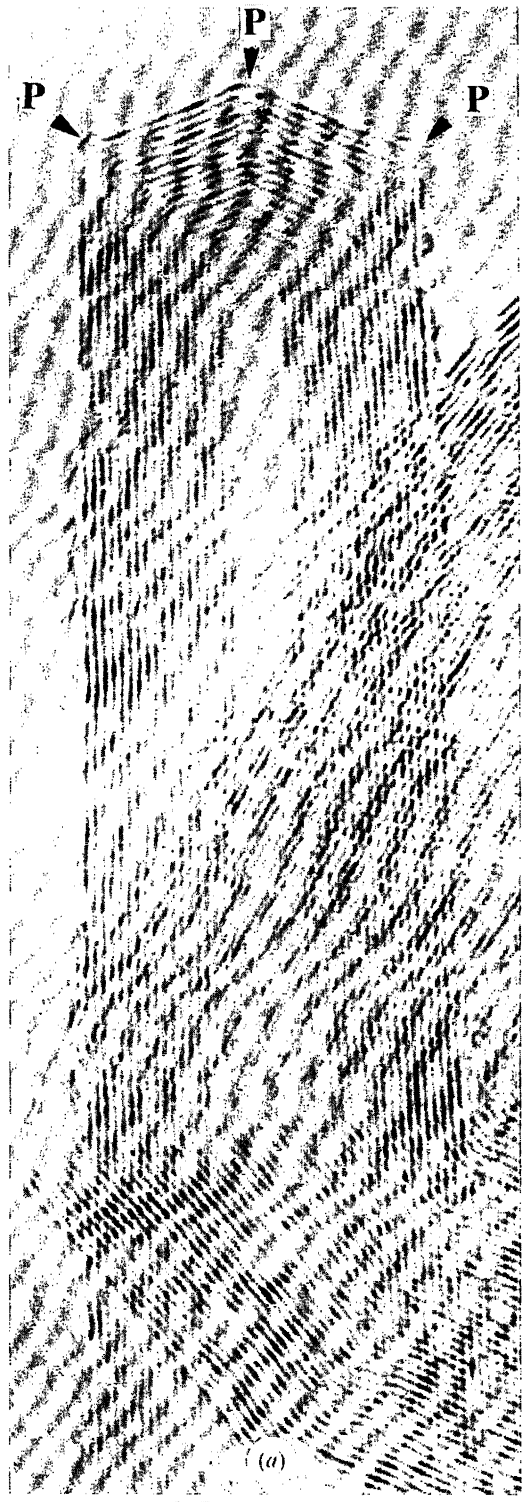
P
P
P
(a)

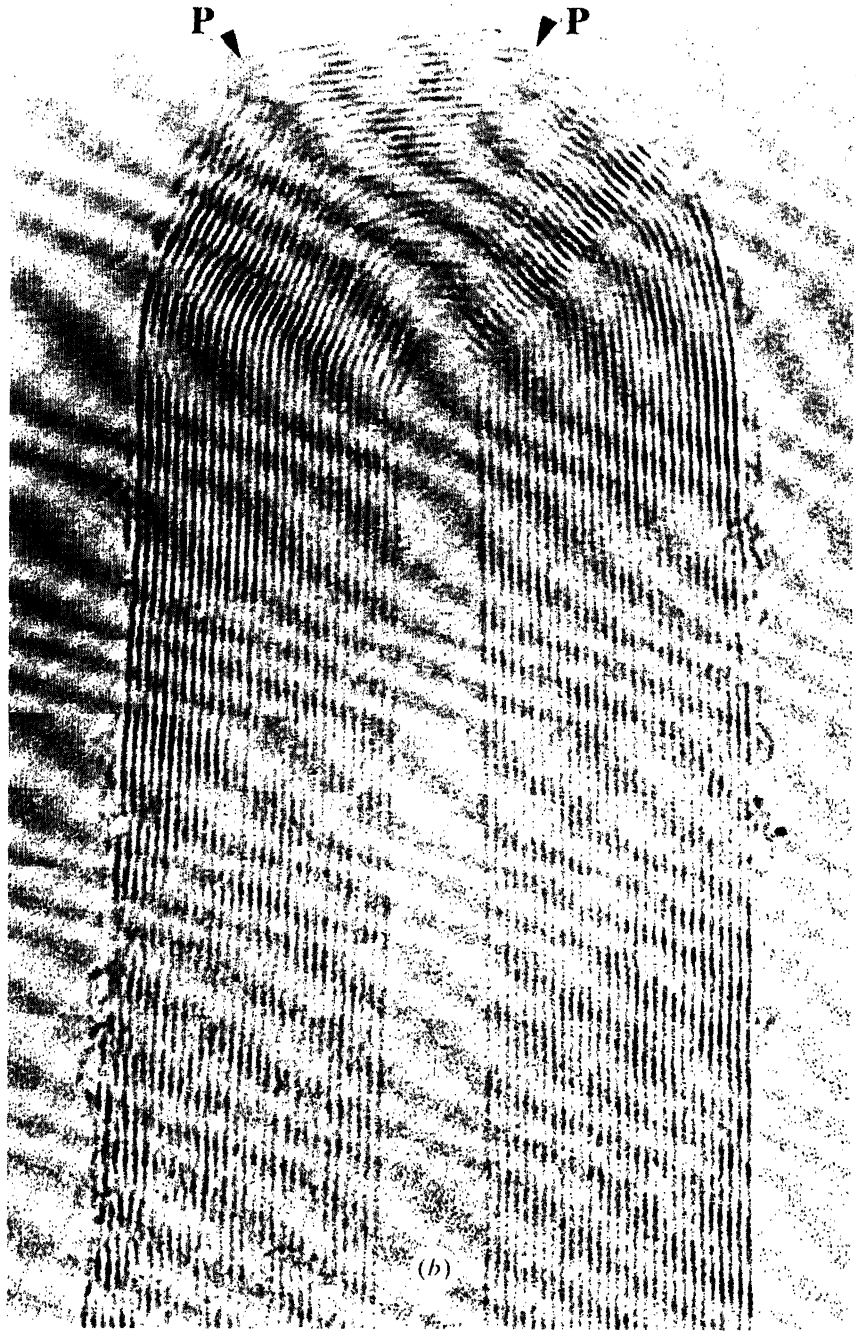

Figure 4. Various types of nanotube caps with different morphologies. **P** denotes likely pentagon sites while **H** denotes likely heptagon regions: (*a*) and (*b*) hemispherical caps where the pentagons are chirally distributed.

temporarily or permanently inhibited. This type of quenching effect is thought to be important in creating defective graphitic structures.

It is also clear from TEM images that tube diameters change when a bend oc-

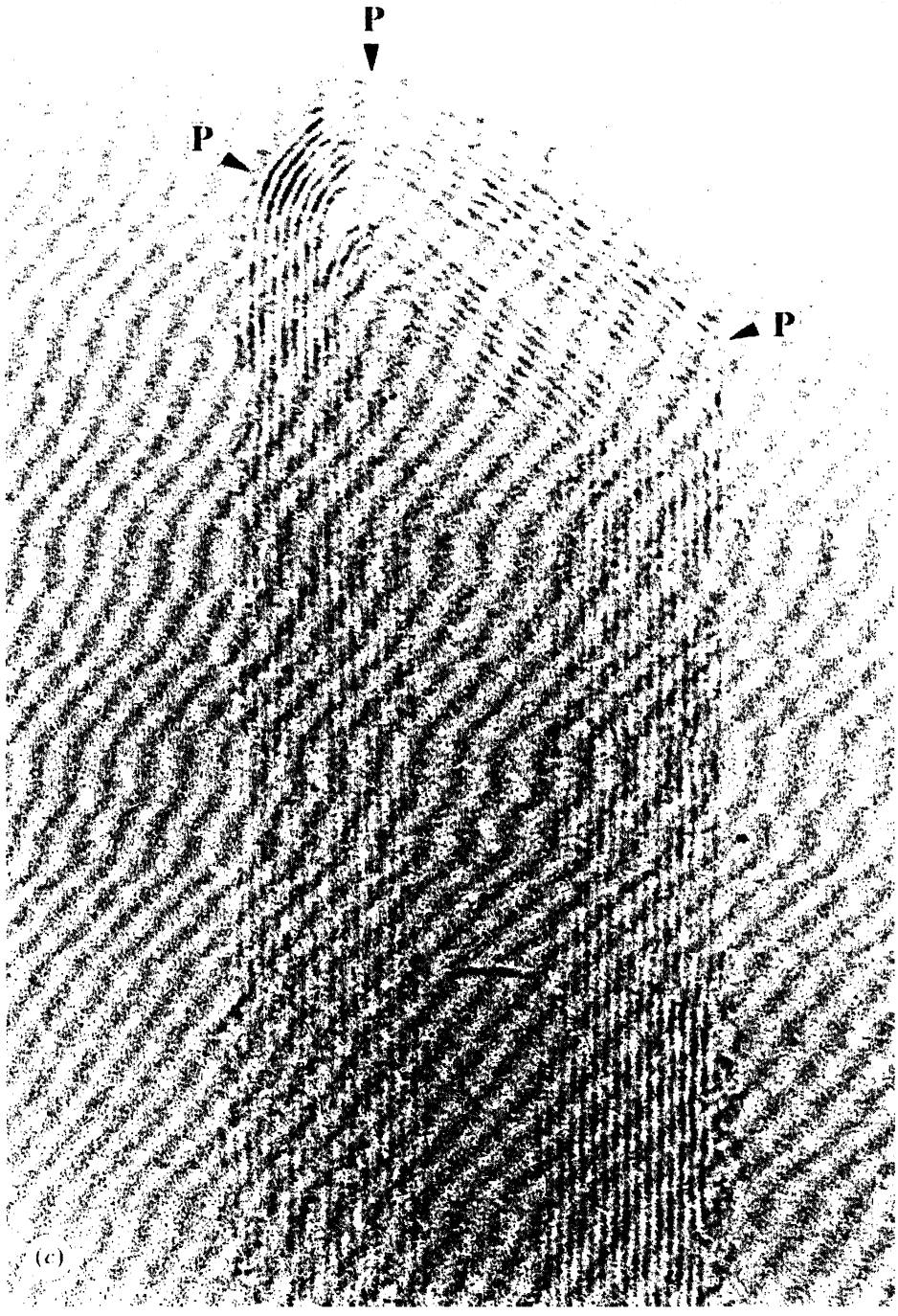

Figure 4. Various types of nanotube caps with different morphologies. **P** denotes likely pentagon sites while **H** denotes likely heptagon regions: (*c*) triangular cap with different pentagon distribution.

curs (figure 6*a*), suggesting that the pitch is also changing due to the inclusion of heptagon–pentagon arrangements (see figure 6*b*). According to theory (Saito *et al.* 1992*b*; Dunlap 1994) and some selected area electron diffraction patterns (SAEDP),

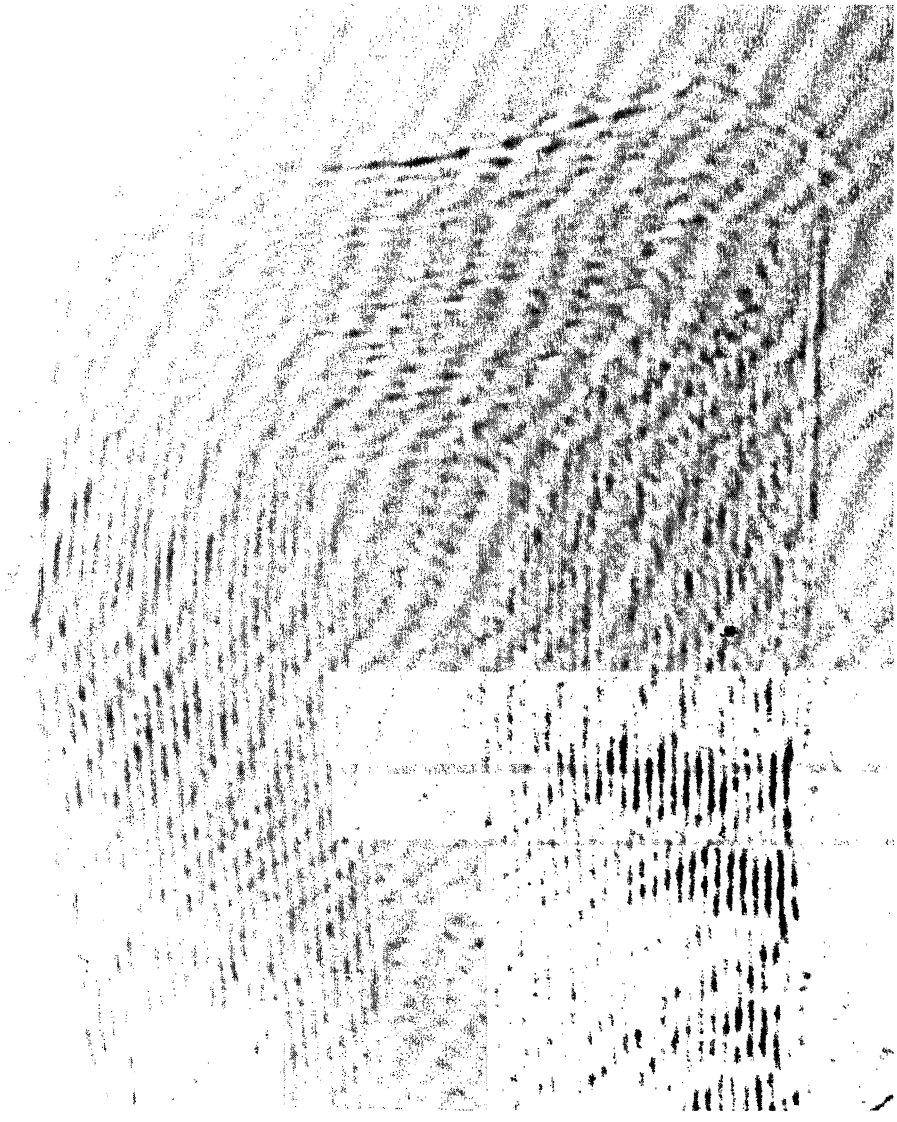

Figure 4. Various types of nanotube caps with different morphologies. **P** denotes likely pentagon sites while **H** denotes likely heptagon regions: (*d*) square cap.

helicity changes of 30° (figure 7) may cause significant changes in the electronic properties (e.g. from metallic conductor to semiconductor). Figure 6*b* shows that a bend can transform a zig-zag configuration into an armchair arrangement. Note that the heptagon–pentagon pair is responsible for the 30° helicity change. The heptagon and pentagon are expected to oppose one another. If this arrangement is not followed the bend becomes less stable with a different angle.

For the helical tubes, if we produce a 30° bend, changes in diameter and helicity occur. Consequently, differences in the electronic properties are possible. By observing bent nanotube caps it is possible to suggest a relationship between the helicity of the tube and the cap shape by invoking different growth velocities around the tube end. For instance, if velocities are identical on every part of the tube, a non-helical

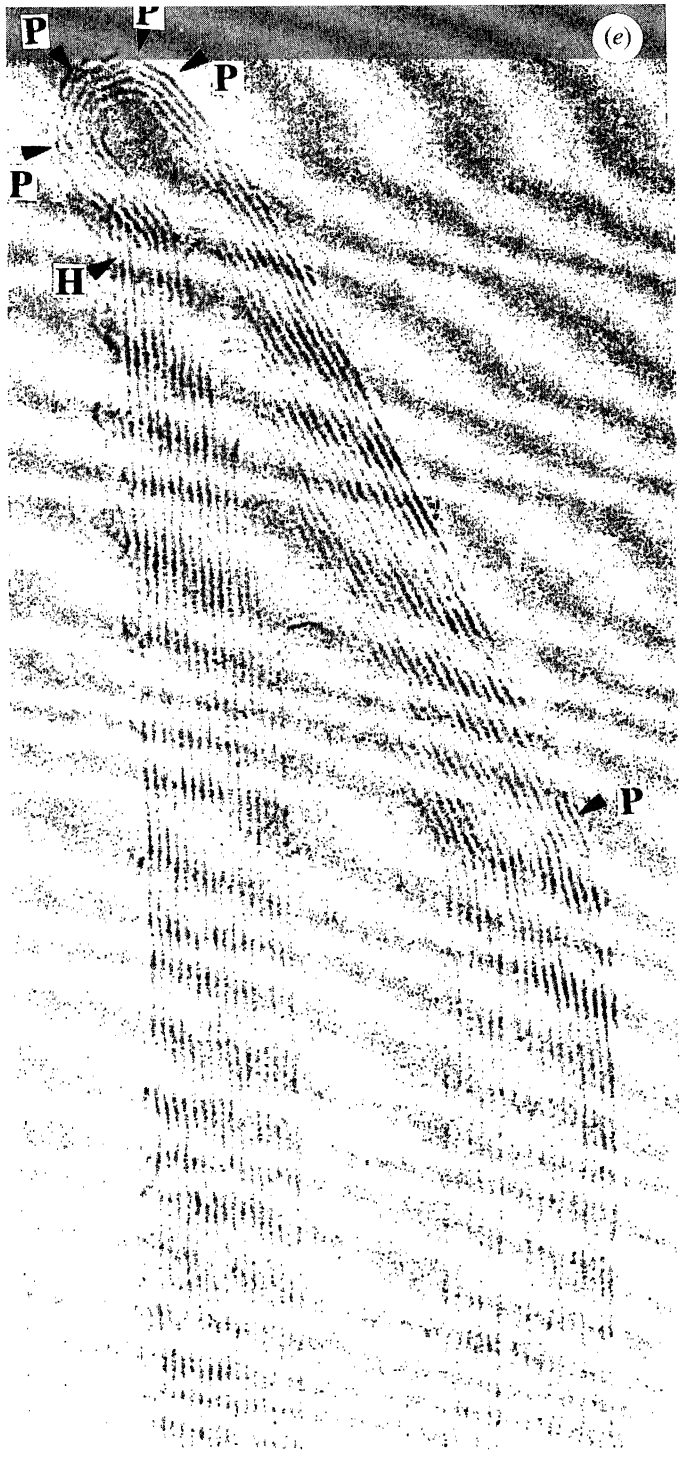

Figure 4. Various types of nanotube caps with different morphologies. **P** denotes likely pentagon sites while **H** denotes likely heptagon regions: (*e*) cap showing negative curvature due to the insertion of heptagons and pentagons. In this image, the 30°-pentagon declination (right-hand bend) cancels the 30°-heptagon inclination (left top bend), ending with six pentagons at the final tip with a hemispherical cap, thus following Euler's Law.

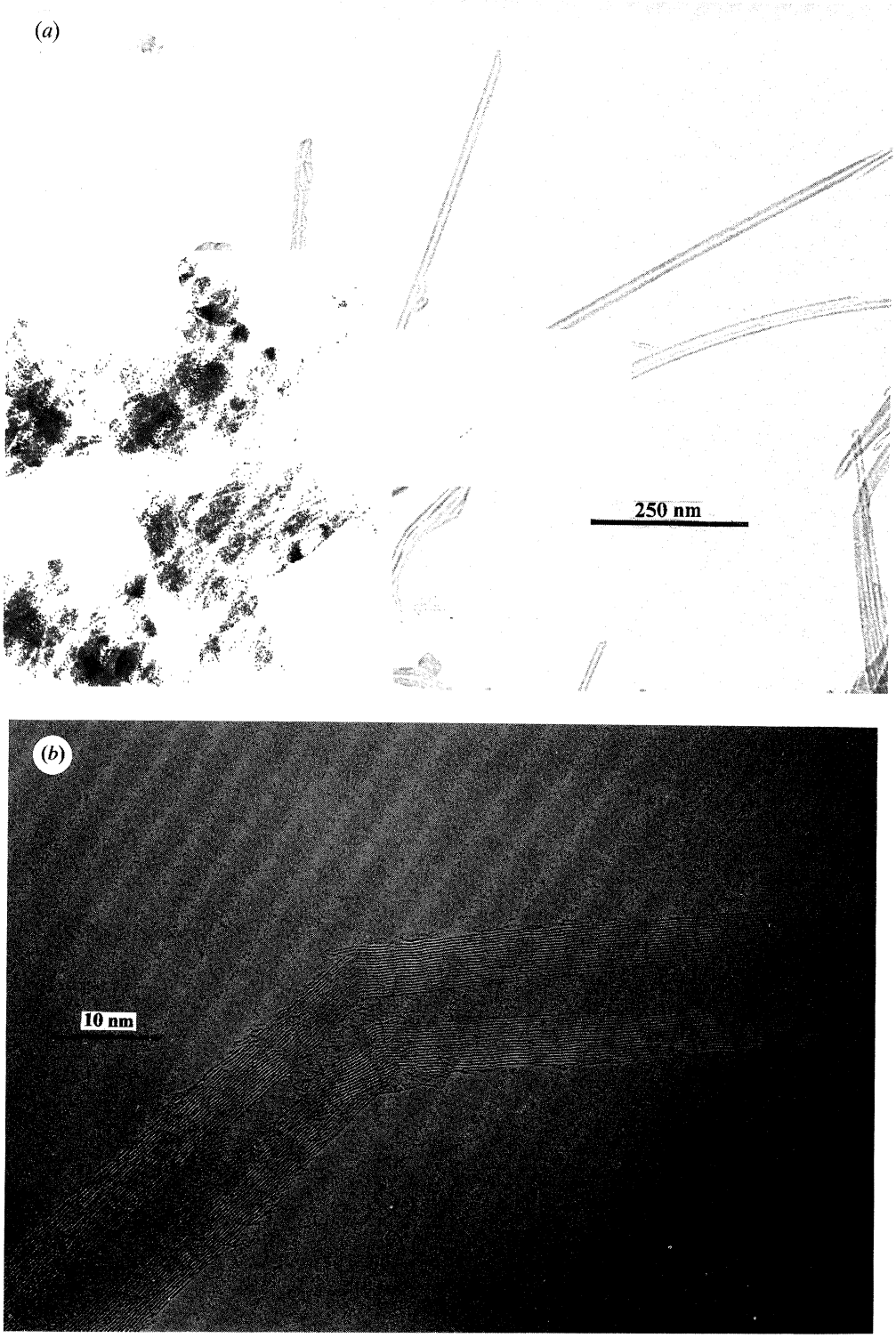

Figure 5. TEM images showing 30°-bent nanotubes: (*a*) low resolution; (*b*) HRTEM of a 30°-bent nanotubes showing some defects and fractures at the bend.

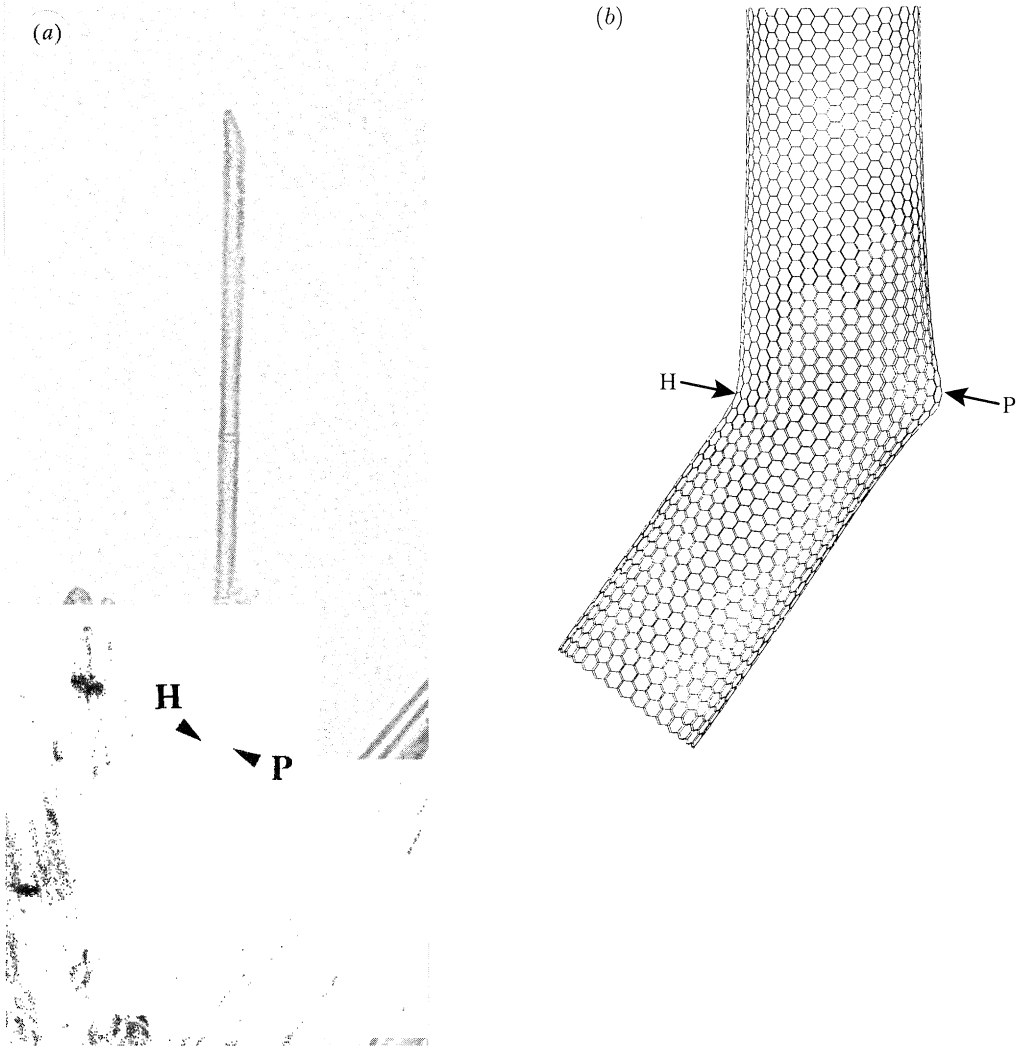

Figure 6. Real 30°-bent nanotube and its possible simulation: (*a*) close-up at the bent nanotube shown in figure 5*a*; (*b*) simulation showing the change in helicity by 30° (from zig-zag to arm-chair) giving up the possibility to have two different electronic properties (e.g. semicondutor and metallic-conductor). In both images a difference in diameters after and before the bend is observed.

tube pitch with a hemispherical cap may result (figure 4*a*, *b*). If the velocities are different, the tubules are likely to posses a helical pitch with a triangularly shaped end cap (figure 4*c*, *e*), possibly with one of the six pentagons necessary for closure, residing offset, in the fast velocity region.

(*d*) *Helix-shaped nanotubes*

Helicoidal graphites (corkscrew-like nanotubes) consisting of arrangements of hexagonal, pentagonal and heptagonal carbon rings (figure 8*a*) were first proposed by Ihara *et al.* (1993). Such fascinating structures have actually been observed among the products of acetylene pyrolysis using a cobalt catalyst (Zhang *et al.* 1994; Amelinckx *et al.* 1994). In these experiments the catalytic particle plays an important role in

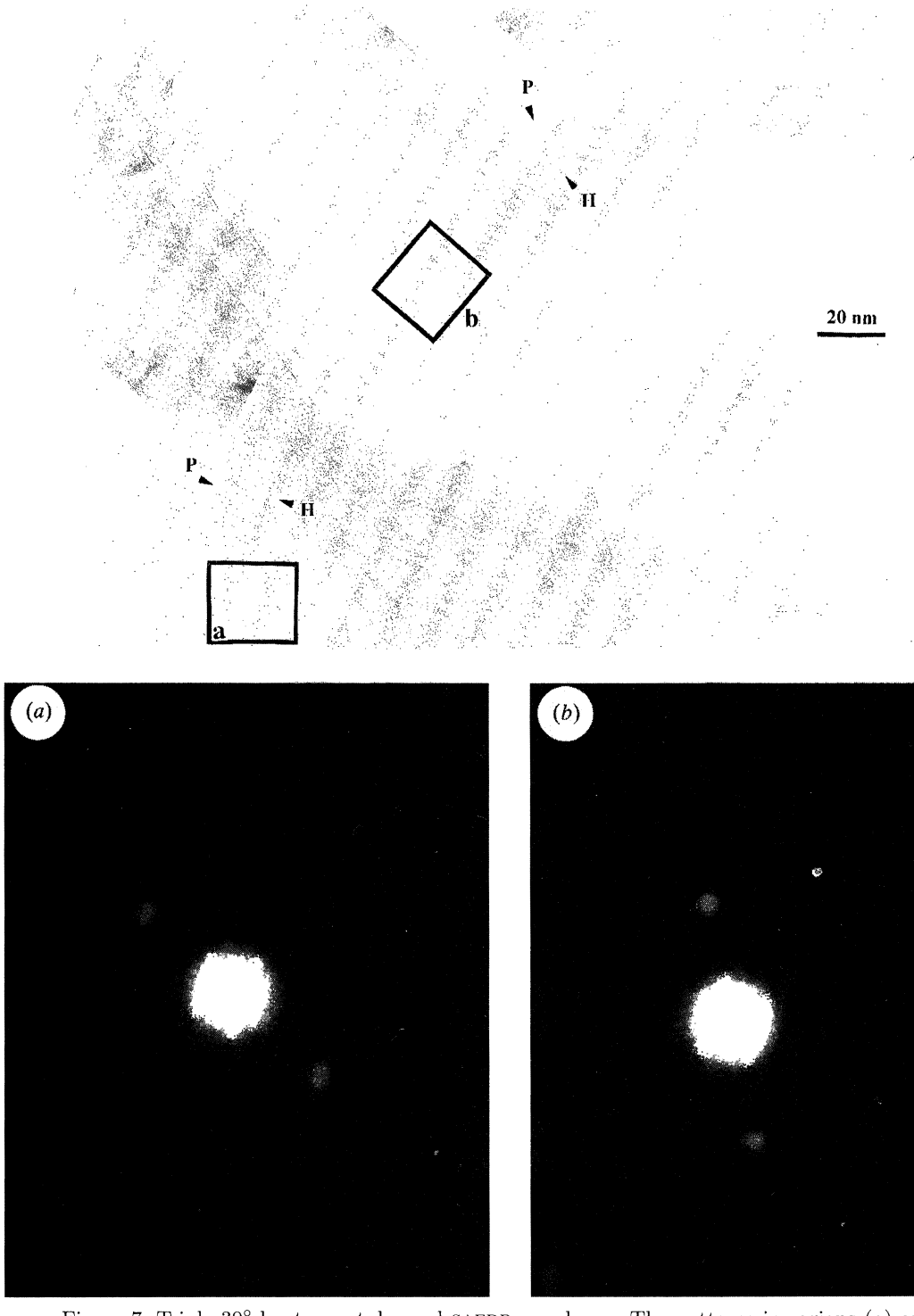

Figure 7. Triple 30°-bent nanotube and SAEDP are shown. The patterns in regions (*a*) and (*b*) show that helicity changes by 30° after and before the bend. This may imply a change in the electronic structure due to the insertion of the pentagon–heptagon pair.

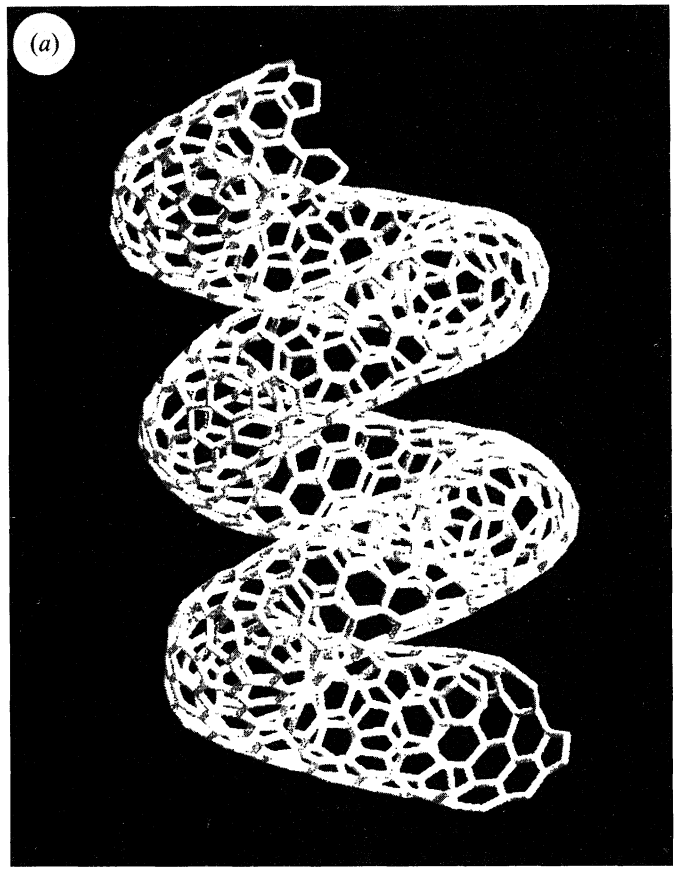

Figure 8. Helicoidal graphite: (*a*) simulated single-wall corkscrew-shaped carbon nanotube produced by interspersing five- and seven-membered rings judiciously within the mainly hexagonal network wall.

the nanotube growth, since the accretion of carbon atoms appears to occur on the metal surface. It is also likely that the growth velocities depend on the surface structure of the exposed area of the catalytic particle. As a result, different wall growth rates arise which may be responsible for the bent structures (e.g. spirals and helices, see figures 8*b*–*e*. These observed helices are multiwalled and complex. However, the simple archetypal single-wall helix (Ihara *et al.* 1993; Kroto *et al.* 1994) is still a hypothetical structure.

Electron diffraction studies on these coiled nanotubes reveal the presence of successive offset 30° bends at regular intervals, which causes the tube to coil systematically (Amelinckx *et al.* 1994; Zhang *et al.* 1994; Bernaerts *et al.* 1995). Recent theoretical calculations on archetypal helices suggest that these structures may possess superconducting or semi-metallic properties, determined by the distributions of five- and seven-membered rings (Akagi *et al.* 1995). The synthesis of such 'perfect' helicoidal graphite crystals and their use in nanoengineering and electronics represents a challenge for the future.

(*e*) *Toroidal and hemitoroidal nanofibres*

Another negatively curved surface is embodied in the torus. Low strain tori can be generated by an appropriate combinations of heptagons, hexagons and pentagons.

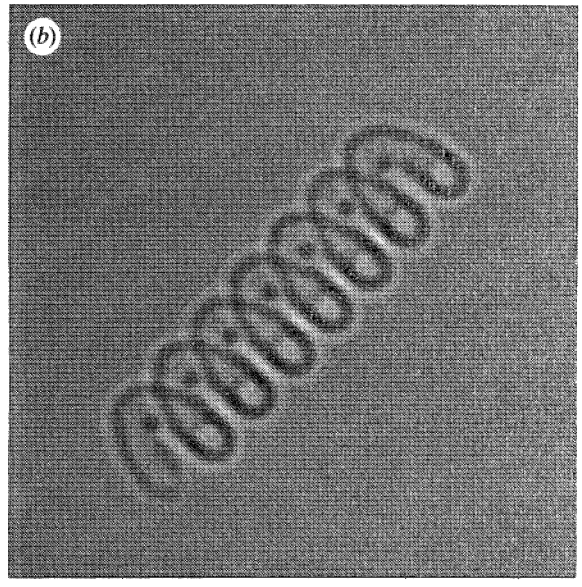

Figure 8. Helicoidal graphite: (*b*) HRTEM simulation from the helix-shaped single wall nanotube represented in 8*a*.

In this case, because the topology is not that of a closed polyhedron, the generalized Euler's law states that the numbers of pentagons and heptagons are equal, and may be zero (Terrones *et al.* 1995*a*); see figure 9*a*.

Hemitoroidal nanotube tip structures (axially elongated concentric doughnuts) have been produced by passage of an arc between graphite rods (Iijima *et al.* 1992*a*; Terrones *et al.* 1995*b*) (figure 10*c*). In addition, the formation of hemi-toroidal linked structures between adjacent concentric walls in pyrolytic carbon nanotubes have been observed and discussed in detail (Sarkar *et al.* 1995; Endo *et al.* 1995). These structures appear to form as a result of optimal graphitization of two or more adjacent concentric graphene tubules (figure 9*b*).

Figure 10*a* shows a molecular model of a hemitoroidal nanotube tip, where negative curvature is produced by the introduction of heptagons. Pentagons are also necessary in order to balance curvature and achieve low strain closure of the adjacent tubes around their periphery. Figure 10*b* shows a HRTEM simulation of the model and figure 10*c* is a real structure observed in the arc discharge. These were produced by inserting hexagonal boron nitride into the graphite anode (see later). The growth mechanism for these hemitoroidal structures remains unclear. It is noteworthy that the arrangement for these 'sock-like' (inwardly folded) structures can be seen as cauterised rim-seals, which link the inner or the outer tubes, thereby avoiding dangling bond reactivity (Sarkar *et al.* 1995). These structures can be thought of as concentric growing nanotubes which have been forced into U-turns in order to generate a more stable graphene configuration. Because of the insertion of non-hexagonal rings, electronic properties for these structures may well diverge from those of conventional nanotubes.

4. Spheroidal graphitic iron (SGI)

Cast irons are essentially iron-carbon alloys or more correctly (Fe–C–Si) alloys containing important, but small, amounts of S, Na and P. Moreover, ductile, nodular

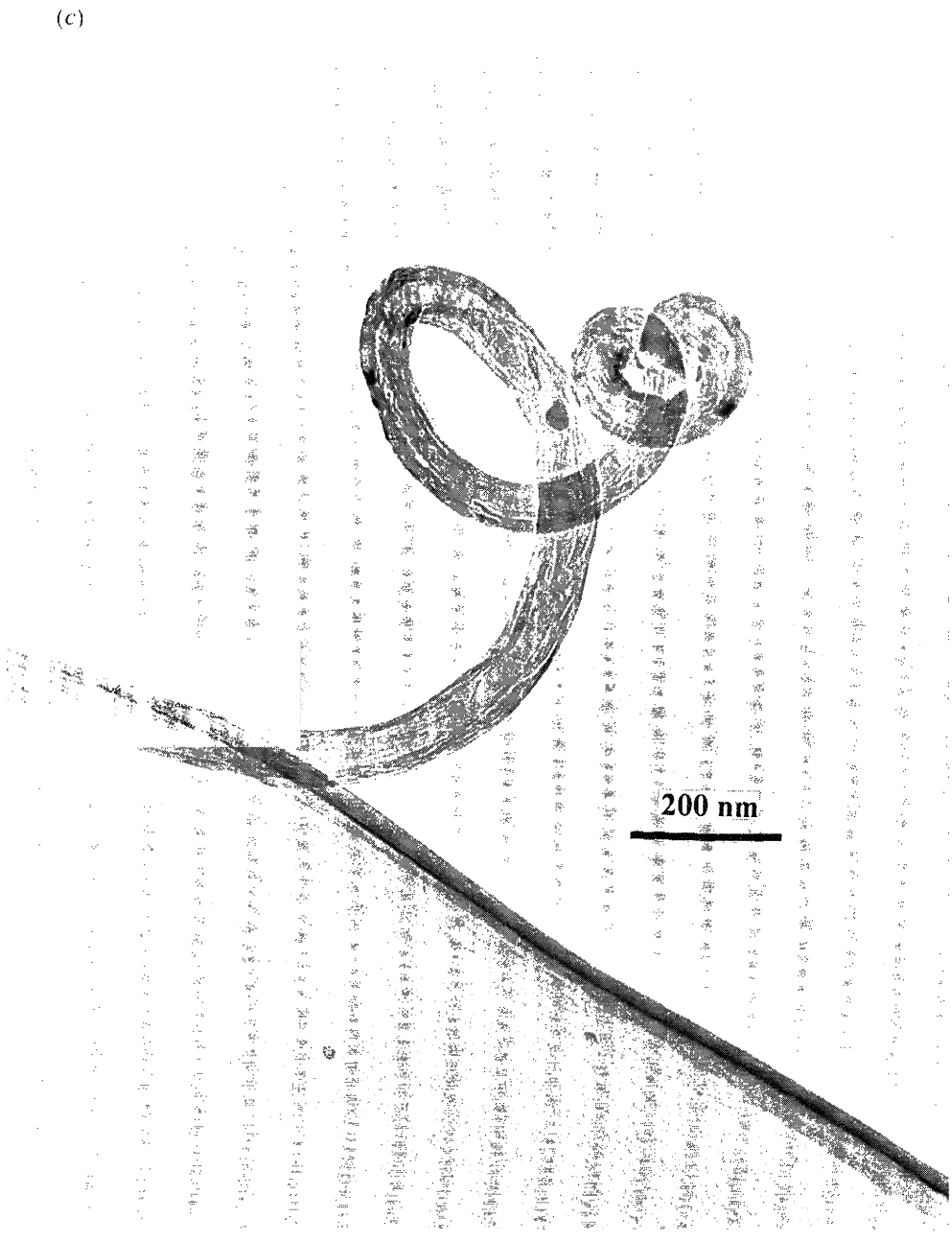

Figure 8. Helicoidal graphite: (*c*) helical nanotube found in acetylene pyrolysis using Co powder as a catalyst at around 800 °C.

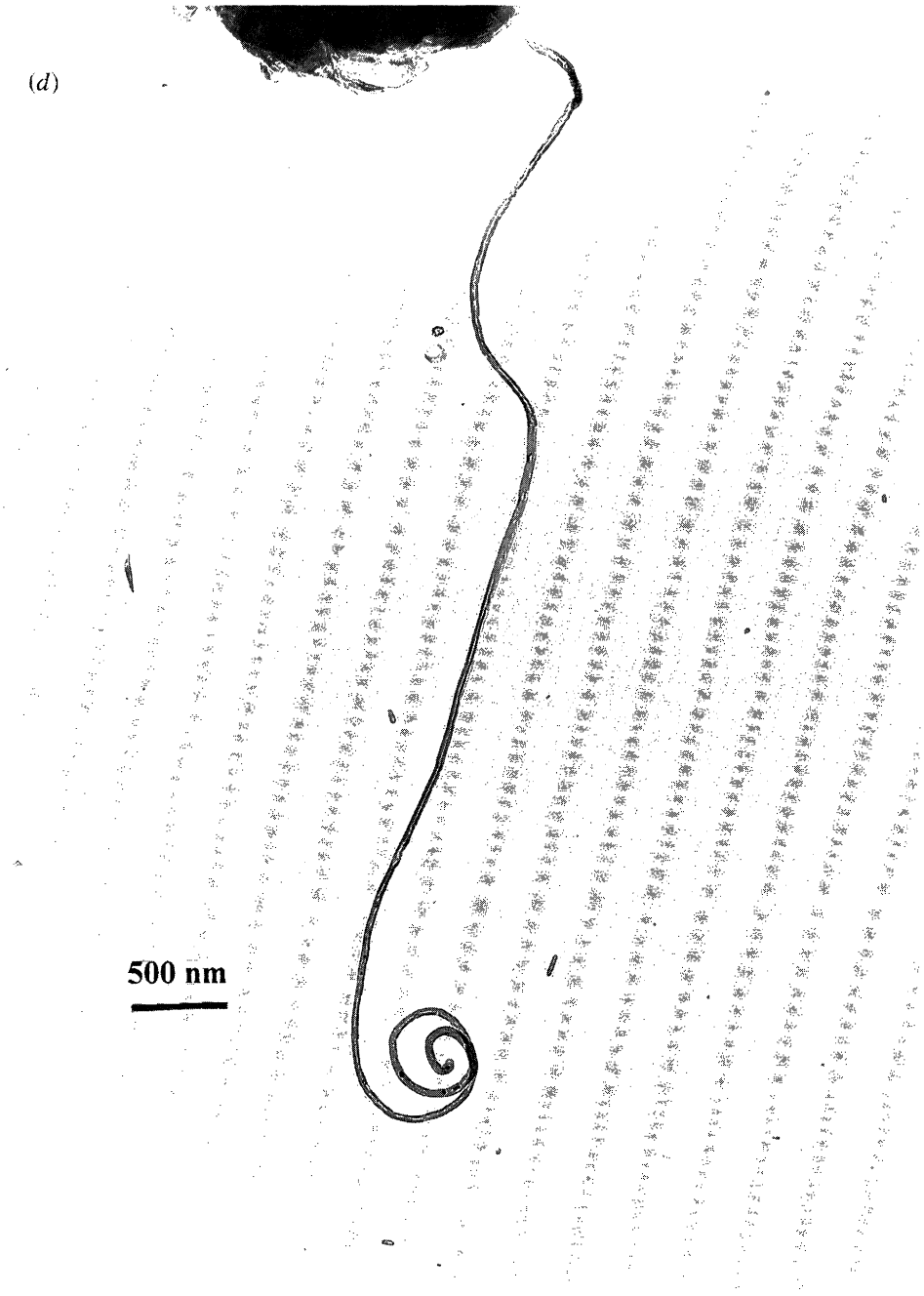

Figure 8. Helicoidal graphite: (*d*) spiral multiwalled nanotube also produced in acetylene pyrolysis with the same conditions as in figure 8*c*.

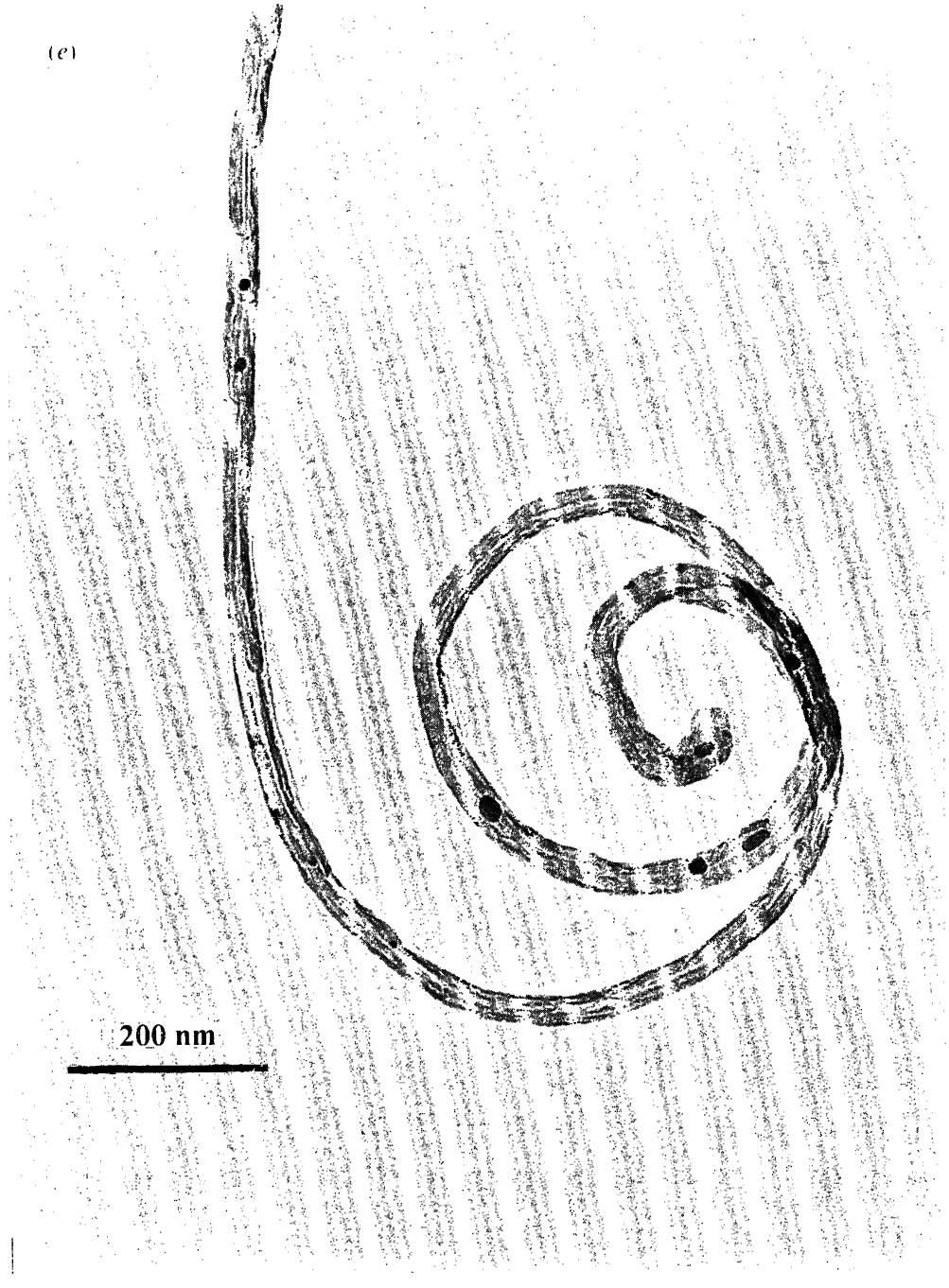

Figure 8. Helicoidal graphite: (*e*) spiral multiwalled nanotube also produced in acetylene pyrolysis with the same conditions as in figure 8*c*.

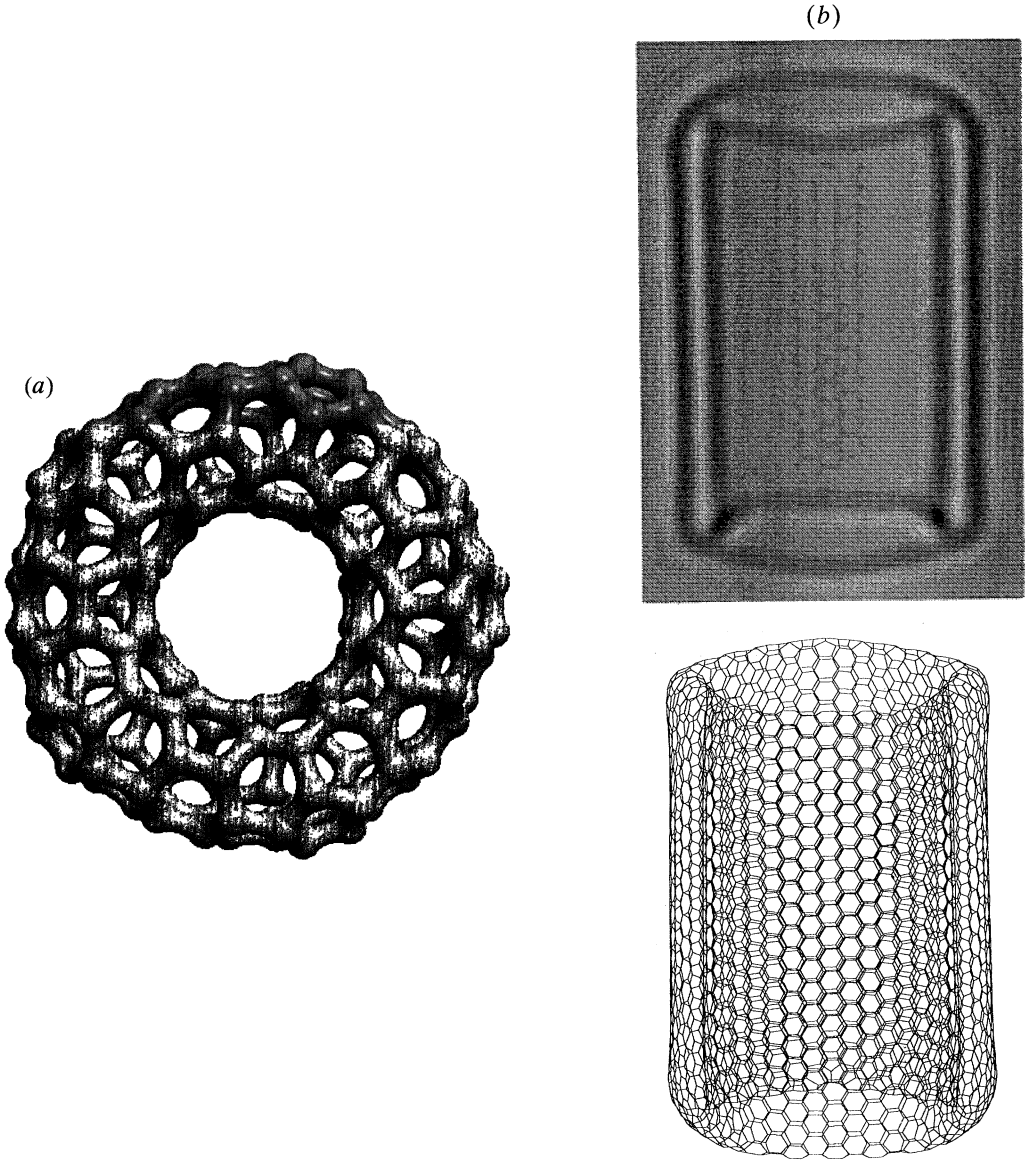

Figure 9. Toroidal graphite: (*a*) doughnut-like structure, where the heptagons are present in the inner rim and the pentagons on the outer rim; (*b*) an elongated doughnut and its HRTEM simulation are presented. The latter image is believed to exist in pyrolytic nanotubes heated at high temperatures (Sarkar *et al.* 1995; Endo *et al.* 1995).

or spheroidal cast iron consists of a high carbon containing iron-based alloy, in which the graphite is present in compact spheroids (SGI) rather than flakes (needle-like graphitic structures). It is noteworthy that in ordinary cast iron, graphite occurs as 'flakes'.

SGI was discovered by Morrogh & Williams (1948), who added Ce and Mn to iron (e.g. a typical spheroidal base iron composition is 3.7% Ce, 2.5% Si, 0.3% Mn, 0.01% S, 0.01% P and 0.04% Mg) (Elliot 1988, p. 13). Spheroidal graphite irons are inferior to flake irons with respect to physical properties such as thermal conductivity,

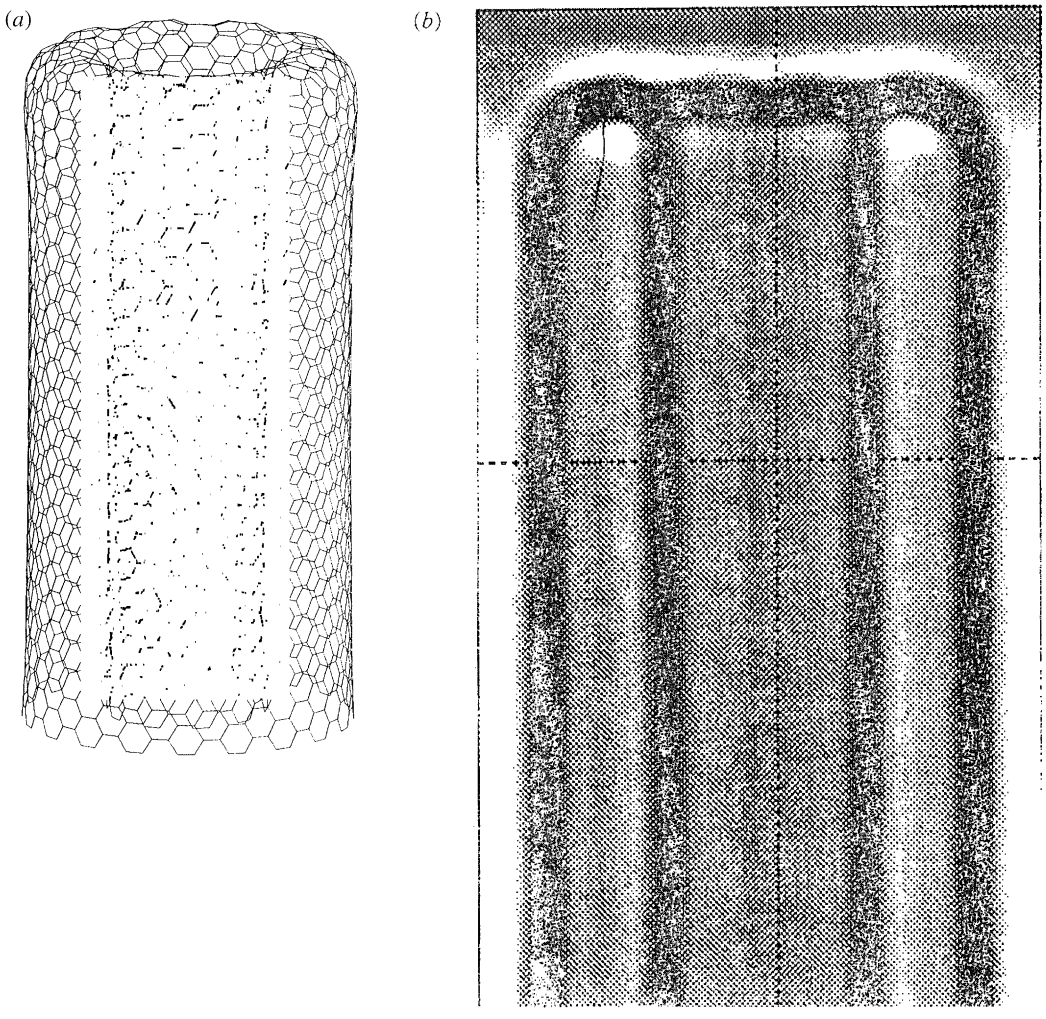

Figure 10. Hemitoroidal nanotube cap 'sock-like' (inwardly folded) structure. (*a*) Simulated structure consisting of two concentric nanotubes joint together from their top rims (inner and outer, respectively); (*b*) HRTEM simulation of the single-wall hemitoroidal structure represented in (*a*).

but exhibit much better mechanical properties. Therefore, SGI is widely used in the construction industry.

The spheroids generated in these irons resemble concentric layers of star-shaped graphitic structures (Karsay 1976, p. 24) similar to concentric giant fullerenes (Iijima 1980; Ugarte 1992; Harris *et al.* 1994). A molecular model can be built by refining a graphene shell structural concept, introducing areas of negative curvature (Mackay & Terrones 1991) by inserting heptagonal rings into an icosahedral giant fullerene (figure 11).

The spheroidal shape in SGI irons may be due to the presence of foreign particles (spheroidizer elements), which act as nuclei causing the graphite to grow, at an angle perpendicular to the basal plane and at the same rate in every direction, creating a sphere or a star-shaped particle. This proposed growth mechanism (Karsay

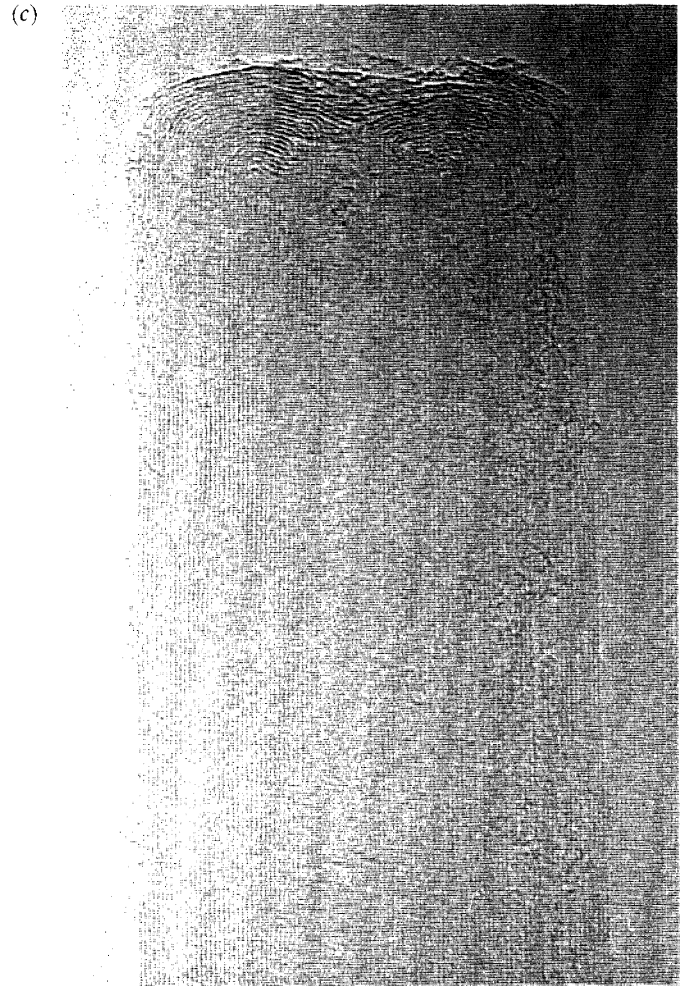

Figure 10. Hemitoroidal nanotube cap 'sock-like' (inwardly folded) structure. (*c*) Hemitoroidal nanotube cap found from the cathode deposit using hexagonal BN in the anode during the arc-discharge experiment. It is noteworthy that the simulated and the real images are in good agreement.

1976, p. 16) is similar to the one advanced for catalytically grown single carbon nanotubes and encapsulated particles using Ni and Co (Saito *et al.* 1994). A second growth mechanism, noted in Karsay (1976, p. 17), states that graphite spheroids start growing from a graphitic flake. If the branching frequency is low, graphite flakes form, but if it is high (due to the presence of spheroidizer) branches overlap one another generating spheroidal shapes. A third mechanism, known as the 'phase boundary' or 'bubble theory' (Karsay 1976, p. 20), proposes that the surface of large CO bubbles, formed by the reaction of SiO_2 and carbon, become partly covered by a thin layer of graphite. The nascent graphite surface absorbs the CO gas, then the bubble collapses resulting in an irregular group of graphite flakes with some unspecified orientation. The latter have, as yet, been studied insufficiently to indicate how SGI really grows.

The similarity in production conditions among graphitic structures in SGI, hydrocarbon pyrolysis and the arc–plasma generator makes it feasible to observe onion-like

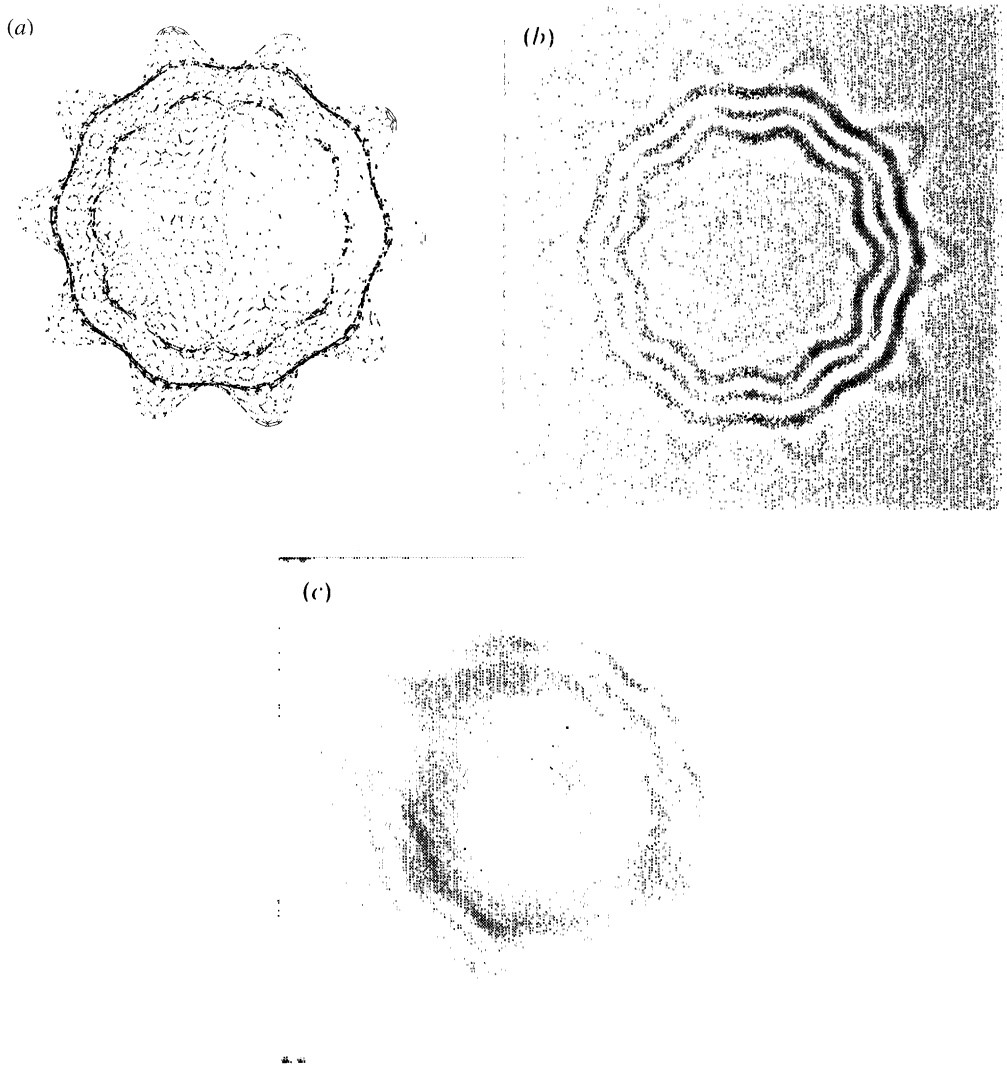

Figure 11. (*a*) Molecular model image of a three-dimensional star-shaped fullerene in which seven and five-membered rings are interspersed to produce negative as well as positive curvature in such a way that blisters occur in the surface; (*b*) and (*c*) HRTEM simulations for three concentric star-shaped fullerenes with different defocus conditions.

structures as well as nanotubes in cast irons. Their growth mechanisms may be similar in some respects and more studies are needed in order to understand the effect of impurities in SGI production. It is possible that nanotubes have been formed in such SGI structures.

5. New production methods

Apart from the arc discharge technique, new methods have been developed in order to produce fullerenes and nanotubes with a better yield and lower costs. An example is the bulk production of nanotubes (e.g. pounds per day) by using pyrolysis of ethy-

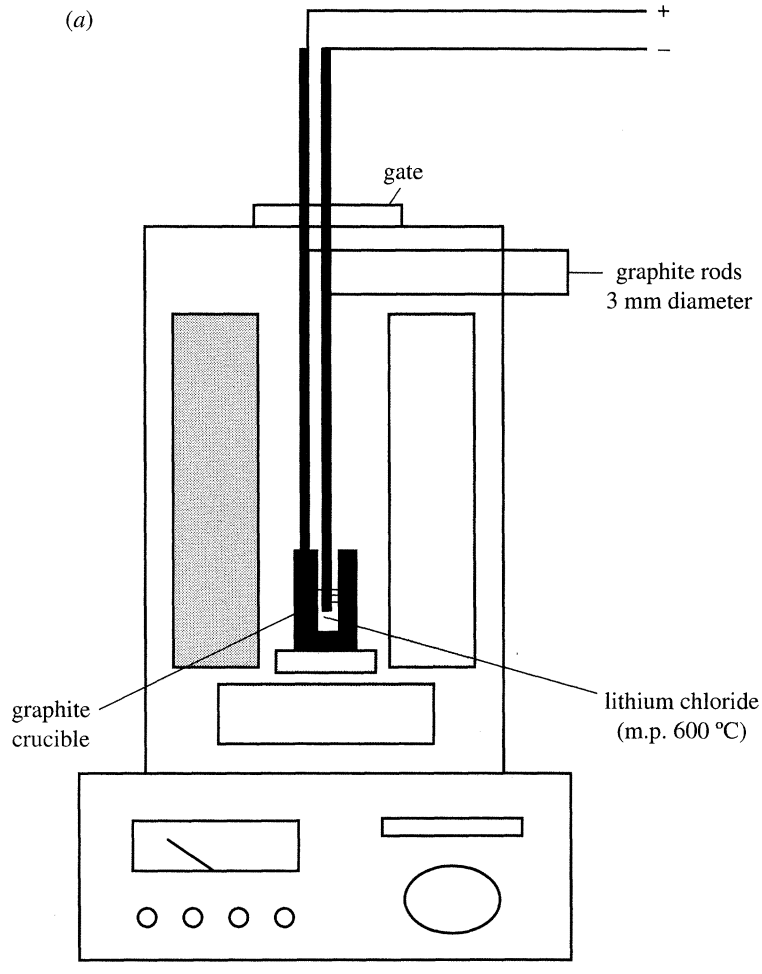

Figure 12. Experimental electrolysis set-up, using a graphite electrode and a graphite crucible as an electrode: (*a*) in air.

lene in the presence of a catalyst (Hausslein 1995) and the fullerene production of C_{60} from naphthalene pyrolysis (Taylor *et al.* 1993). In addition to this, the production of nanotubes by using high-energy laser irradiation of graphite in an inert atmosphere (He or Ar) at high temperatures (900–1200 °C) is possible (Guo *et al.* 1995; Abeysinghe *et al.* 1994, unpublished work). The latter can be explained in terms of a gas-phase scheme, in which carbon atoms attach to the adjacent edges of the growing multiwalled graphite sheets prolonging the life-time of the open structure, finally ending up with a multilayered nanotube (Guo *et al.* 1995). This mechanism suggests that a graphitic flake, with at least one pentagon, is first created from the carbon vapour which results from the graphite vaporization. Under certain high-temperature conditions this flake may anneal creating fullerenes, which may nucleate and form onions. If the carbon density is high enough, successive concentric graphite layers form around the template and multiwalled nanotubes are produced.

It is interesting to note that all the production techniques mentioned previously indicate that gas-phase nucleation is involved in the creation process: e.g. laser vaporization (Kroto *et al.* 1985; Guo *et al.* 1995); carbon arc evaporation (Krätschmer

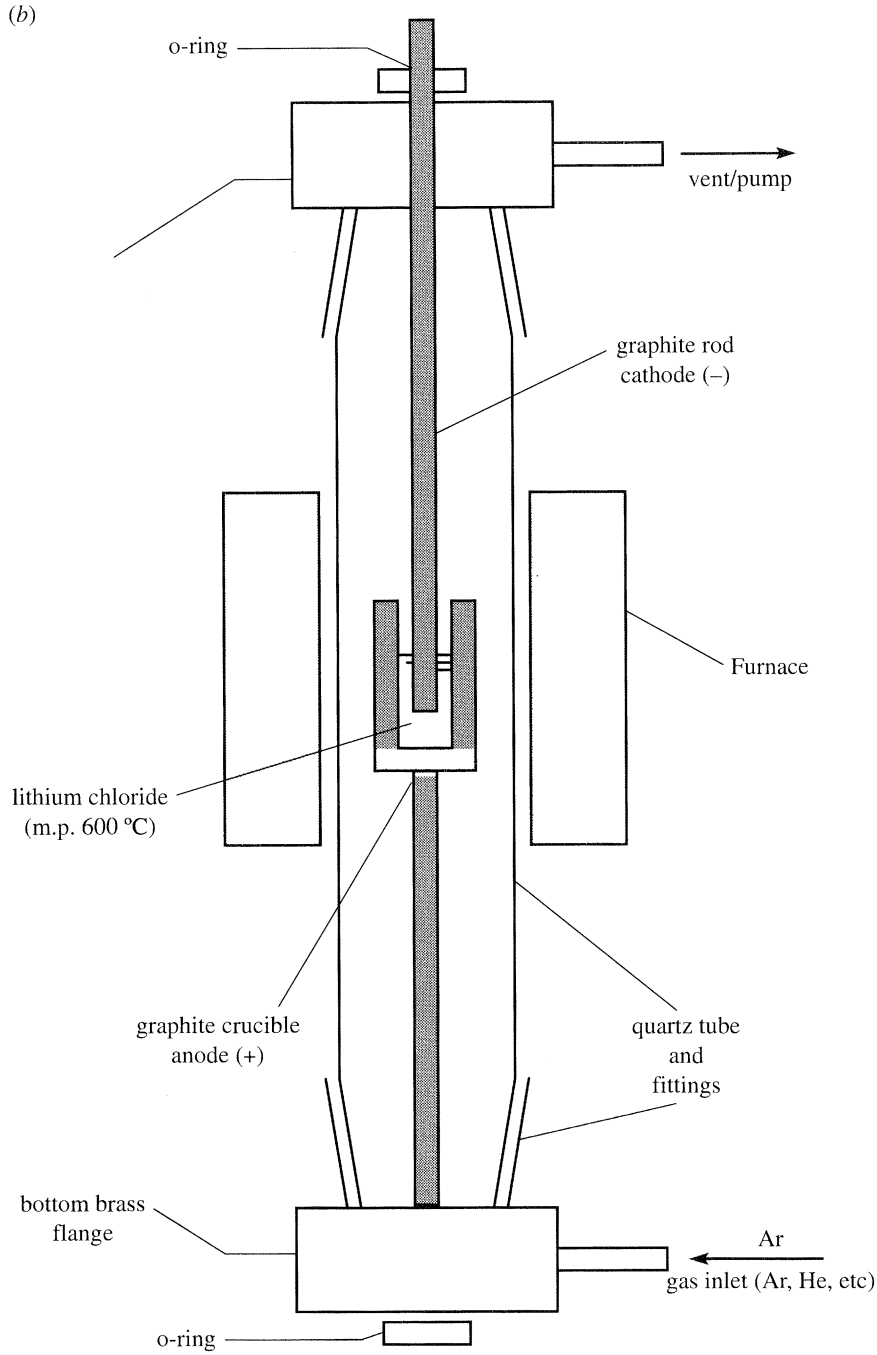

Figure 12. Experimental electrolysis set-up, using a graphite electrode and a graphite crucible as an electrode: (*b*) under Ar atmosphere. Both experiments produce carbon nanotubes and graphitic particles such as concentric onions.

et al. 1990; Iijima 1991); incomplete combustion (Iijima 1991; Ebbesen & Ajayan 1992); gas phase polymerization of synthetic carbons (Diederich *et al.* 1989; McElvaney *et al.* 1993); and the heterogeneous pyrolysis of vapour phase feedstocks (Taylor

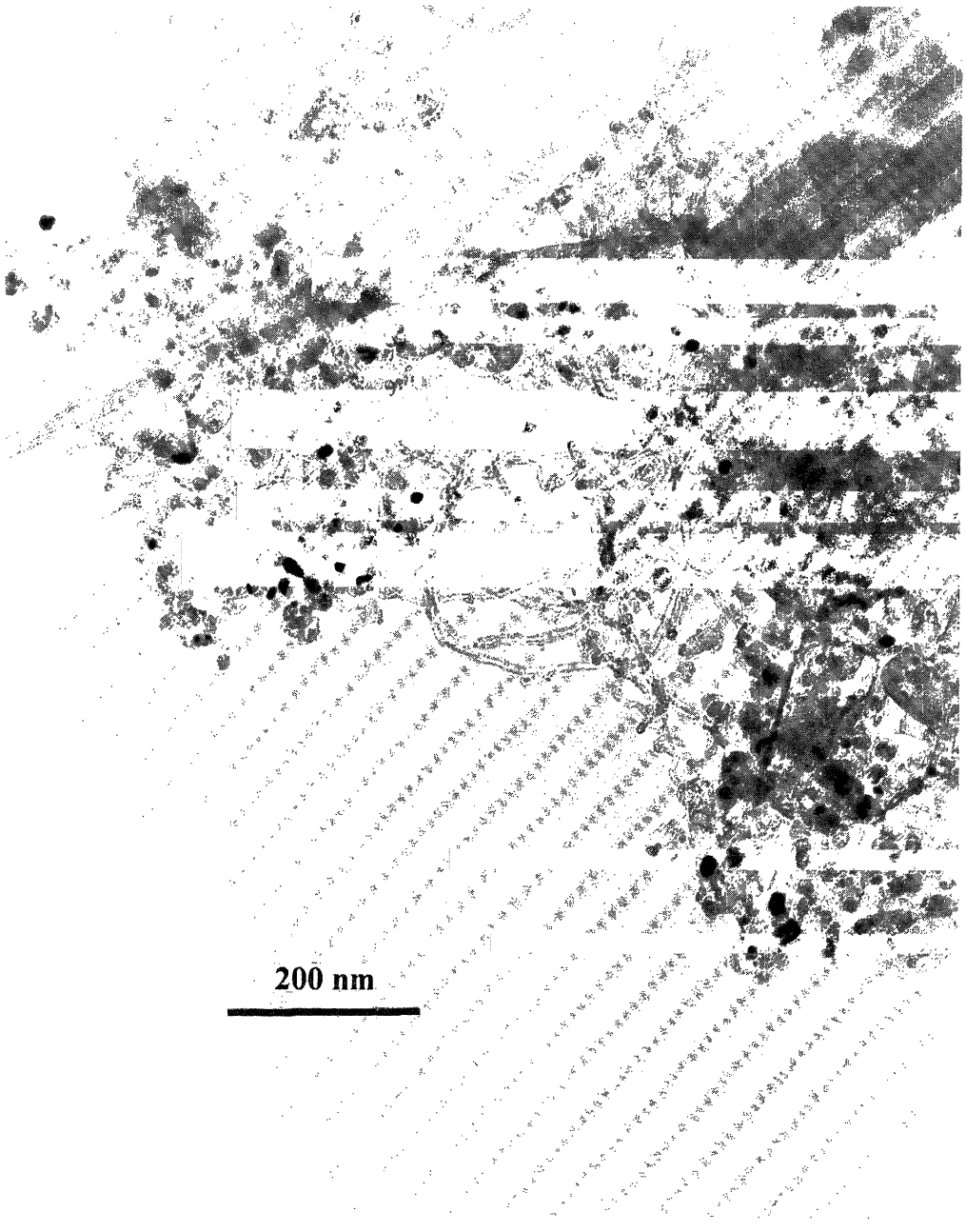

Figure 13. TEM image showing a representative area where nanotubes, produced by electrolysis in LiCl, possess curled morphologies.

et al. 1993; Howard *et al.* 1992; Endo *et al.* 1994). Recently, it has been found that nanotubes can also be produced by condensed-phase electrolysis between carbon electrodes in a molten electrolyte (Hsu *et al.* 1995). This appears to be the first report of the creation of fullerene-related material in the condensed phase, and represents a major advance which opens up the possibility of the development of controlled mass-production techniques for carbon nanotubes. In particular, these nanotubes

were produced by immersing two graphite electrodes, 3 mm in diameter, in molten LiCl salt (600 °C) (figure 12) with a current of *ca.* 30 A for *ca.* 30 s. After cooling, the solid melt was dissolved in water and particulate material was precipitated. Electron microscopy studies reveal that onion-like polyhedral particles as well as carbon nanotubes are present. Furthermore, some of these nanotubes show material encapsulation (e.g. LiO, LiC, LiCl or Li) with unusual morphologies (creating loops) in comparison with the ones produced in the arc–plasma generator (figure 13).

6. Conclusion

An overview has been presented of different forms of graphite which may possess practical uses in the future. The insertion of heptagons and pentagons into the graphitic hexagonal network is responsible for closed, curly and bent structures (spheres, hemi-toroids, spirals, helices, etc.) which are also stable. Carbon and other layered materials offer the possibility of creating tubules with applications in nanoscale engineering. Moreover, the encapsulation of ferromagnetic materials may have potential applications in magnetic data storage, magnetic toners for xerography, magnetic inks, etc. (McHenry *et al.* 1994). Another possibility is the insertion of superconducting material into these graphite-like structures, which also may offer important applications in solid-state electronics (Murakami *et al.* 1993; Terrones *et al.* 1995*c*). The production of graphite as well as other layered materials which bend and close opens up a new era in material science and chemistry with enormous potential for the coming century.

We are very grateful to P. J. F. Harris (Reading), D. Hutchinson (Oxford), J. Critchell (JEOL, UK), J. Thorpe (Sussex) and L. Rendón (UNAM-México) for electron microscopy facilities. We are also in debt to A. Sarkar, A. M. Benito, N. Boivin and D. Reid for their help and useful discussions. We thank EPSRC (UK), Royal Society (UK) and CONACYT-México (scholarship and grant No. 3348) for financial support.

References

Akagi, K., Tamura, R., Tsukada, M., Itoh, S., Ihara, S. 1995 Electronic structure of helically coiled cage of graphitic carbon. *Phys. Rev. Lett.* **74**, 2307–2310.

Amelinckx, S., Zhang, X. B., Bernaerts, D., Zhang, X. F., Ivanov, V. & Nagy, J. B. 1994 A formation mechanism for catalytically grown helix-shaped graphite nanotubes. *Science* **265**, 635–639.

Bernaerts, D., Zhang, X. B., Zhang, X. F., Amelinckx, S., Van Tendeloo, G., Van Landuyt, J., Ivanov, V. & Nagy, J. B. 1995 Electron microscopy study of coiled carbon tubules. *Phil. Mag.* A **71**, 605–630.

Brabec, C. J., Maiti, A. & Bernholc, J. 1994 Structural defects and the shape of large fullerenes. *Chem. Phys. lett.* **219**, 473–478.

Chopra, N. S., Luyken, R. J., Cherrey, K., Crespi, V. H., Cohen M. L., Louie, S. G. & Zettl, A. 1995 Boron nitride nanotubes. *Science* **269**, 966–967.

Diederich, F., Rubin, Y., Knobler, C. B.,Whetten, R. L., Schriever, K. E., Houk, K. N. & Li, Y. 1989 All carbon molecules, evidence for the generation of cyclo [18] carbon from a stable organic precursor. *Science* **245**, 1088–1090.

Dresselhaus, M. S., Dresselhaus, G., Sugihara, K., Spain, I. L. & Goldberg, H. A. 1988 Synthesis of graphite fibers and filaments. In *Graphite fibers and filaments* (Series in Material Sciences 3), pp. 12–34. Berlin: Springer.

Dunlap, B. I. 1994 Relating carbon tubules. *Phys. Rev.* B **49**, 5643–5650.

Ebbesen, T. W. & Ajayan, P. M. 1992 Large scale synthesis of carbon nanotubes. *Nature* **358**, 220–222.

Ebbesen, T. W., Ajayan, P. M., Hiura, H. & Tanigaki, K. 1994 Purification of nanotubes. *Nature* **367**, 519.

Elliot, R. 1988 An introduction to cast irons. In *Cast iron technology*, pp. 1–45. London: Butterworths.

Else, G. E. 1983 The first two years, operating experience at the Hallam plant of Stanton and Staveley. *Br. Foundryman* **76**, 145.

Endo, M., Katoh, A., Sugiura, T. & Shiraishi, M. 1987. In *Extended Abstracts of the 18th. Biennial Conf. on Carbon* (Worcester, MA), p. 151. University Park, PA: American Carbon Society.

Endo, M. & Kroto, H. W. 1992 Formation of carbon nanofibres. *J. Phys. Chem.* **96**, 6941–6944.

Endo, M., Takeuchi, K., Shiraishi, M. & Kroto, H. W. 1993 The production and structure of pyrolytic carbon nanotubes (PCNT's). *J. Phys Chem. Solids* **54**, 1841–1848.

Endo, M., Takeuchi, K., Kobori, K., Takahashi, K., Kroto, H. W. & Sarkar, A. 1995 Pyrolytic carbon nanotubes from vapor-grown carbon fibers. *Carbon* **33**, 873–881.

Guo, T., Nikolaev, P., Rinzler, A. G., Tománek D. Colbert, D. T. & Smalley, R. E. 1995 Self-Assembly of tubular fullerenes. *J. Phys. Chem.* **99**, 10 694–10 697.

Hamada, N., Sawada, S. & Oshiyama, A. 1992 New one-dimensional conductors—graphite microtubules. *Phys. Rev. Lett.* **68**, 1579–1581.

Harris, P. J. F., Tsang, S. C., Claridge, J. B. & Green, M. L. H. 1994 High resolution electron microscopy studies of a microporous carbon produced by arc-evaporation. *J. Chem. Soc. Faraday Trans.* **90**, 2799–2802.

Hausslein, R. W. 1995 Commercial manufacture and uses of carbon nanotubules. In *Abstracts of the 18th Electrochemical Society Meeting*, p. 175. Pennington, NJ: Electrochemical Society. (In the press.)

Howard, J. B., Lafleur, A. L., Markarovsky, Y., Mitra, S., Pope, C. J. & Yadav, T. K. 1992 Fullerene synthesis in combustion. *Carbon* **30**, 1183–1201.

Hsu, W. K. & Terrones, M. 1994 Bent nanotubes. First year report, University of Sussex.

Hsu, W. K., Hare, J. P., Terrones, M., Harris, P. J. F., Kroto, H. W. & Walton, D. R. M. 1995 Condensed phase nanotubes. *Nature* **377**, 687.

Ihara, S., Itoh, S. & Kitakami, J. 1993 Helically coiled cage forms of graphite carbon. *Phys. Rev.* B **48**, 5643–5647.

Iijima, S. 1980 Direct observations of tetrahedral bonding in graphitized carbon black by high resolution electron microscopy. *J. Cryst. Growth* **5**, 675–683.

Iijima, S. 1991 Helical microtubules of graphitic carbon. *Nature* **354**, 56–58.

Iijima, S. 1993 Growth of carbon nanotubes. *Mat. Sci. Engng* B **19**, 172–180.

Iijima, S., Ajayan, P. M. & Ichihashi, T. 1992*a* Growth model for carbon nanotubes. *Phys. Rev. Lett.* **69**, 3100–3103.

Iijima, S., Ichihashi, T., Ando, Y. 1992*b* Pentagons, heptagons and negative curvature in graphite microtubule growth. *Nature* **356**, 776–778.

Karsay, S. I. 1976 The fundamentals of ductile iron metallurgy. In *Ductile iron*, 4th edn, pp. 9–40. Québec: Québec Iron and Titanium Corporation.

Krätschmer, W., Lamb, L. D., Fostiropoulos, K. & Huffman, D. R. 1990 Solid C_{60}: a new form of carbon. *Nature* **347**, 354–358.

Kroto, H. W. & McKay, K. 1988 The formation of quasi-icosahedral spiral shell carbon particles. *Nature* **331**, 328–331.

Kroto, H. W., Heath, J. R., O'Brien, S. C., Curl, R. F. & Smalley, R. E. 1985 C_{60}—Buckminsterfullerene. *Nature* **318**, 162–163.

Kroto, H. W., Hare, J. P., Sarkar, A., Hsu, K., Terrones, M. & Abeysinghe, J. R. 1994 New horizons in carbon chemistry and materials science. *MRS Bull.* **19**, 51–55.

Mackay, A. L. & Terrones, H. 1991 Diamond from graphite. *Nature* **352**, 762.

Margulis, L., Saltra, G., Tenne, R. & Tallanker, M. 1993 Nested fullerene-like structures. *Nature* **365**, 113–114.

McElvany, S. W., Ross M. M., Goroff, N. S., Diederich, F. 1993 Mechanisms for tailor-made fullerene formation. *Science* **259**, 1594–1596.

McHenry, M. E., Nakamura, Y., Kirkpatrick, S., Johnson, F., Curtin, S., DeGraef, M., Uhfer, N. T., Majetich, S. A. & Brunsman, E. M. 1994 Carbon-coated fine particle ferromagnets produced by a carbon-arc technique. In *Recent advances in the chemistry and physics of fullerenes and related materials* (ed. K M. Kadish & R. S. Ruoff), vol. 1, pp. 1463–1475. Pennington, NJ: Electrochemical Society.

Morrogh, H. & Williams, W. J. 1948 The production of nodular graphite structures in cast iron. *J. Iron Steel Inst.* **150**, 306.

Murakami, Y., Shibata, T., Okuyama, K., Arai, T., Suematsu, H. & Yoshida, Y. 1994 Structural, magnetic and superconducting properties of graphite nanotubes and their encapsulation compounds. *J. Phys. Chem. Solids* **54**, 1861–1970.

Saito, R., Fujita, M., Dresselhaus, G. & Dresselhaus, M. S. 1992*a* Electronic structure of graphene tubules based on C_{60}. *Phys Rev.* B **46**, 1804–1811.

Saito, R., Fujita, M., Dresselhaus, G., Dresselhauss, M. S. 1992*b* Electronic structure of chiral graphene tubules. *Appl. Phys. Lett.* **60**, 2204–2206.

Saito, Y., Okuda, M., Fujimoto, M., Yoshikawa, T., Tomita, M. & Hayashi, T. 1994 Single-wall carbon nanotubes growing radially from Ni fine particles formed by arc evaporation. *Jap. J. Appl. Phys.* **33**, 526–529.

Sarkar, A. K. 1994 Fullerene and non-planar graphitic networks: a physicochemical analysis. Ph.D. thesis, University of Sussex, p. 98.

Sarkar, A. K., Kroto, H. W. & Endo, M. 1995 Hemi-toroidal networks in pyrolytic carbon nanotubes. *Carbon* **33**, 51–55.

Sarkar, A. K., Kroto, H. W., Abeysinghe, J. R. & Ugarte, D. 1996 The structure and dynamics of carbon nanoparticles. (In the press.)

Stone, A. J. & Wales, D. J. 1986 Theoretical studies of icosahedral C_{60} and some related species. *Chem. Phys. Lett.* **128**, 501–503.

Taylor, R., Langley, G. J., Kroto, H. W. & Walton, D. R. M. 1993 Formation of C_{60} by pyrolysis of Naphthalene. *Nature*, **366**, 728–731.

Tenne, R., Margulis, L., Genut, M. & Hodes, G. 1992 Polyhedral and cylindrical structures of tungsten disulfide resonance. *Nature* **360**, 444–446.

Terrones, H., Terrones, M., Hsu, W. K. 1995*a* Beyond C_{60}: graphite structures for the future. *Chem. Soc. Rev.* **24**, 341–350,

Terrones, H., García-Cruz., R. A., Castillo, R., Ramos, S., Terrones, M., Hsu, W. K., Prassides, K., Walton, D. R. M. & Kroto, H. W. 1995*b* The role of boron nitride in the production of long graphite nanotubes. In *Proc. IV Int. Conf. on Adanced Materials.* S3-P1.12.

Terrones, M., Hare, J. P., Hsu, W., Kroto, H. W., Lappas, A., Maser, W. K., Pierik, A. J., Prassides, K., Taylor, R. & Walton, D. R. M. 1995*c* Physico-chemical studies on nanotubes and their encapsulated compounds. In *Recent advances in the chemistry and physics of fullerenes and related materials* (ed. K. M. Kadish & R. S. Ruoff), vol. 2, pp. 599–620. Pennington, NJ: Electrochemical Society.

Ugarte, D. 1992 Curling and closure of graphitic networks under electron beam irradiation. *Nature* **359**, 707–709.

Ugarte, D. 1993 Formation mechanism of quasi-spherical carbon particles induced by electron bombardment. *Chem. Phys. Lett.* **207**, 473–479.

Wang, X. K., Lin, X. W., Dravid, V. P., Ketterson, J. B. & Chang, R. P. H. 1995 Carbon nanotubes synthesized in a hydrogen arc discharge. *Appl. Phys. Lett.* **66**, 2430–2432.

Wengsieh, Z., Cherrey, K., Chopra, N. G., Blase, X., Miyamoto, Y., Rubio, A., Cohen, M. L., Louie, S. G., Zettl, A. & Gronsky, R. 1995 Synthesis of $B_xC_yN_z$ nanotubules. *Phys. Rev.* B **51**, 11 229–11 232.

Zhang, X. B., Zhang, X. F., Bernaerts, D., Van Tendeloo, G., Amelinckx, S., Van Landuyt, J., Ivanov, V., Nagy, J. B., Lambin, P. & Lucas, A. A. 1994 The texture of catalytically grown helix-shaped graphitic nanotubes. *Europhys. Lett.* **27**, 141–146.

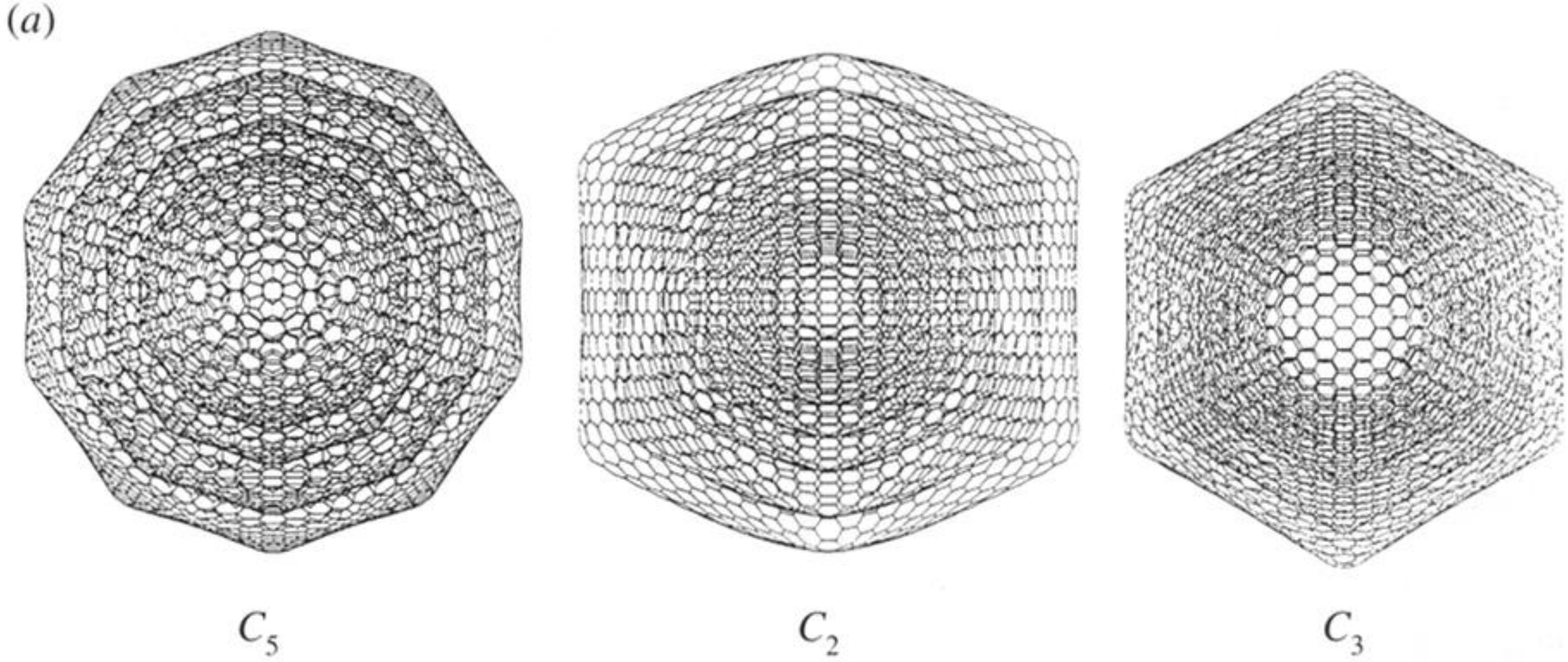

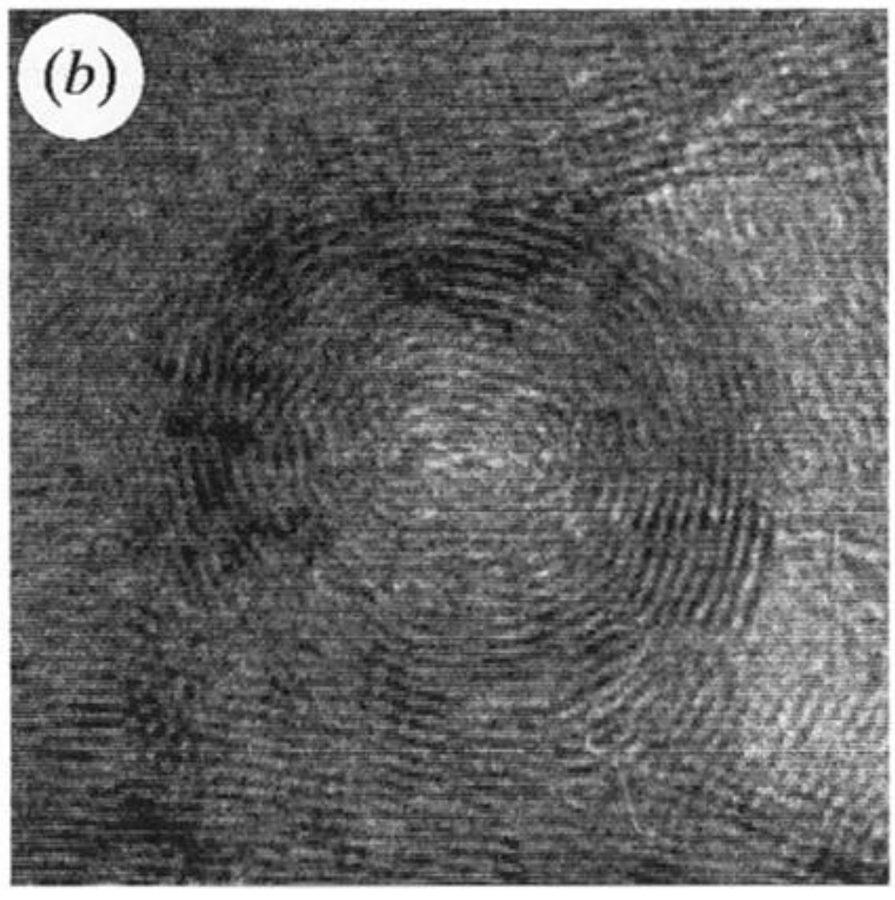

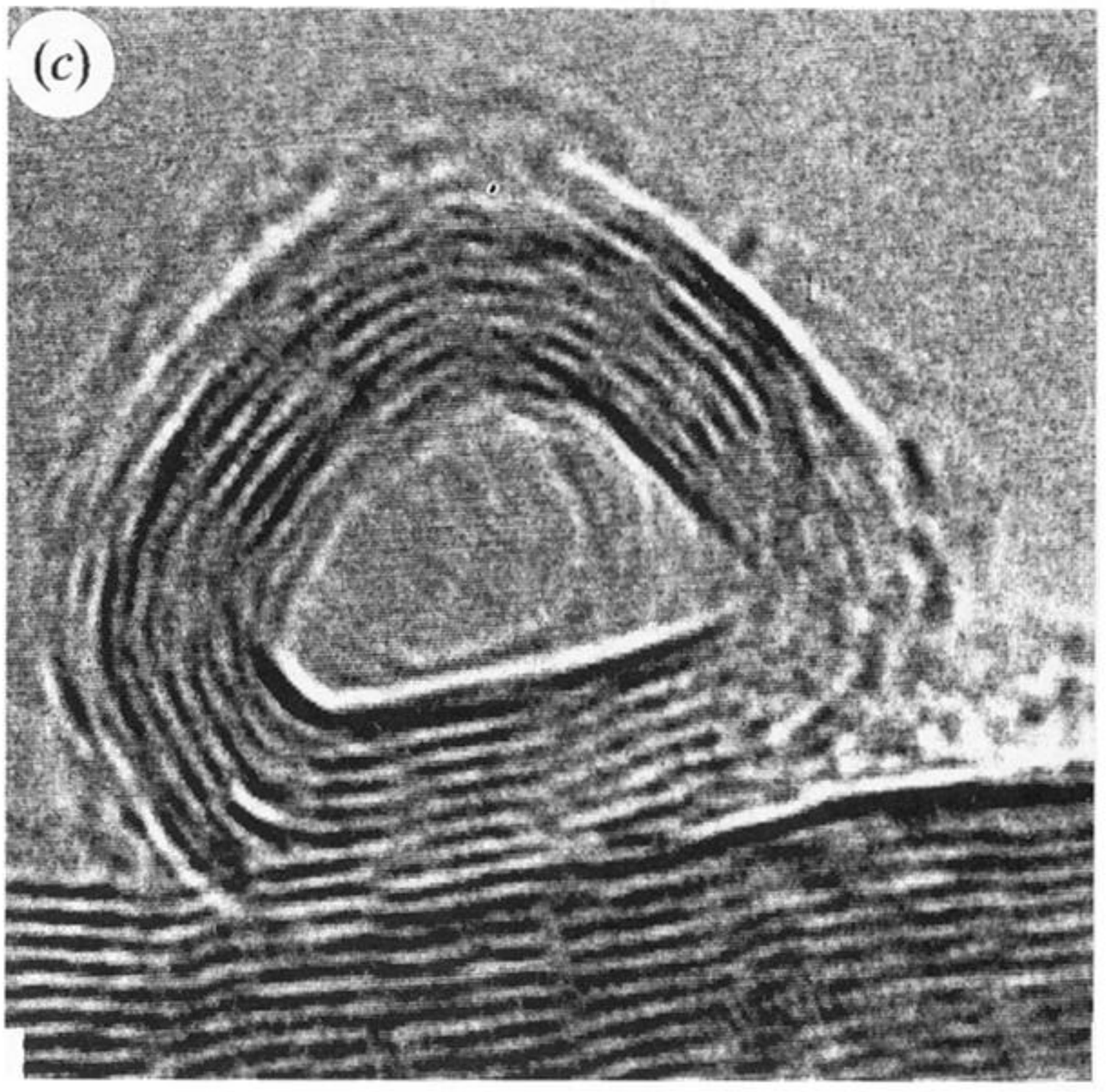

Figure 1. (*a*) Molecular modelling image of the structure $C_{960}@C_{1500}@C_{2160}@C_{2940}$ composed of four concentric perfect icosahedral giant fullerenes. The particle is viewed along three different symmetry axes (C5, C2 and C3, respectively) to show the way the shape varies with orientation to the observer. (*b*) Real round onion-like structure with *ca.* 15–20 layers. (*c*) Polyhedral (tetrahedron-like) structure possessing 8–10 layers. In (*b*) and (*c*) the interlayer spacing is close to that of graphite (e.g. 3.35 Å).

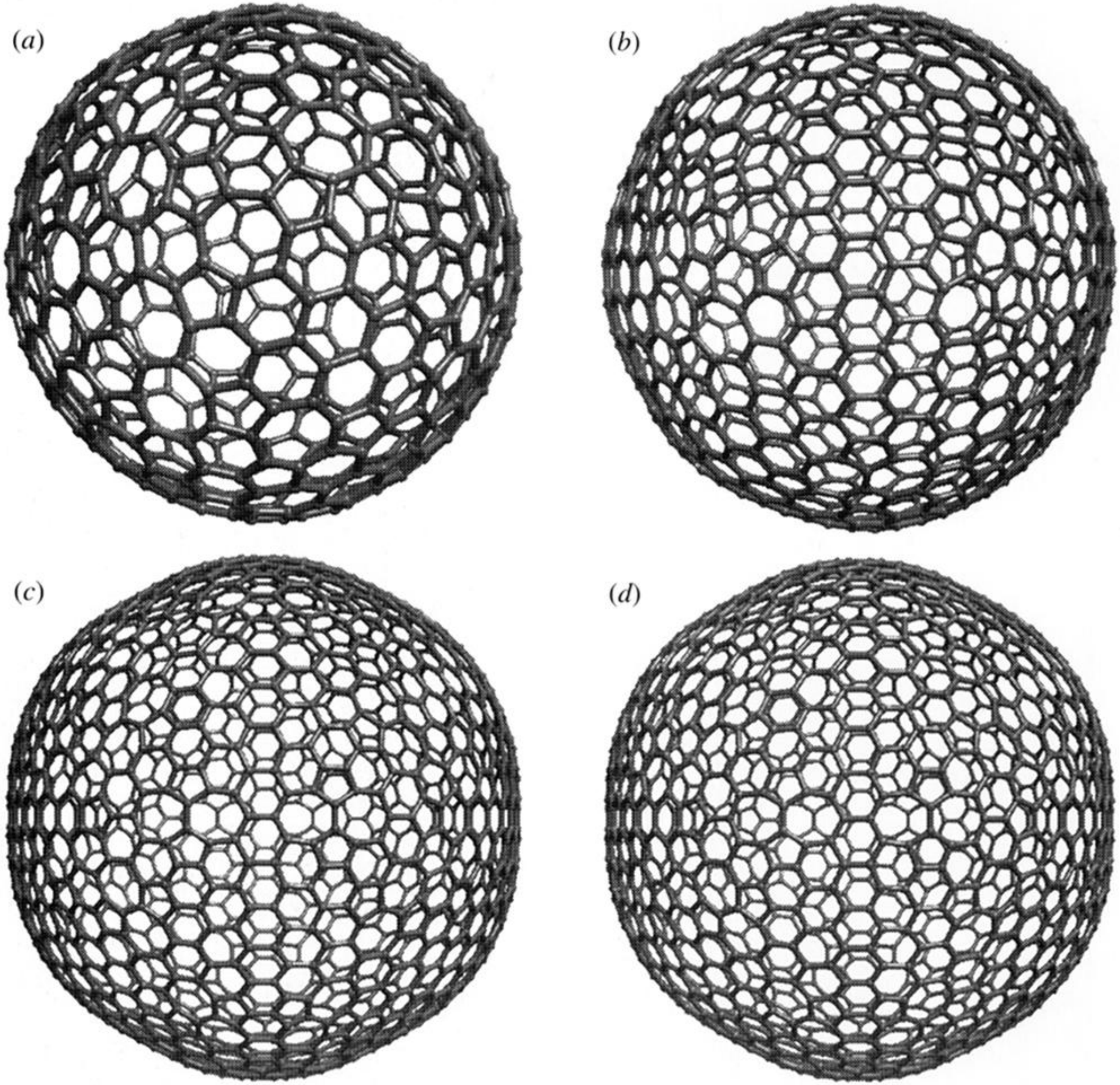

Figure 2. Quasi-spherical fullerenes with additional heptagonal and pentagonal rings: (*a*) D_{2h} C_{540} with 76 pentagons and 64 heptagons (non-cubic, non-icosahedral); (*b*) ico C_{888}-A with 60 heptagons and 72 pentagons (with traces of icosahedral symmetry); (*c*) ico C_{1500}-A with 132 pentagons and 120 heptagons (icosahedral I_h); (*d*) ico C_{1020}-B with 132 pentagons and 120 heptagons (icosahedral I_h symmetry).

(*e*)

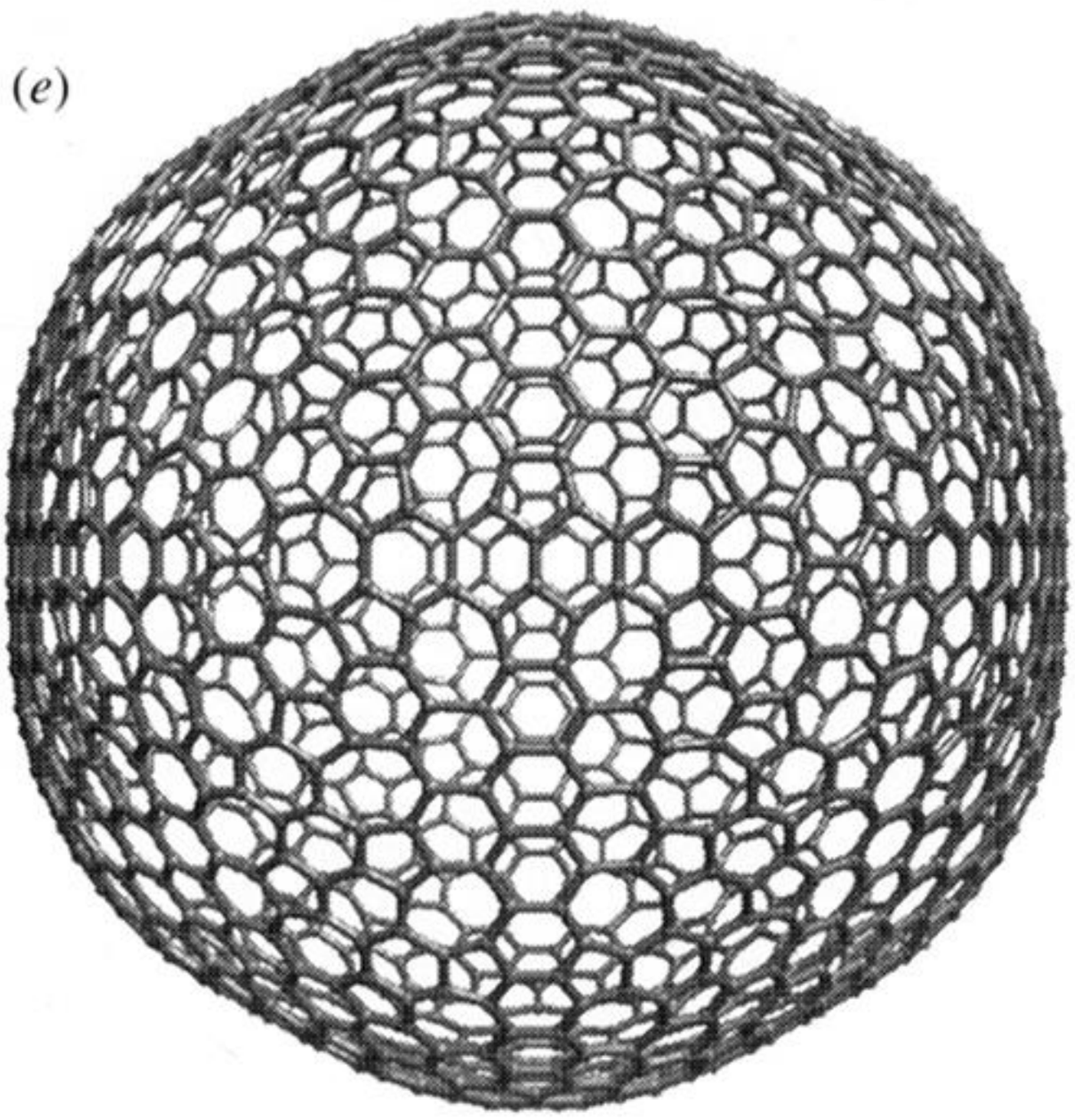

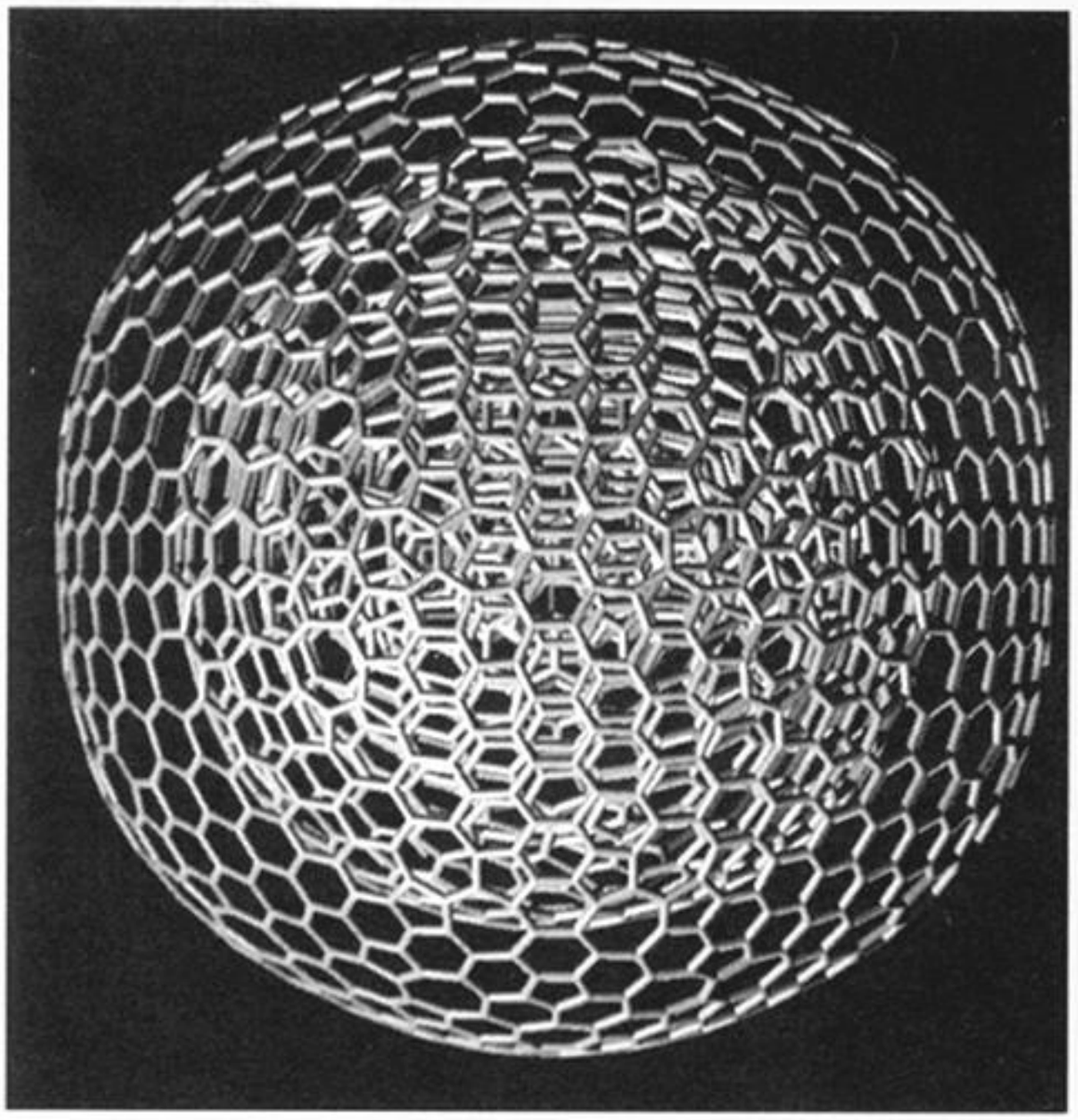

(*f*)

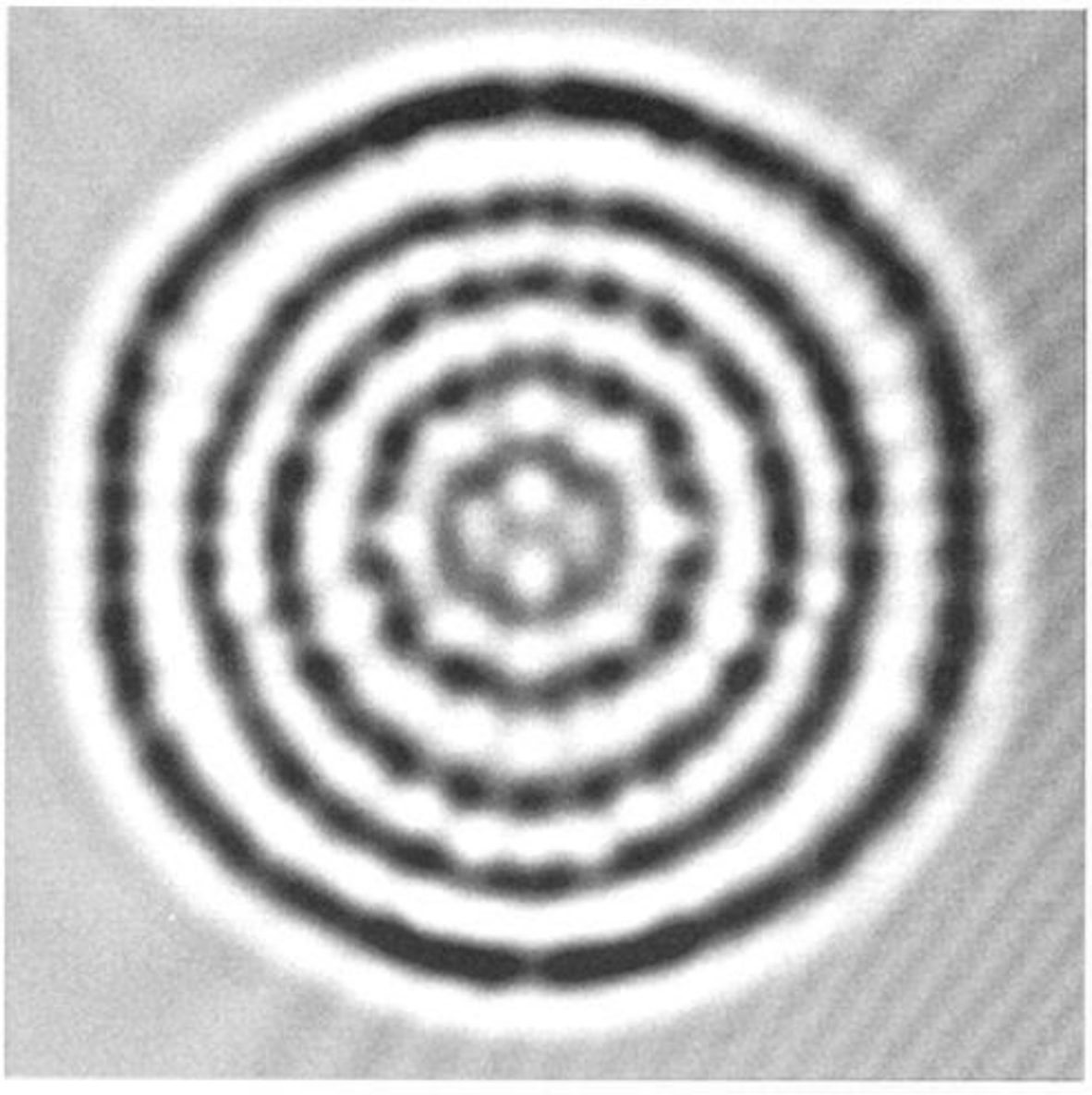

Figure 2. Quasi-spherical fullerenes with additional heptagonal and pentagonal rings: (*e*) ico C_{1620}-B (with traces of icosahedral symmetry) containing 192 pentagons and 180 heptagons; (*f*) nested quasi-spherical fullerenes made by introducing heptagonal and pentagonal carbon rings (along C_2 axes). The onion (top) and HRTEM simulation (bottom) are composed of $C_{60}@C_{240}@D_{2h}$ $C_{540}@C_{888}$-A@C_{1500}-A.

(a) (b) (c) (d)

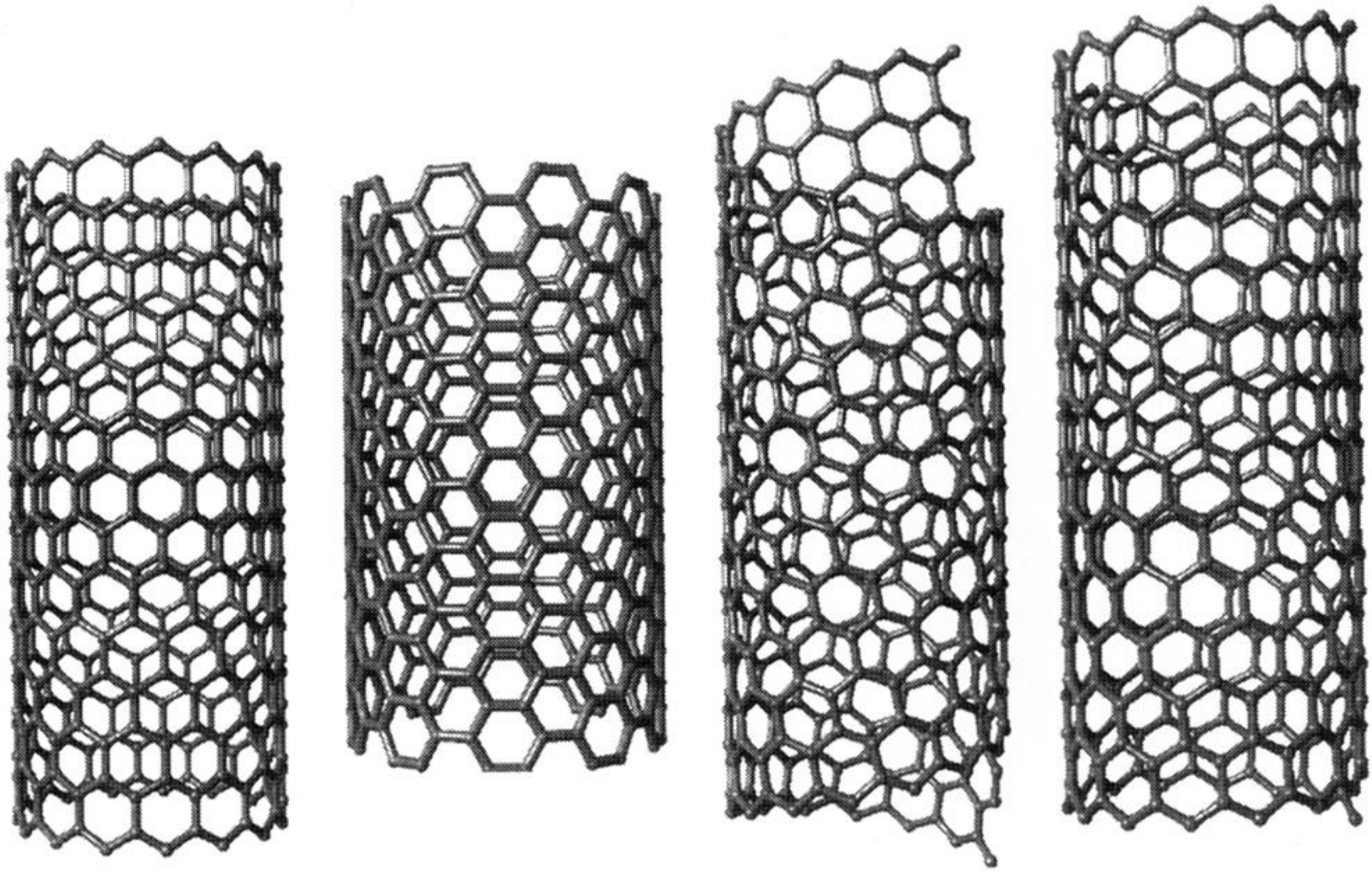

Figure 3. Simulated single-walled nanotubes with different helicities: (*a*) zig-zag arrangement; (*b*) armchair configuration; (*c*) and (*d*) two different helicities.

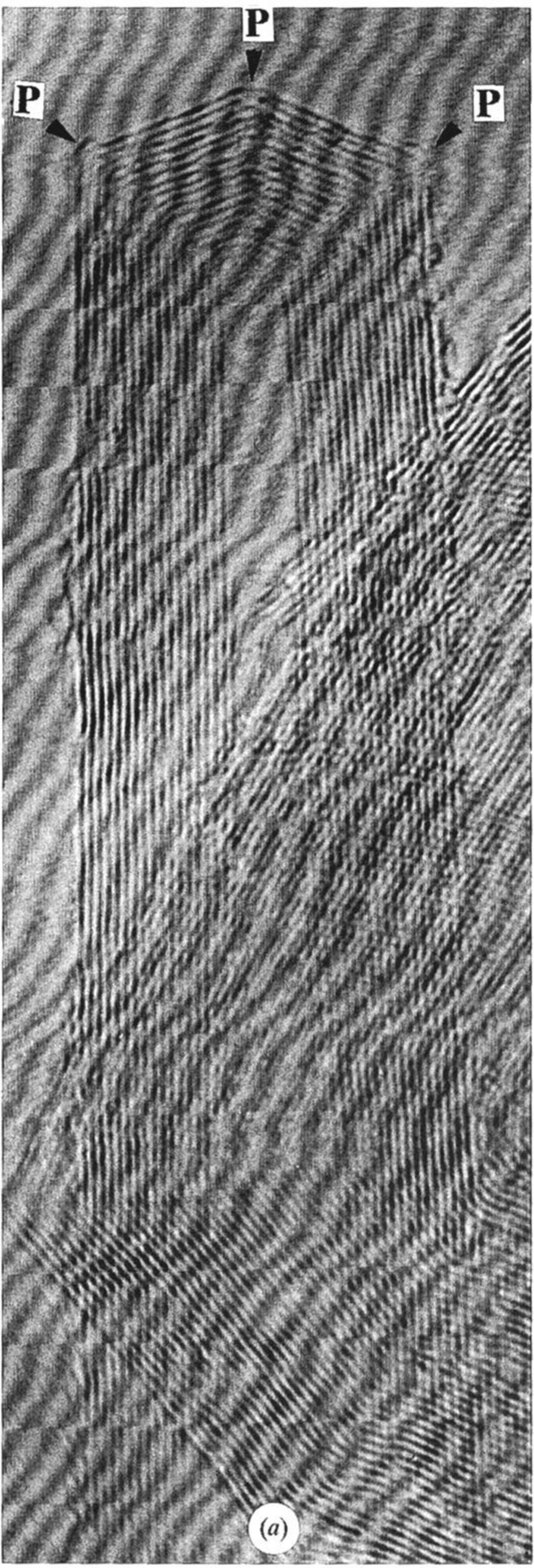
P
P
P
(a)

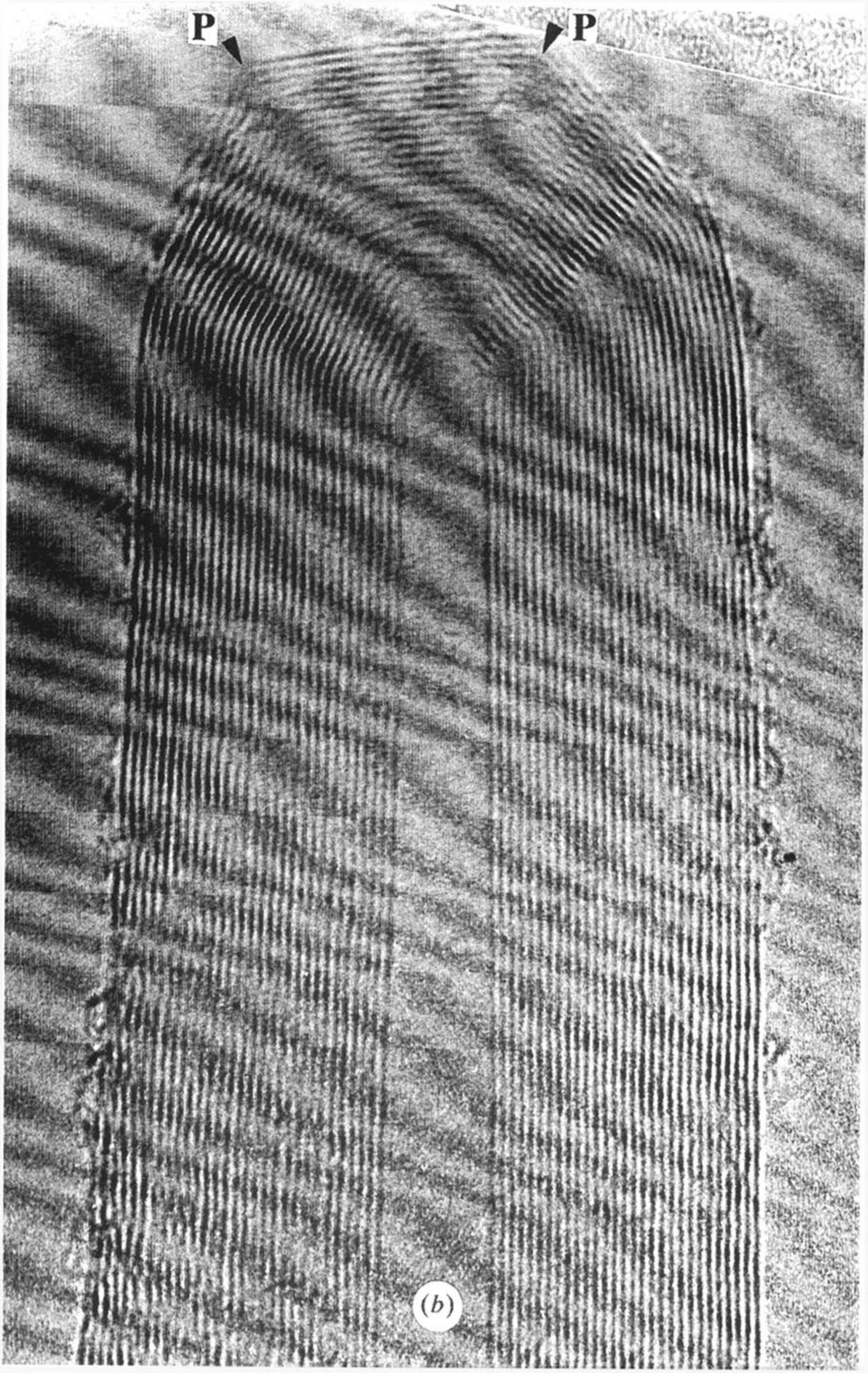

Figure 4. Various types of nanotube caps with different morphologies. **P** denotes likely pentagon sites while **H** denotes likely heptagon regions: (*a*) and (*b*) hemispherical caps where the pentagons are chirally distributed.

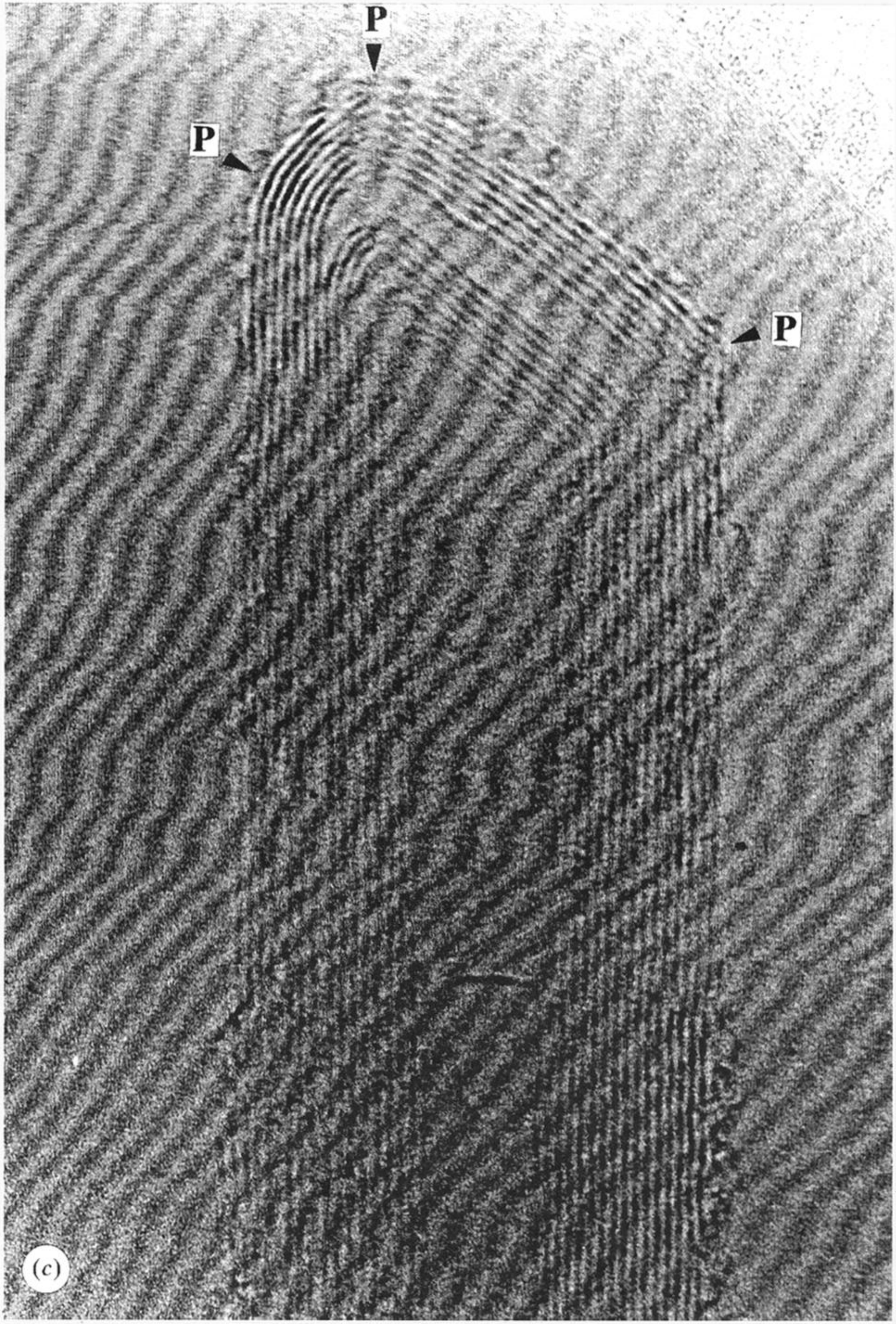

Figure 4. Various types of nanotube caps with different morphologies. **P** denotes likely pentagon sites while **H** denotes likely heptagon regions: (*c*) triangular cap with different pentagon distribution.

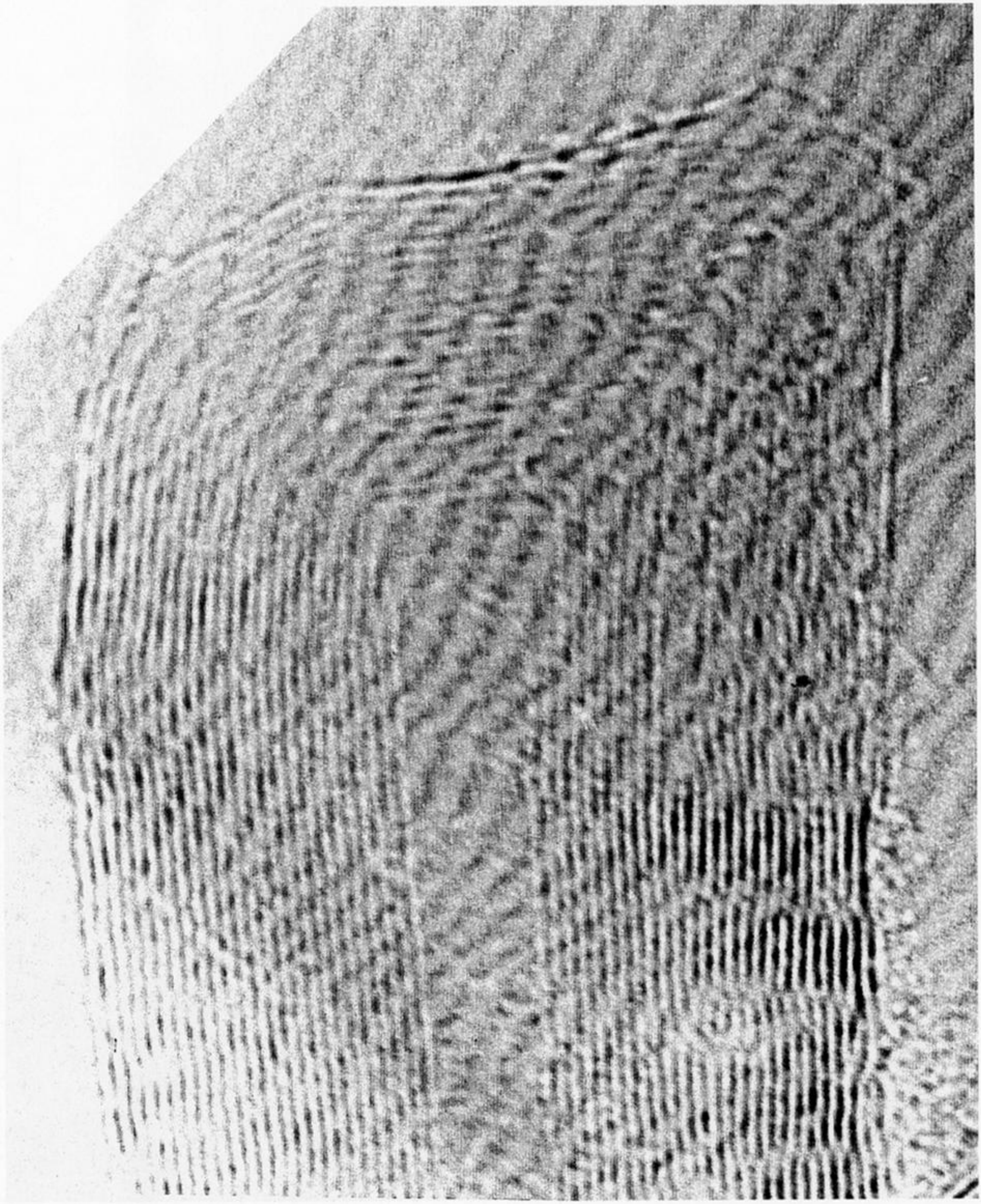

Figure 4. Various types of nanotube caps with different morphologies. **P** denotes likely pentagon sites while **H** denotes likely heptagon regions: (*d*) square cap.

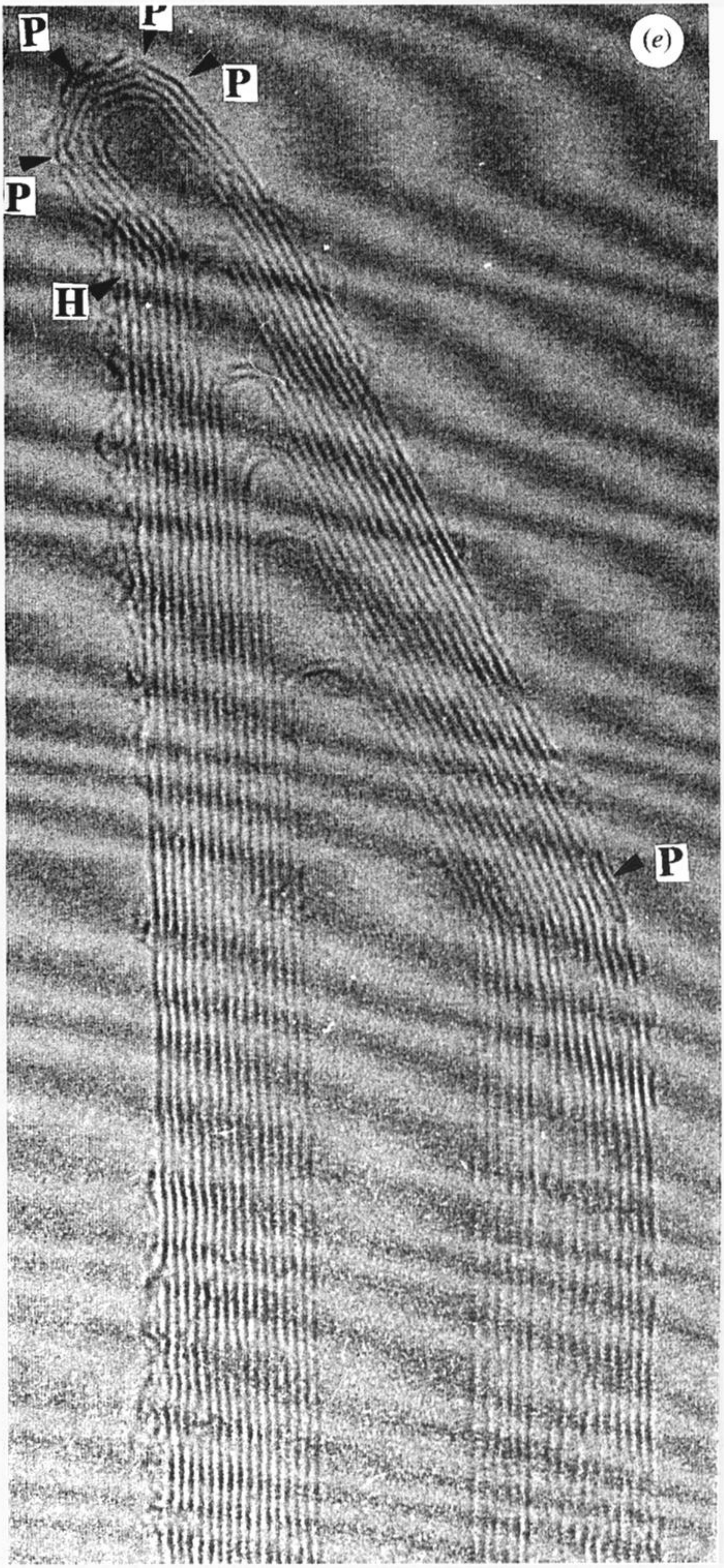

Figure 4. Various types of nanotube caps with different morphologies. **P** denotes likely pentagon sites while **H** denotes likely heptagon regions: (*e*) cap showing negative curvature due to the insertion of heptagons and pentagons. In this image, the 30°-pentagon declination (right-hand bend) cancels the 30°-heptagon inclination (left top bend), ending with six pentagons at the final tip with a hemispherical cap, thus following Euler's Law.

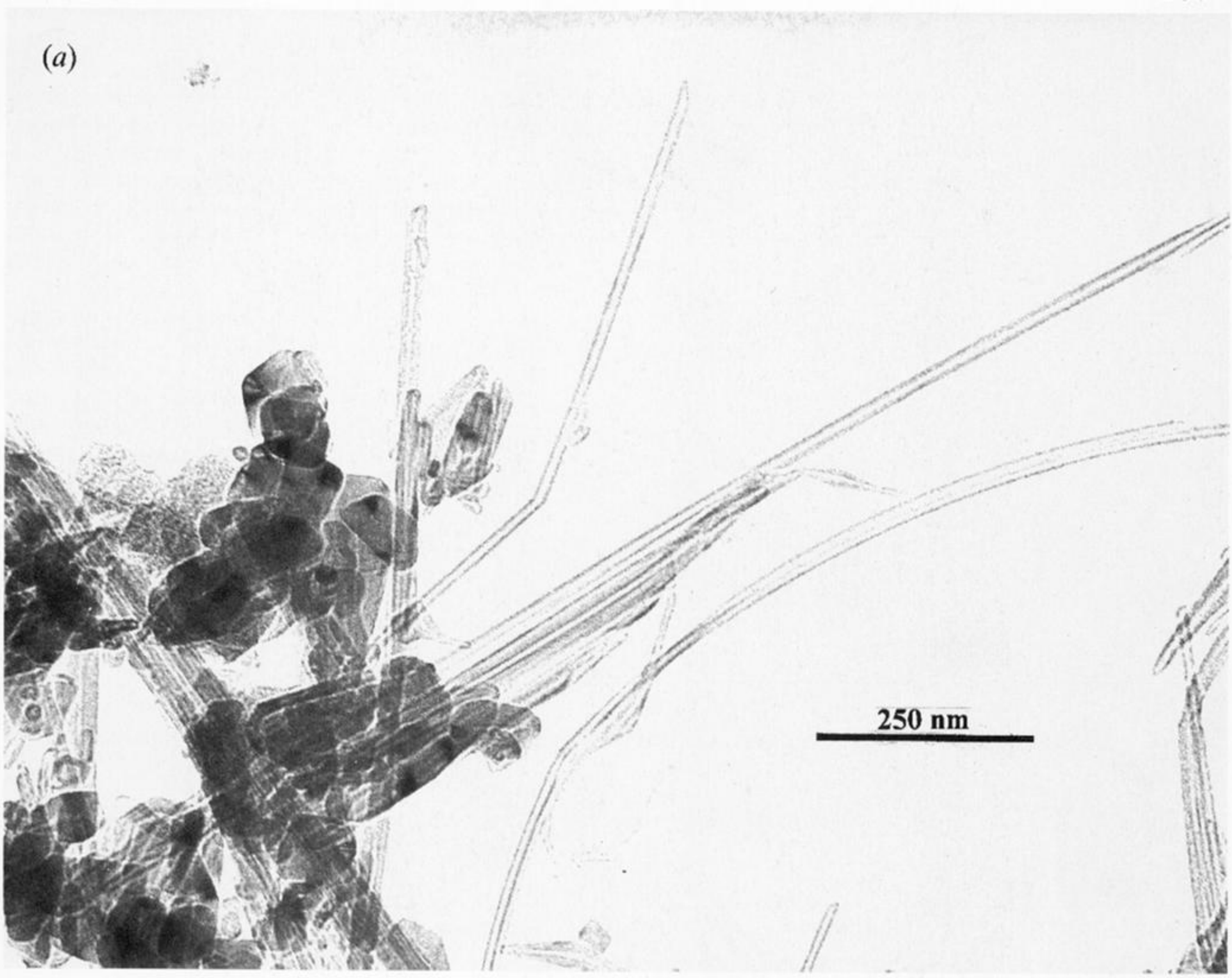

Figure 5. TEM images showing 30°-bent nanotubes: (*a*) low resolution; (*b*) HRTEM of a 30°-bent nanotubes showing some defects and fractures at the bend.

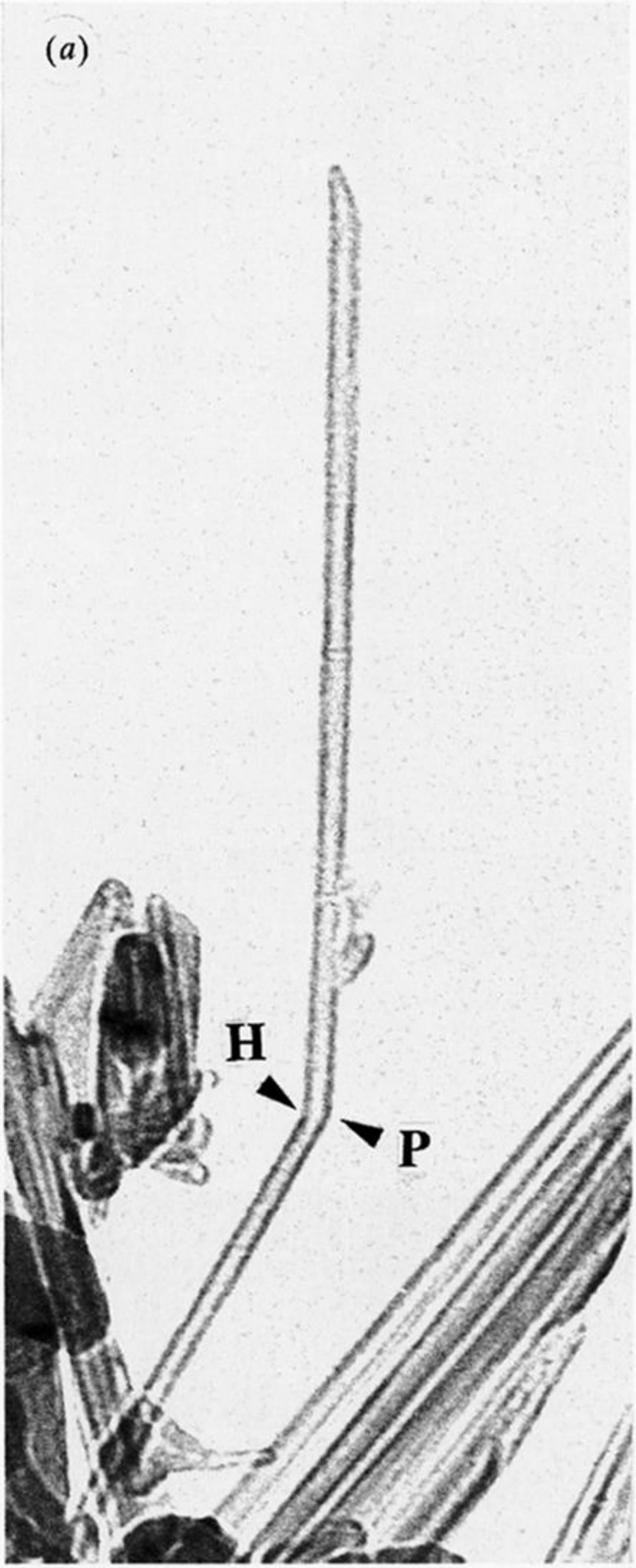

Figure 6. Real 30°-bent nanotube and its possible simulation: (*a*) close-up at the bent nanotube shown in figure 5*a*; (*b*) simulation showing the change in helicity by 30° (from zig-zag to arm-chair) giving up the possibility to have two different electronic properties (e.g. semicondutor and metallic-conductor). In both images a difference in diameters after and before the bend is observed.

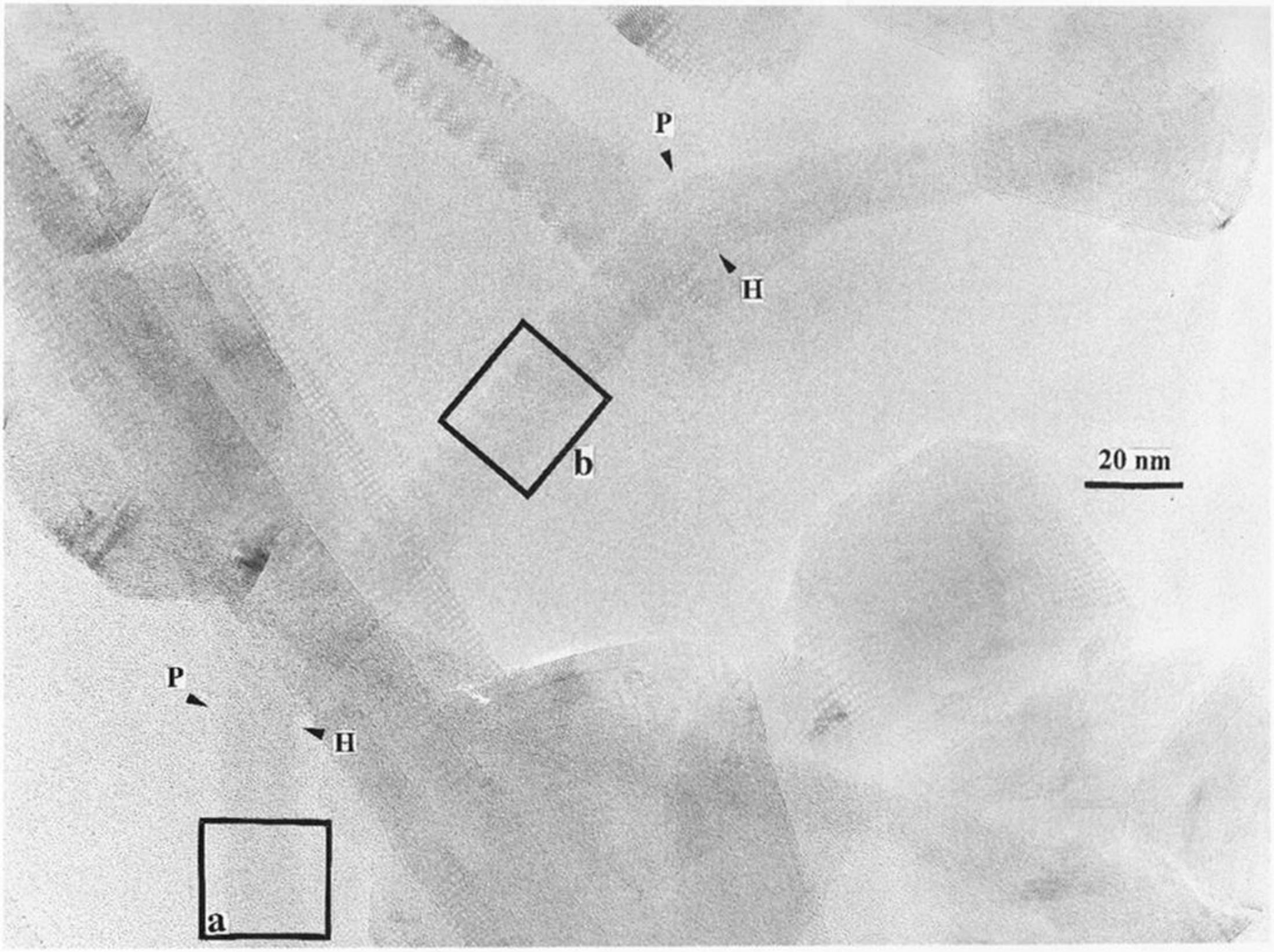

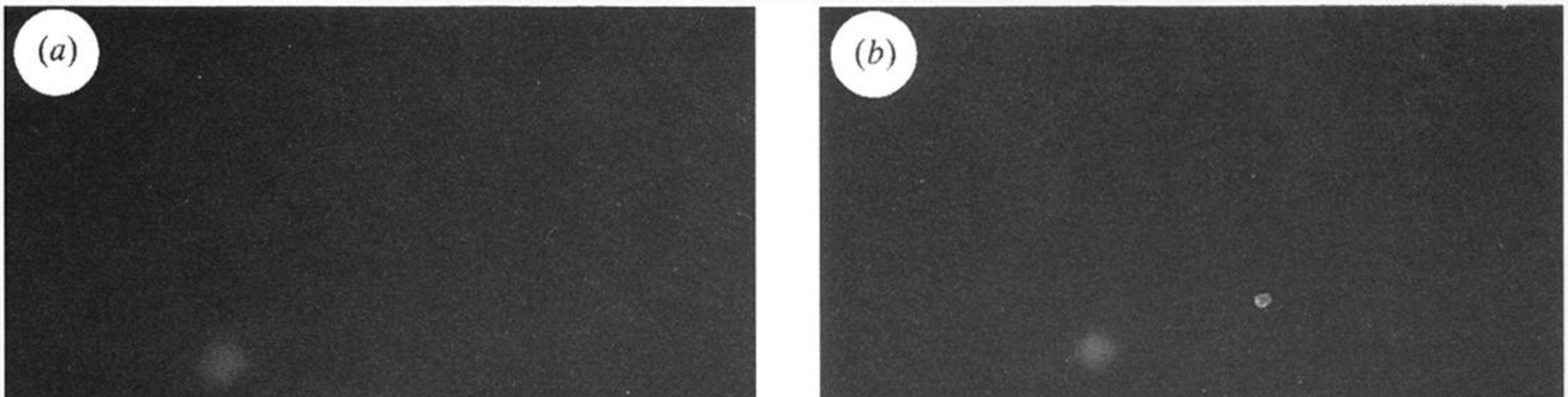

Figure 7. Triple 30°-bent nanotube and SAEDP are shown. The patterns in regions (*a*) and (*b*) show that helicity changes by 30° after and before the bend. This may imply a change in the electronic structure due to the insertion of the pentagon–heptagon pair.

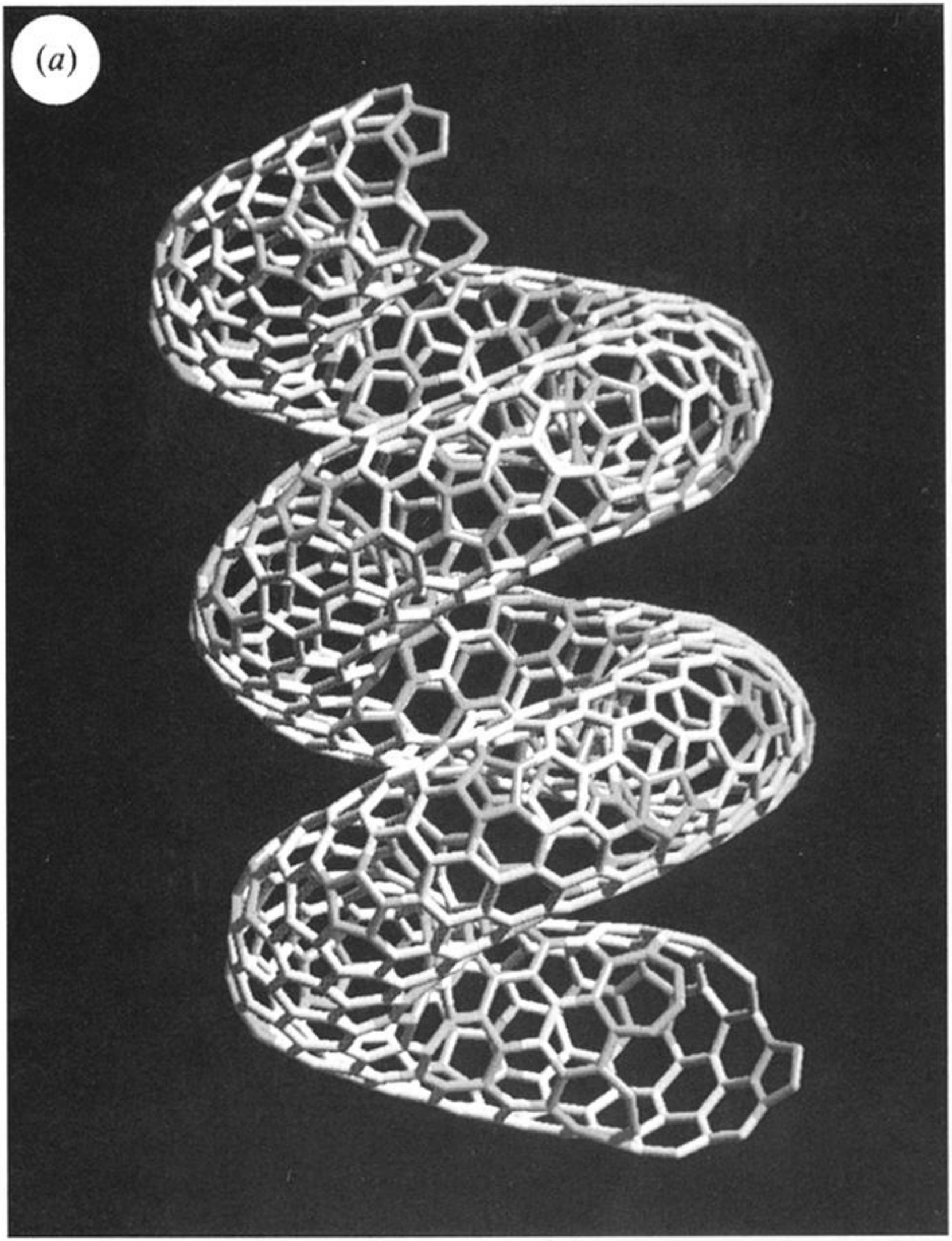

Figure 8. Helicoidal graphite: (a) simulated single-wall corkscrew-shaped carbon nanotube produced by interspersing five- and seven-membered rings judiciously within the mainly hexagonal network wall.

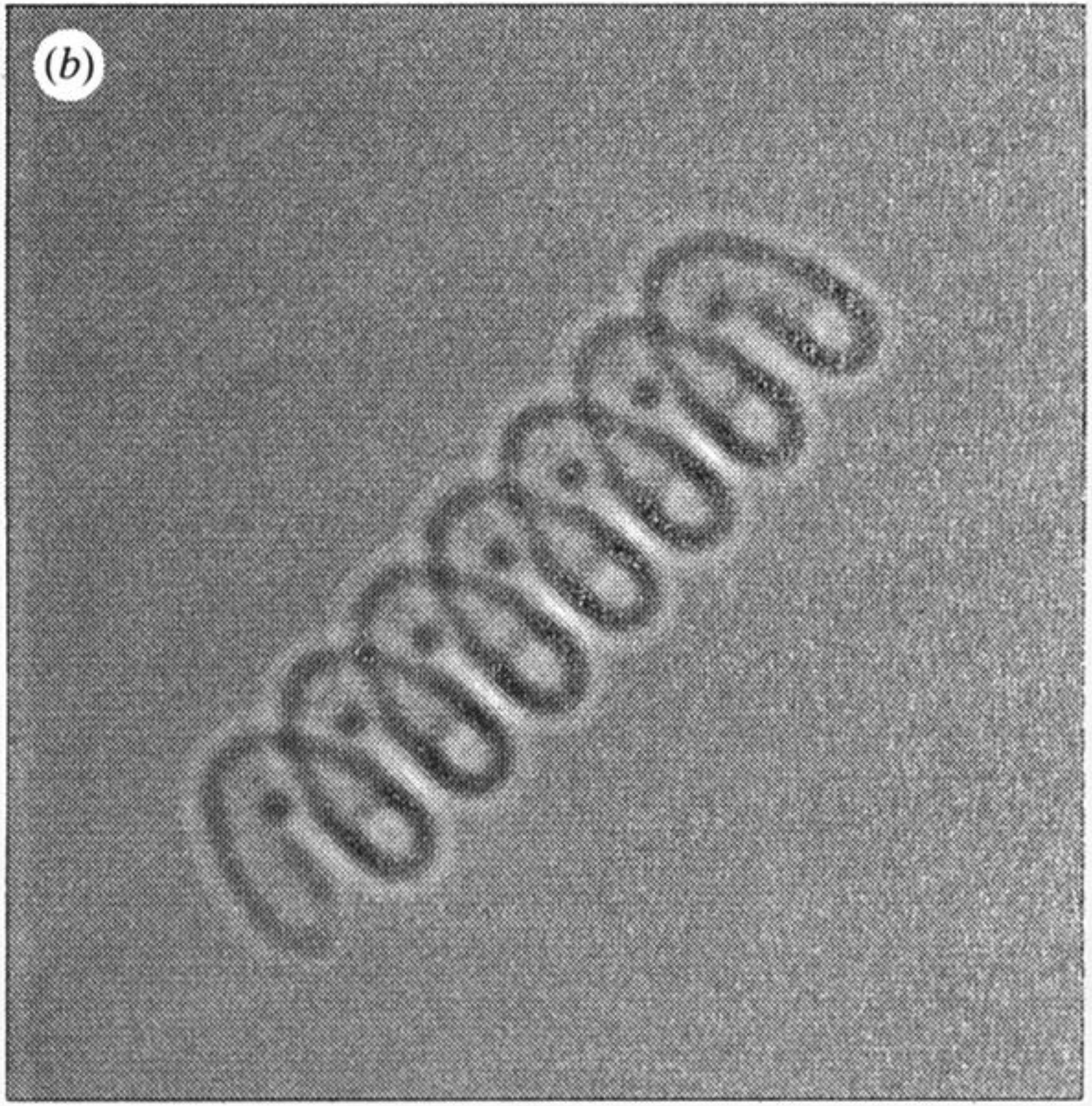

Figure 8. Helicoidal graphite: (*b*) HRTEM simulation from the helix-shaped single wall nanotube represented in 8*a*.

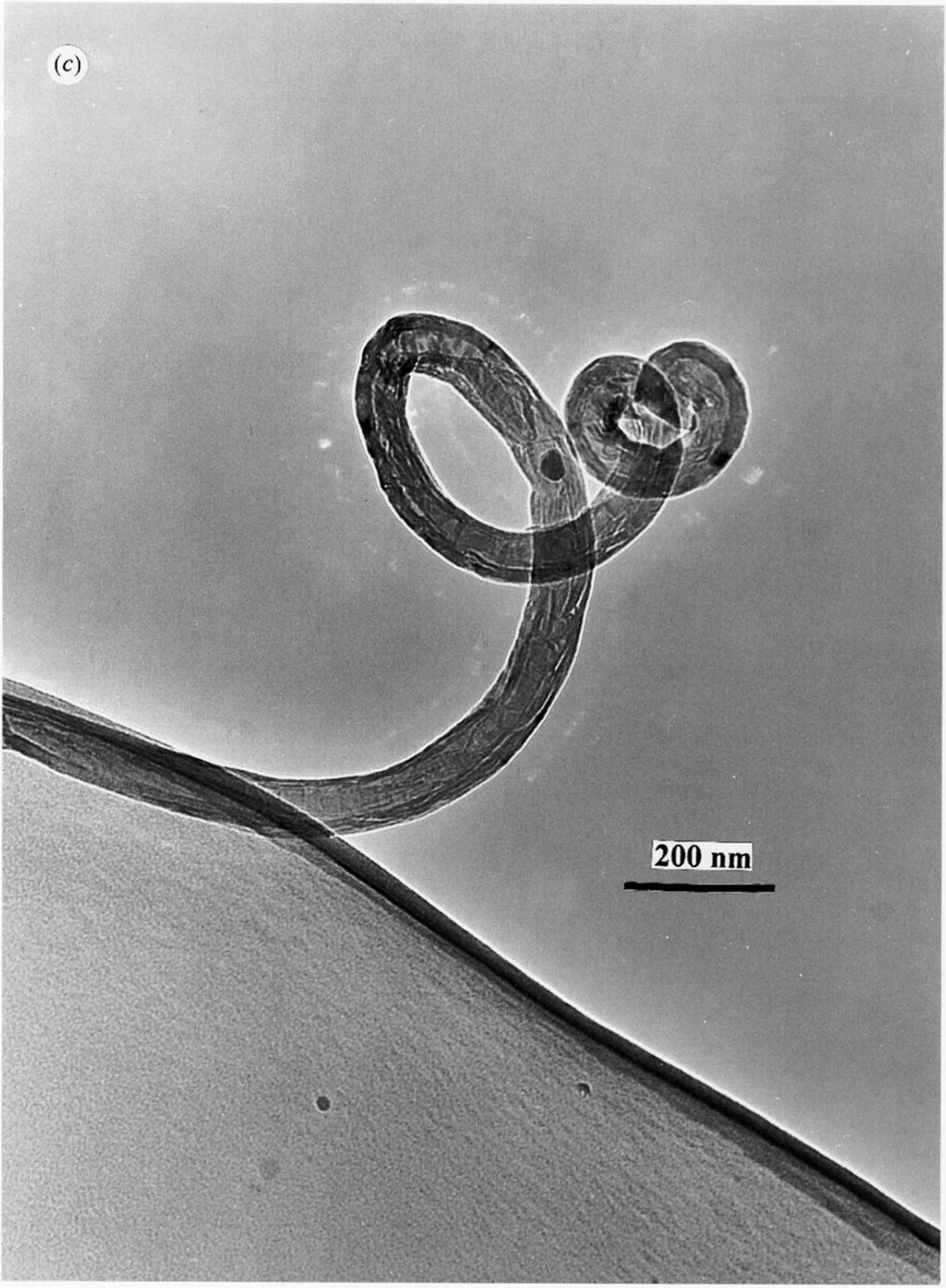

Figure 8. Helicoidal graphite: (*c*) helical nanotube found in acetylene pyrolysis using Co powder as a catalyst at around 800 °C.

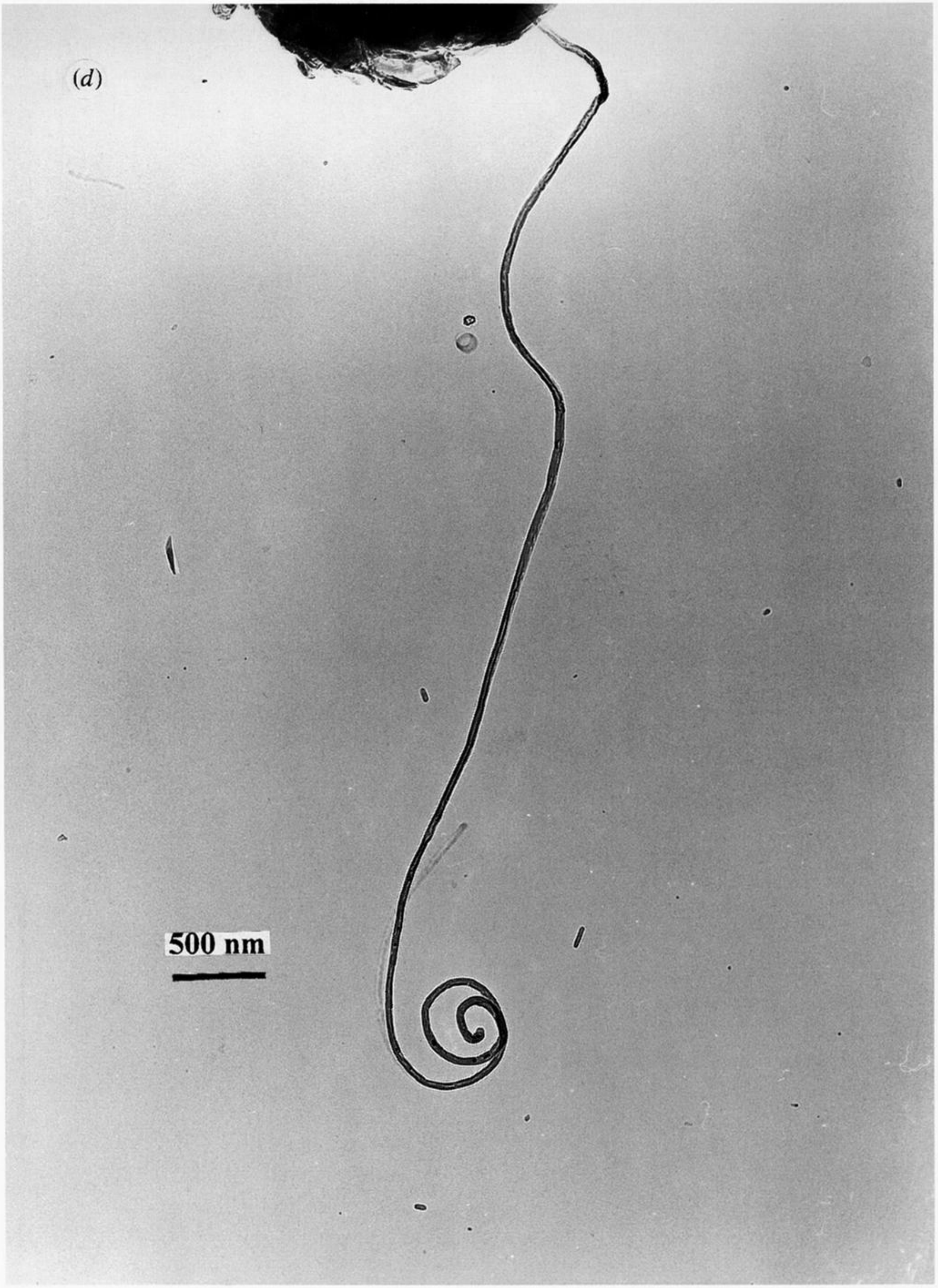

Figure 8. Helicoidal graphite: (*d*) spiral multiwalled nanotube also produced in acetylene pyrolysis with the same conditions as in figure 8*c*.

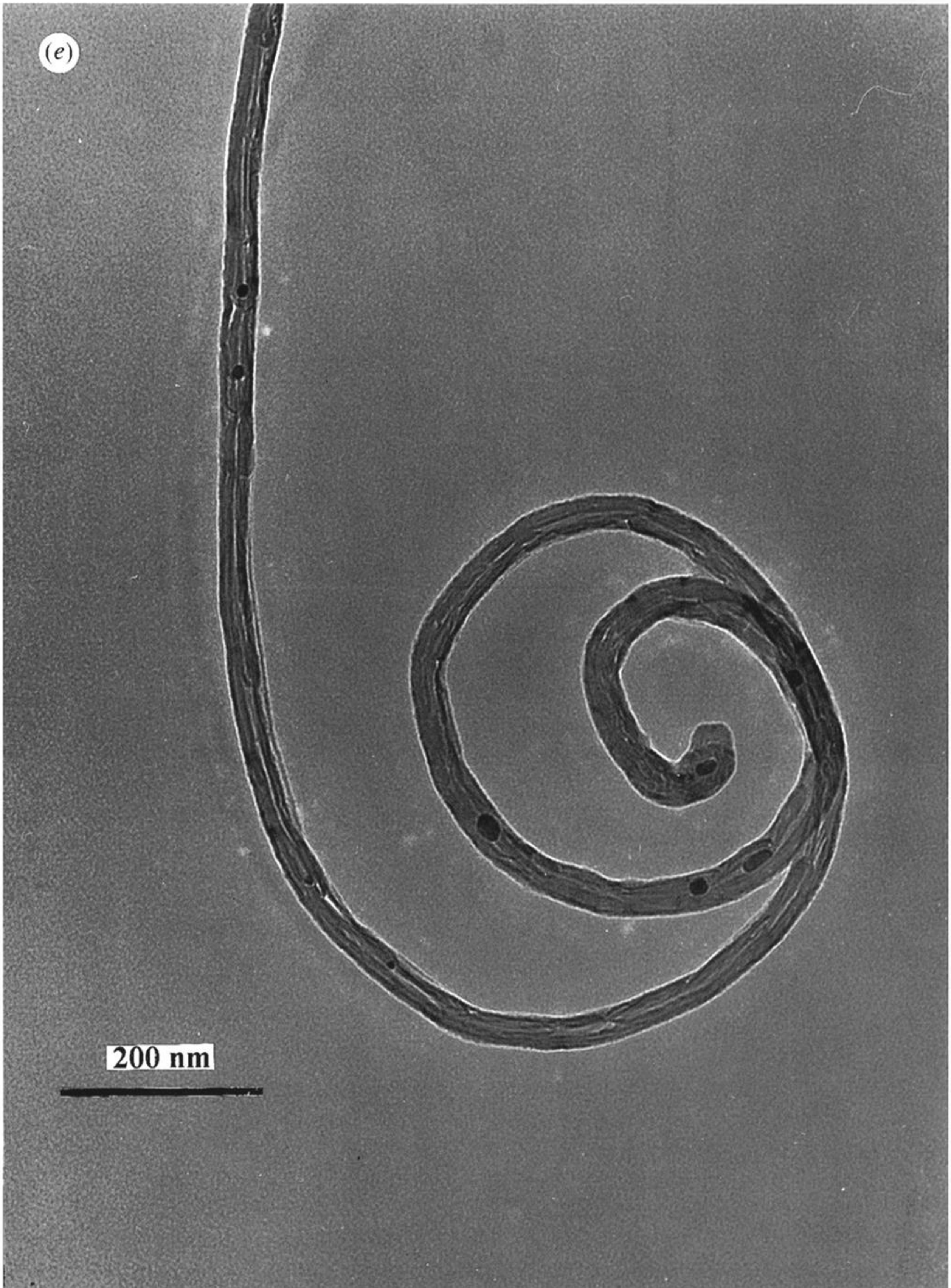

Figure 8. Helicoidal graphite: (*e*) spiral multiwalled nanotube also produced in acetylene pyrolysis with the same conditions as in figure 8*c*.

(*a*)

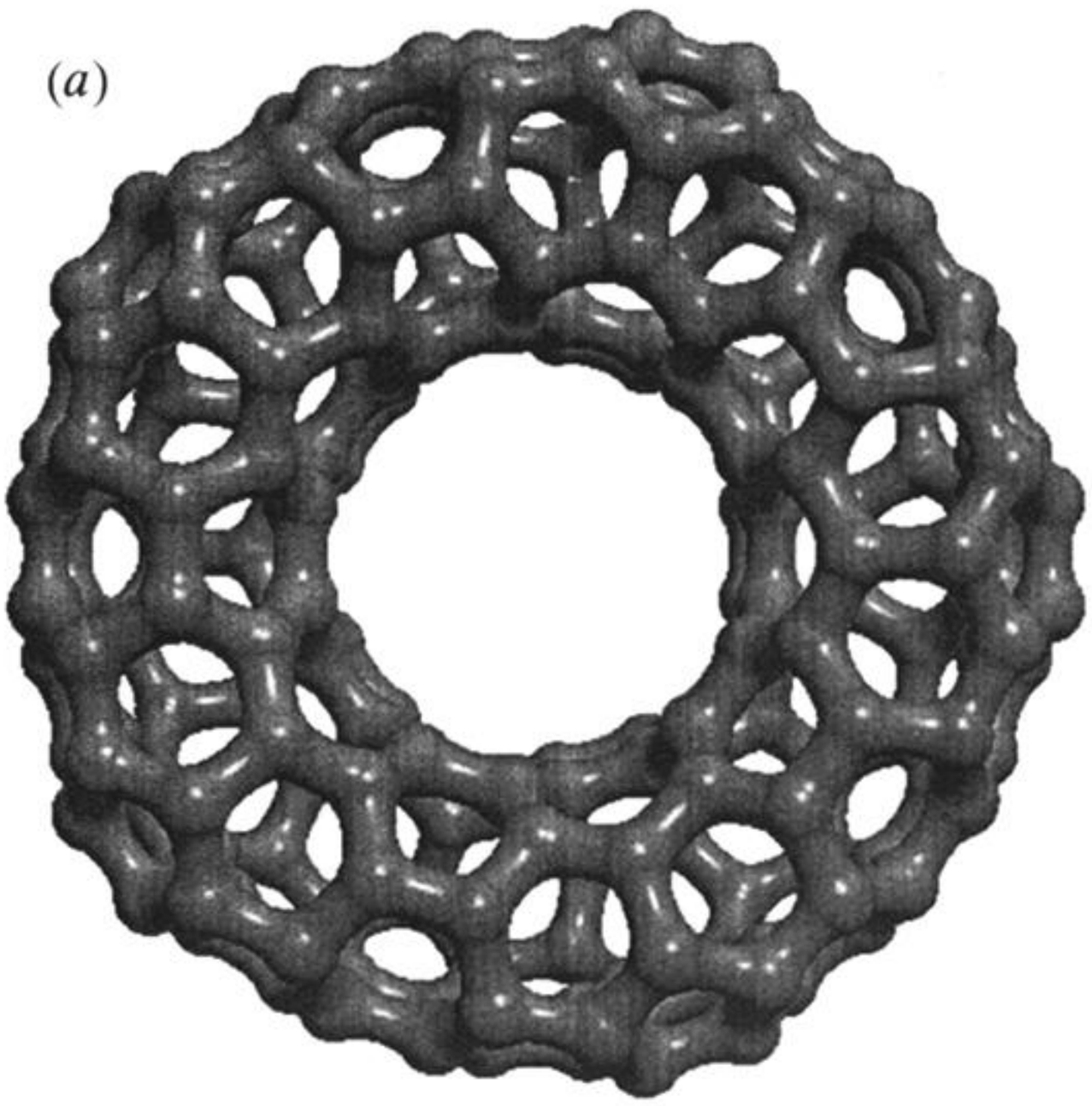

(*b*)

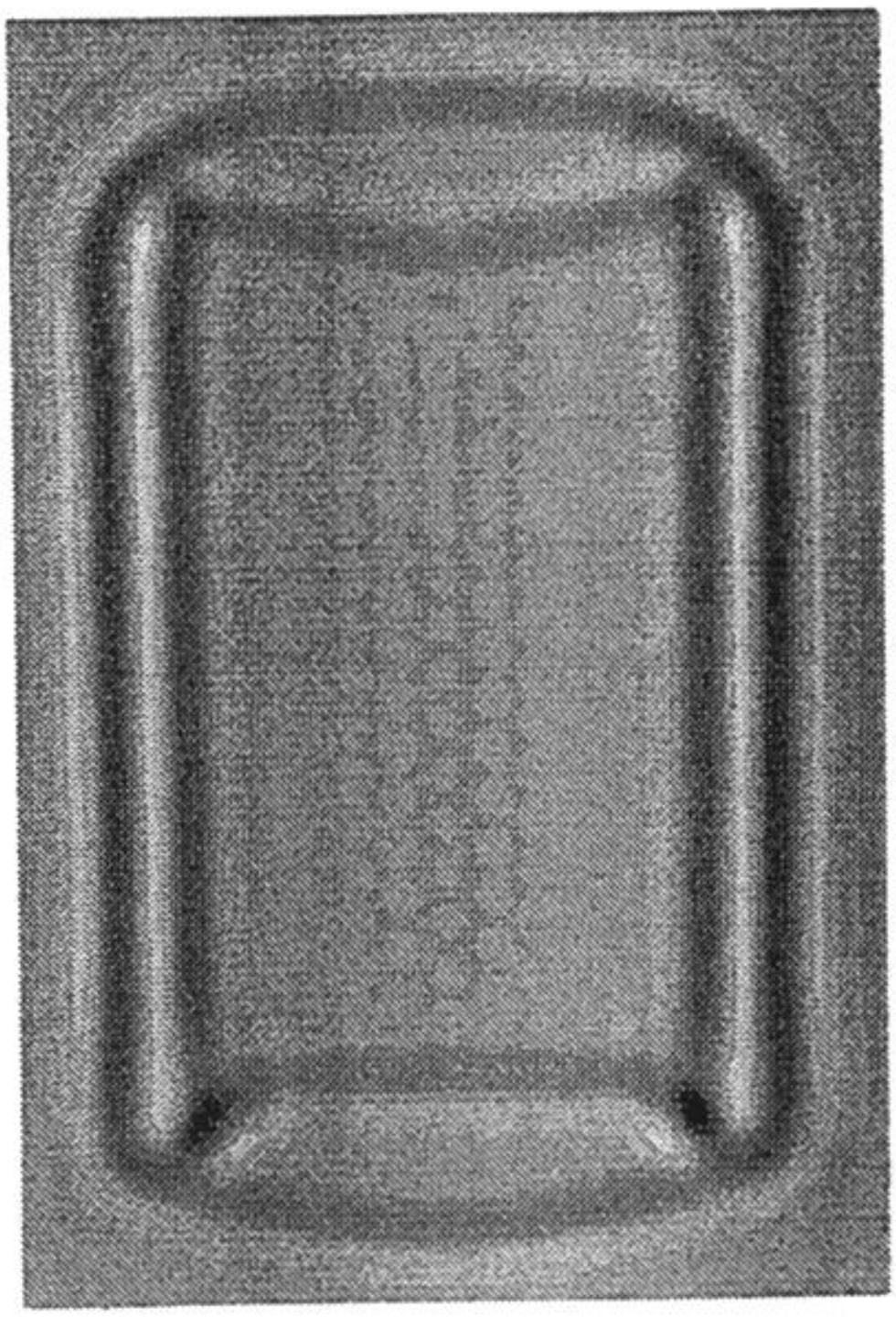

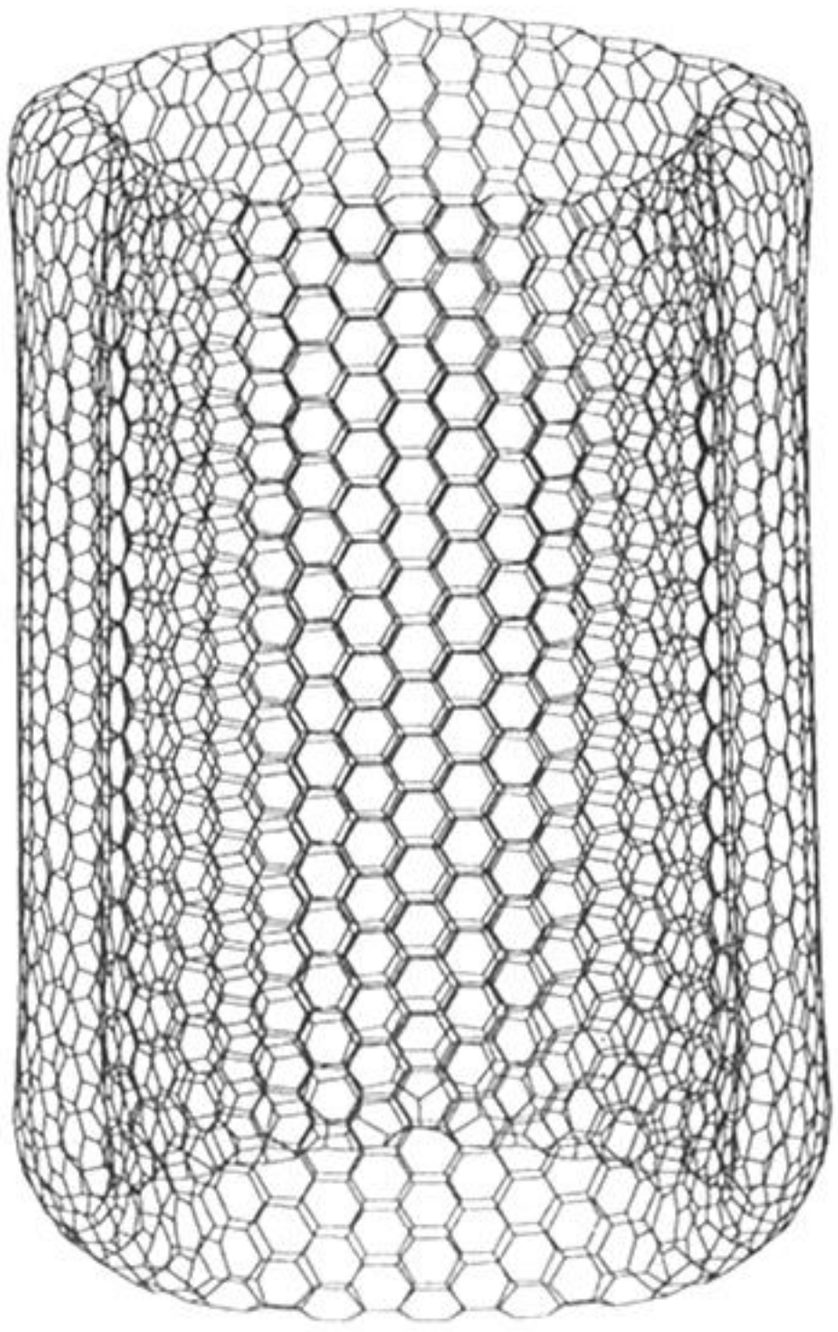

Figure 9. Toroidal graphite: (*a*) doughnut-like structure, where the heptagons are present in the inner rim and the pentagons on the outer rim; (*b*) an elongated doughnut and its HRTEM simulation are presented. The latter image is believed to exist in pyrolytic nanotubes heated at high temperatures (Sarkar *et al.* 1995; Endo *et al.* 1995).

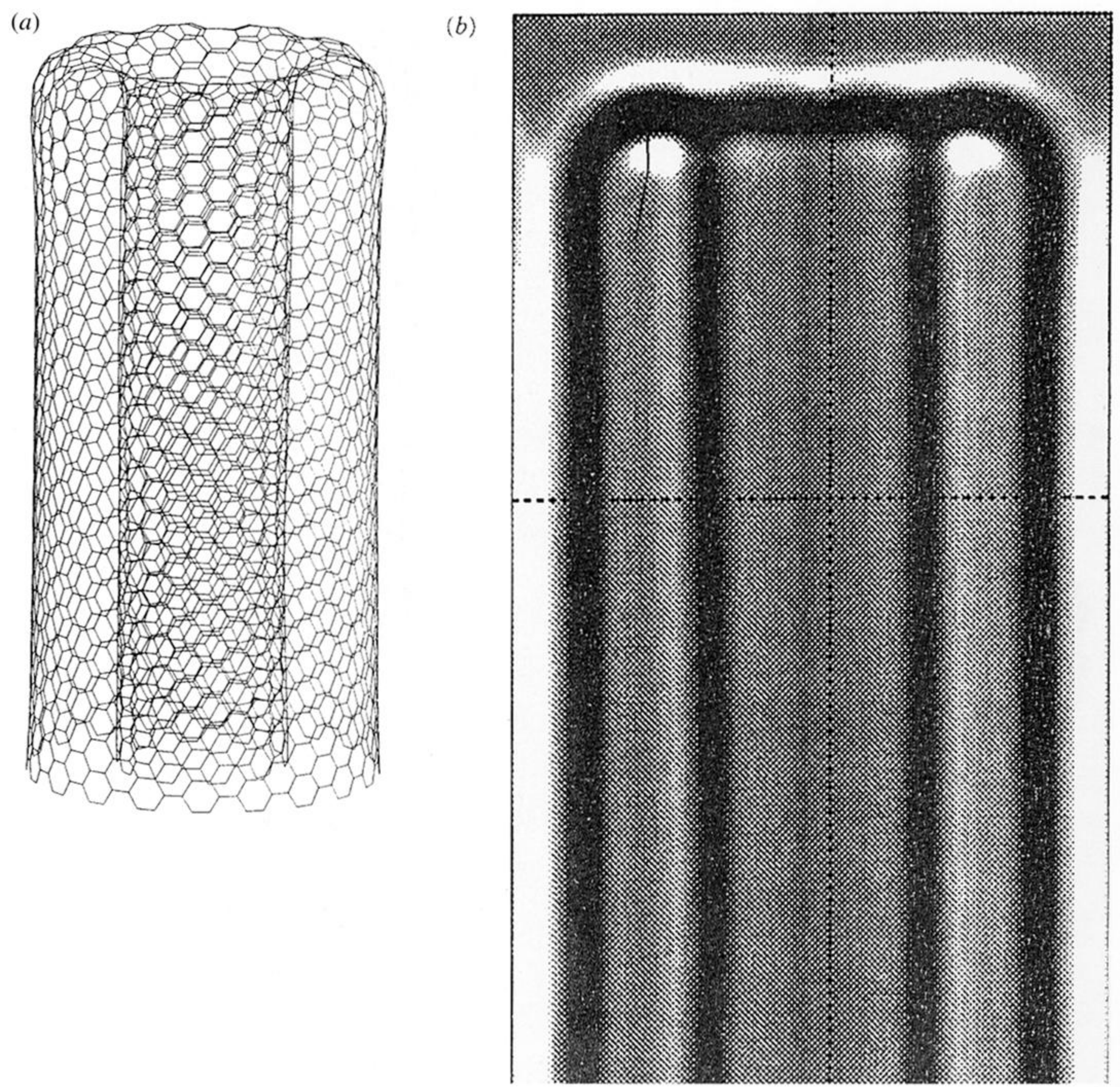

Figure 10. Hemitoroidal nanotube cap 'sock-like' (inwardly folded) structure. (a) Simulated structure consisting of two concentric nanotubes joint together from their top rims (inner and outer, respectively); (b) HRTEM simulation of the single-wall hemitoroidal structure represented in (a).

(*c*)

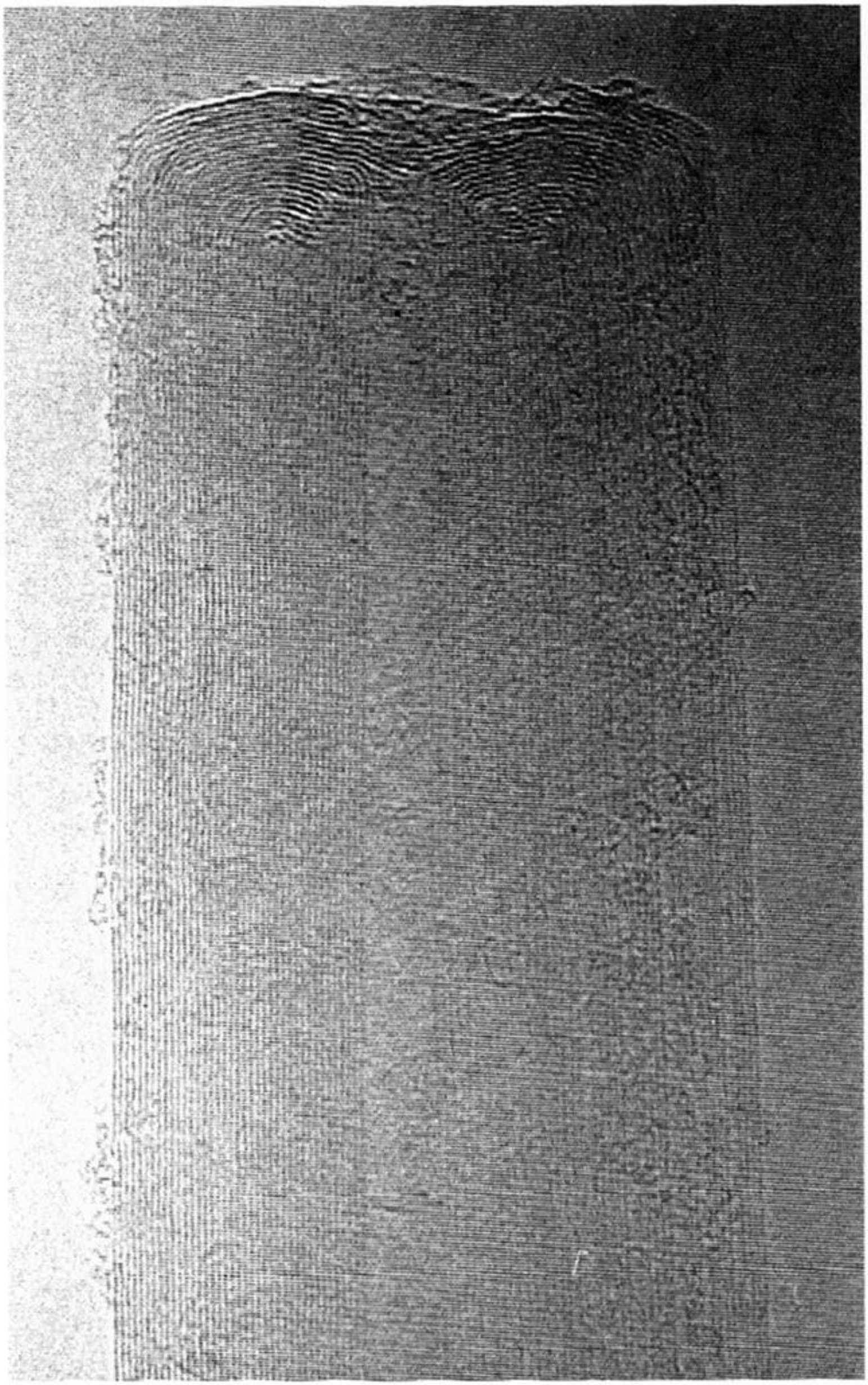

Figure 10. Hemitoroidal nanotube cap 'sock-like' (inwardly folded) structure. (*c*) Hemitoroidal nanotube cap found from the cathode deposit using hexagonal BN in the anode during the arc-discharge experiment. It is noteworthy that the simulated and the real images are in good agreement.

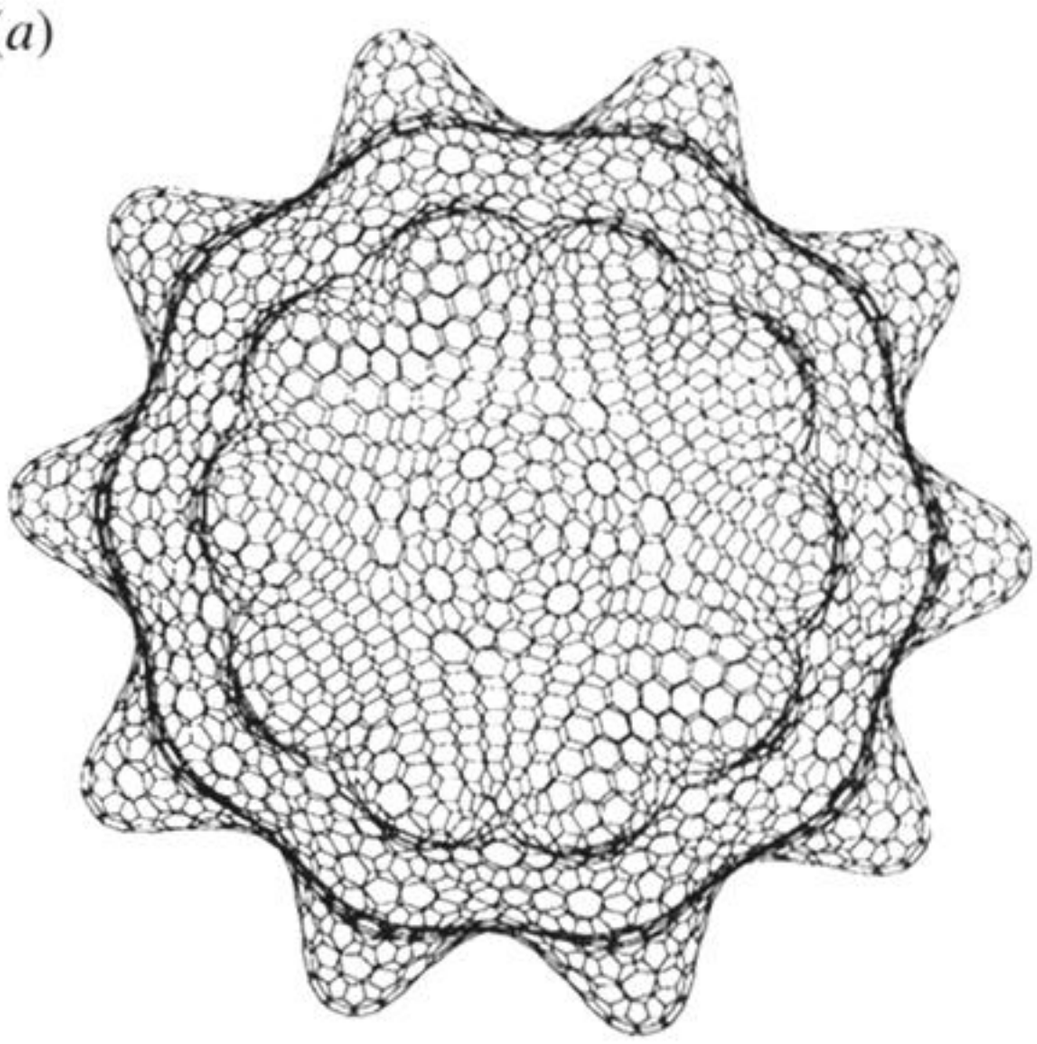

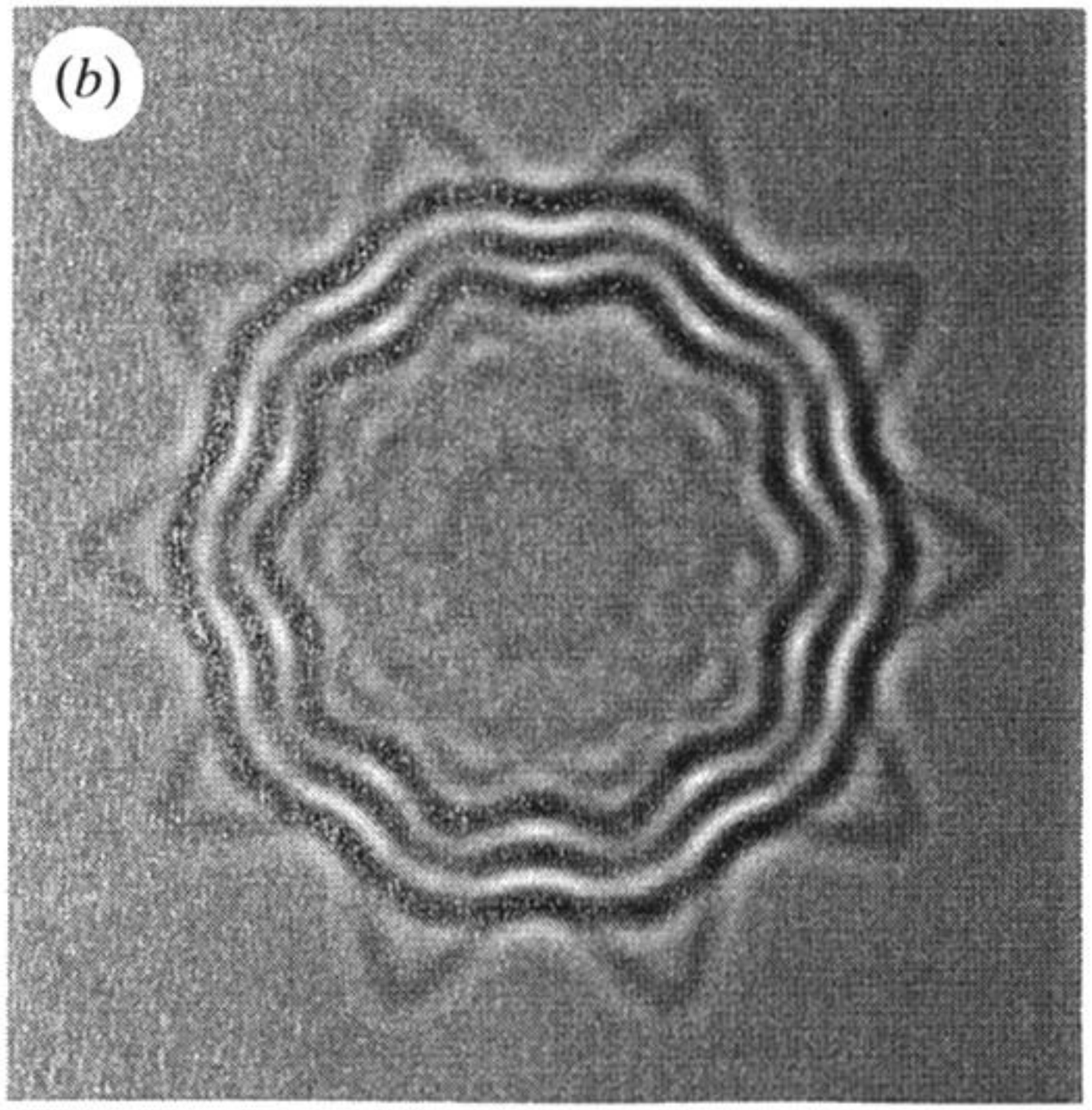

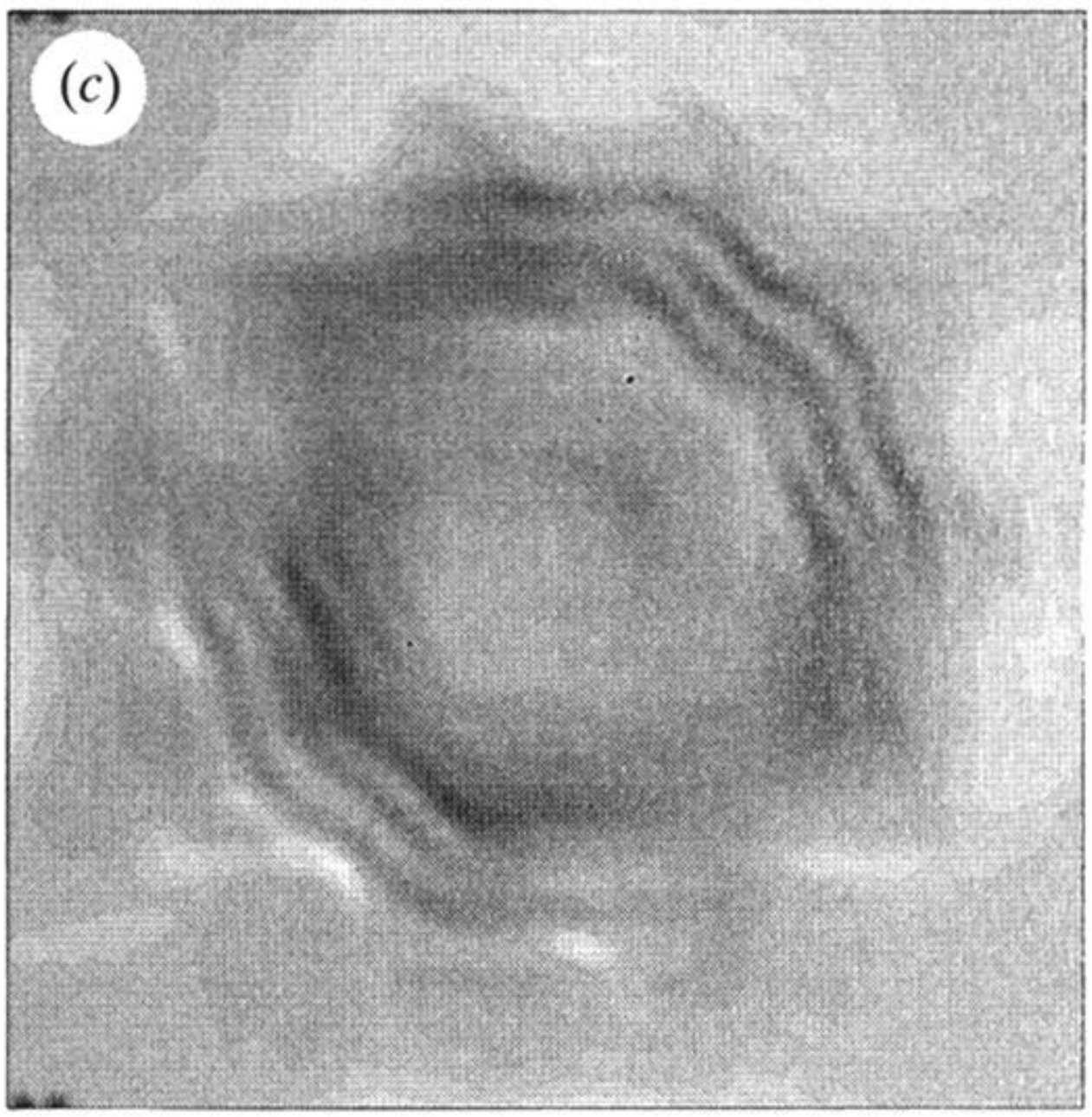

Figure 11. (a) Molecular model image of a three-dimensional star-shaped fullerene in which seven and five-membered rings are interspersed to produce negative as well as positive curvature in such a way that blisters occur in the surface; (b) and (c) HRTEM simulations for three concentric star-shaped fullerenes with different defocus conditions.

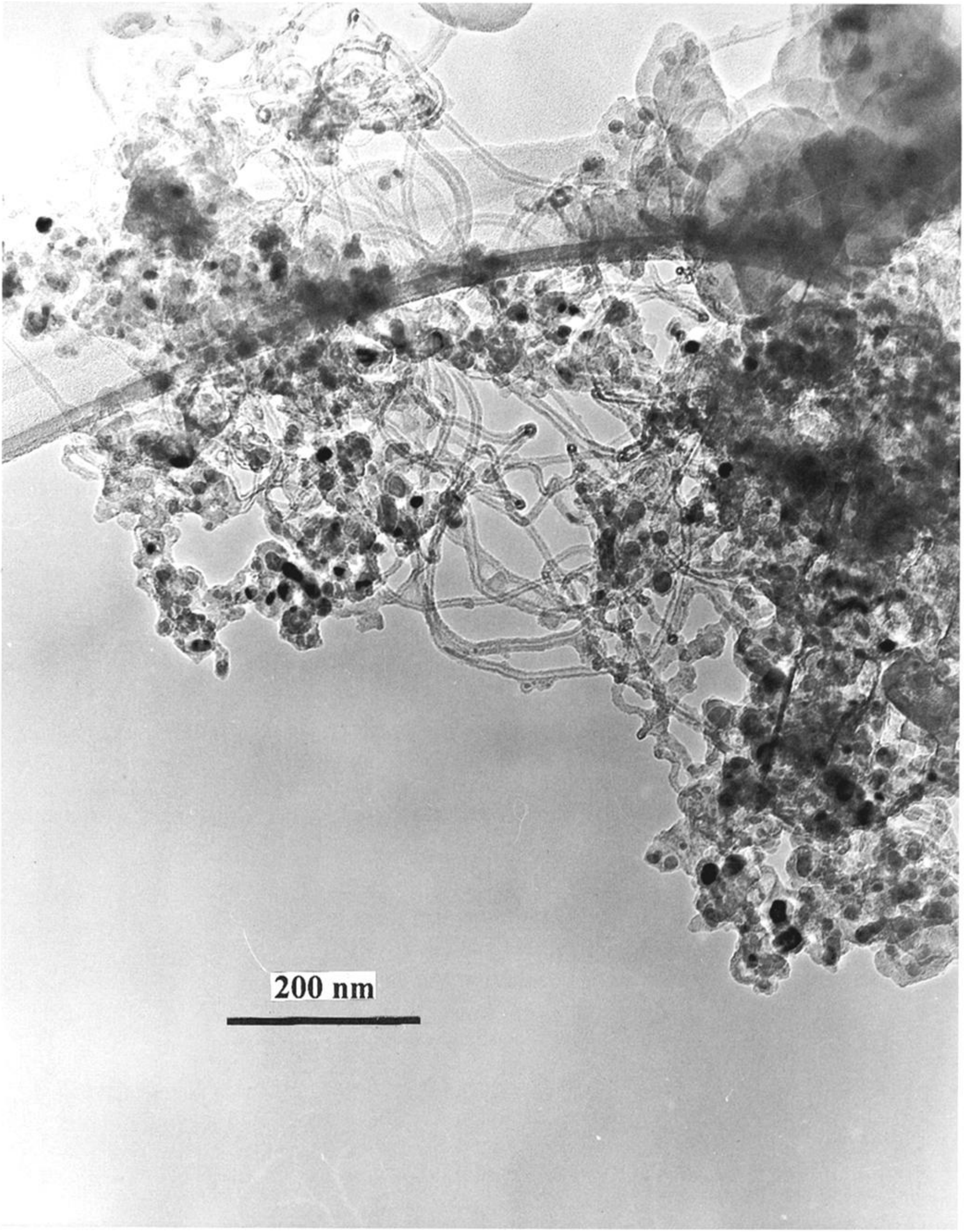

Figure 13. TEM image showing a representative area where nanotubes, produced by electrolysis in LiCl, possess curled morphologies.